ROLE OF THE NUCLEAR RECEPTOR PPARγ IN CLEAR CELL RENAL AND BLADDER UROTHEIAL CARCINOMA

Danielle J. Sanchez

A DISSERTATION

in

Cell and Molecular Biology

Presented to the Faculties of the University of Pennsylvania

in

Partial Fulfillment of the Requirements for the

Degree of Doctor of Philosophy

2019

Supervisor of Dissertation

_____

M. Celeste Simon, Ph.D.
Arthur H. Rubenstein, MBBCh Professor

Graduate Group Chairperson

_____

Daniel S. Kessler, Ph.D.
Associate Professor of Cell and Developmental Biology

Dissertation Committee
Patrick Seale, Ph.D., Associate Professor of Cell and Developmental Biology
Kathryn E. Wellen, Ph.D., Associate Professor of Cancer Biology
Katalin Susztak, M.D., Ph.D., Professor of Medicine
Mitchell A. Lazar, M.D., Ph.D., Willard and Rhoda Ware Professor in Diabetes and Metabolic Diseases

A mi abuelita querida, Isabel.

ACKNOWLEDGMENTS

With sincere appreciation for:

My advisor, Celeste Simon, for her example in science and faith. For teaching me countless life lessons about working with and for others. For the encouragement and support she provides her trainees. Brian Keith, for all those things as well as his mentorship on golf.

Mentors I have had throughout my life: Anne Tei, Cheryl Whiteman, Patrick and Anita Mason, Michael Graf, Fr. Andrea Vicini and Fr. Joseph Nolan (*AMDG*), Glenn Maclean and the other postdocs of the Orkin lab (for what I aspired to be as a graduate student).

My thesis committee, lab mates, and collaborators: Patrick Seale, Katy Wellen, Katalin Susztak, and Mitch Lazar. Karin Eisinger, Nico Skuli, Bo Qiu, Ankita Bansal, Sanika Khare, Pearl Lee, Jay Godfrey, Nicole Anderson, Michelle Spata, and John Tobias. Steve Dinardo (for ukulele and guitar jam sessions) and Dan Kessler. For my IDOM friends: Dave Steger (for teaching me ChIP-seq and a two-handed backhand), Liming Pei, Suzi Shapira, and Jeff Ishibashi.

My friends from high school and Boston College: Tori Berman, Manju Varughese, Elsy Thayil-Blanchard, Erica Lewis (for constantly reminding me of the ideals of our Jesuit education), and Marlena Papavaritis. My grad school friends, particularly Terra Kuhn and Colleen Harrington, for always making time to chat over coffee, wine, ice cream, or dinner.

My teammates and opponents in flag football, softball, soccer, squash, tennis, and golf. Finding a community of people in Philadelphia to share these activities with has been one of the most rewarding parts of my grad school experience.

Every single one of the words I wrote of the novellas *The Sound Sentinel* and *Debates*. You are the true treasure of the past few years of my life. Without the mental respite you brought me from the disappointments of grad school, *there is absolutely no way* I would have made it to the end of this program. "*Junts som més forts."*

My Mom and Dad. Thank you for your constant love and support.

ABSTRACT

ROLE OF THE NUCLEAR RECEPTOR PPARγ IN CLEAR CELL RENAL AND BLADDER UROTHEIAL CARCINOMA

Danielle J. Sanchez

M. Celeste Simon, Ph.D.

The nuclear receptor peroxisome proliferator-activated receptor gamma (PPARγ) has a well-characterized role in the developmental process of adipogenesis and transcriptional regulation of lipid metabolism. However, its expression patterns and functions in various cancer subtypes are less understood. My studies investigate the role of PPARγ in two distinct cancers of the urinary tract: clear cell renal cell carcinoma (ccRCC) and bladder urothelial carcinoma (UC). In ccRCC, I hypothesized that PPARγ activity contributes to the aberrant lipid accumulation phenotype characteristic of this disease, thereby promoting tumor progression. Through ChIP-seq, I demonstrated that PPARγ and its heterodimeric DNA binding partner retinoid X receptor (RXR) occupy both adipose-shared and ccRCC-specific sites throughout the genome. However, based on a number of *in vitro* and *in vivo* assays evaluating ccRCC viability, proliferation, migration, and effects on lipid metabolism, I concluded that PPARγ was dispensable for these processes and ccRCC progression. I also studied the role of PPARγ in UC, a cancer which displays copy number amplification and mRNA overexpression of *PPARG* or *RXRA* in ~30% of tumors. In contrast to the results obtained in ccRCC, I demonstrated that genetic and pharmacological inhibition of PPARγ reduces tumor growth via cell cycle arrest. Furthermore, I identified a candidate list of PPARγ-regulated genes in UC based on ChIP- and RNA-seq analyses of cell culture models, as well as gene expression data from primary patient samples. Together, my studies illuminate the remarkable cell type-specific functions of PPARγ in urinary tract cancers, and provide rationale for the pharmacological targeting of its transcriptional effectors in a subset of tumors.

TABLE OF CONTENTS

LIST OF TABLES

LIST OF FIGURES

Chapter 1: General Introduction

A portion of this chapter has been adapted with modifications from: Sanchez, DJ, Simon, MC. Genetic and metabolic hallmarks of clear cell renal cell carcinoma. *Biochim Biophys Acta Rev Cancer.* 2018 Aug;1870(1):23-31. doi: 10.1016/j.bbcan.2018.06.003.

1.1 Introduction to nuclear receptors and the peroxisome proliferator-activated receptor gamma (PPARγ)

Nuclear receptor structure and mechanism of action

Nuclear receptors (NRs) are a family of ligand-activated transcription factors that couple metabolic cues from the external environment to the regulation of gene expression. The human genome encodes 48 NRs, many of which were initially classified as “orphan” receptors, as their activating ligands and physiological functions were unknown (Chawla et al., 2001b). NRs share common structural domains, including an N-terminal regulatory domain containing a ligand-independent transcriptional activation function (AF-1); DNA-binding domain composed of two zinc finger motifs; hinge region, and a large C-terminal region containing the ligand-binding domain; dimerization region; and ligand-dependent activation function (AF-2) (Tsai and O'Malley, 1994). Type I NRs are located in the cytosol and bound to chaperone proteins in the absence of ligand. Upon ligand-binding, these NRs dissociate from chaperones, homodimerize, and translocate to the nucleus to activate target gene expression. Type II NRs, such as PPARs, are generally bound on DNA as heterodimers regardless of activation state (Sever and Glass, 2013). Briefly, ligand-binding induces a conformational change that dissociates co-repressor molecules and facilitates binding of co-activators. NR co-activator proteins contain intrinsic histone acetyltransferase activity to facilitate chromatin decondensation, while co-repressors recruit histone deacetylase to compact chromatin (Dasgupta et al., 2014). CBP/p300, the SRC family, TRAP220 (MED1), and PGC-1α all function as NR co-activators; silencing mediator for retinoid and thyroid hormone receptors (SMART), nuclear receptor co-repressor (NCoR), and RIP140 are co-repressors (Hu and Lazar, 1999; Tontonoz and Spiegelman, 2008).

Peroxisome proliferator-activated receptors

The peroxisome proliferator-activated receptor (PPAR) family are type II NRs and contain three members: PPARα, PPARδ, and PPARγ. PPARs have distinct tissue expression patterns and biological functions, but are all broadly important for the regulation of lipid metabolism and

energy homeostasis. The retinoid X receptor (RXR) is the heterodimeric partner of PPAR transcription factors, which together bind a consensus motif containing a hexameric DNA sequence repeated with a single nucleotide spacer AGGTCA(N)AGGTCA (known as DR1) (Kliewer et al., 1992). PPARα is a critical regulator of fatty acid catabolism and lipoprotein assembly, and is most highly expressed in the liver, kidney, and heart (Mandard et al., 2004). PPARδ is expressed ubiquitously and has also been implicated in fatty acid oxidation, although the specific biological functions of this family member are the least studied of the three (Luquet et al., 2005). PPARγ is the master regulator of adipogenesis (discussed below), and is expressed in fat cells as PPARγ1 and PPARγ2, isoforms that differ by 30 amino acids at the N-terminus of the protein. This is achieved through alternative promoter usage and differential splicing of the mRNA transcript (Fajas et al., 1997; Zhu et al., 1995). *PPARG* expression in non-adipocyte cells predominantly results in the production of the PPARγ1 isoform. Endogenous ligands of PPARγ include polyunsaturated fatty acids, prostanoids such as 15-deoxy-Δ12–14-PGJ2, and the oxidized fatty acids 9-hydroxyoctadecadienoic acid (HODE) and 13-HODE. However, the identity of the biological ligand(s) important for PPARγ activation *in vivo* remains unknown (Sauer, 2015; Tontonoz and Spiegelman, 2008). Post-translational modifications can also change the activity of the receptor, such as phosphorylation of mPPARγ2 at serine 112 by mitogen-activated protein kinase (MAPK), which decreases its transcriptional activity by inhibiting ligand binding (Adams et al., 1997; Hu et al., 1996; Shao et al., 1998).

1.1a Roles of PPARγ in development and metabolic disease

PPARγ works coordinately with CCAAT-enhancer-binding proteins (C/EBP) alpha and beta to direct the terminal differentiation of mesenchymal stem cell-derived precursors into adipocytes. Specifically, hormonal treatment of preadipocytes induces C/EBPβ/δ, which binds to the promoter of *PPARG* and activates its expression (Wu et al., 1996; Wu et al., 1995). PPARγ then induces C/EBPα, which participates in a positive-feedback loop with its activator to drive the

expression of genes important for triglyceride uptake and storage (Rosen et al., 2002). As C/EBPα cannot promote adipogenesis in the absence of PPARγ, the latter is considered the "master regulator" of adipogenesis and has been shown to be both necessary and sufficient for this process *in vitro* (Tontonoz et al., 1994) and *in vivo* (Wang et al., 2013).

Since homozygous knockout of *PPARG* results in embryonic lethality (Barak et al., 1999), several groups have created conditional, adipose-specific deletions of *PPARG* in mice to investigate its function postnatally. Early studies from the Evans group reported progressive lipodystrophy in an *FABP4* driven (*ap2*-Cre) *PPARG*$^{-/-}$ model, which was accompanied by hyperlipidemia, fatty liver (hepatosteatosis), and hepatic insulin resistance (He et al., 2003). These results were corroborated by tamoxifen-inducible *PPARG* deletion in mature white and brown adipocytes, which died within a few days of knockout and were replaced by newly differentiated PPARγ-positive adipocytes (Imai et al., 2004). A more dramatic phenotype was observed using an independent Cre-driver of *PPARG* deletion in fat by the adiponectin promoter (*Aqipoq*-Cre) (Wang et al., 2013). These results from mouse models are also supported by studies of polymorphisms linked to human metabolic disease. For example, heterozygous, R425C mutation of *PPARG* was reported in a patient with familial partial lipodystrophy (Agarwal and Garg, 2002). Collectively, these data demonstrate the critical role for PPARγ in mammalian adipose tissue development and function throughout the lifespan.

Metabolic syndrome is a collection of symptoms including obesity, hyperlipidemia, hypertension, insulin resistance, and hepatosteatosis, all of which are influenced by the "Western" diet, genetics, and sedentary lifestyle. Collectively, type 2 diabetes and other metabolic diseases pose a significant health risk for both adults and children in the United States, and incidence has been rising dramatically over the past decades (Eckel et al., 2005). The synthetic PPARγ agonists thiazolidinediones (TZDs) are one class of medication commonly used for the treatment of type 2 diabetes. TZDs exert pleiotropic effects on a number of tissues, but are thought to predominantly work by activating PPARγ function in adipocytes (Yki-Jarvinen, 2004). Proposed mechanisms of TZD action include increasing small adipocyte number and increasing fatty acid uptake into

adipose tissue, thereby preventing it from being deposited in ectopic tissues such as the liver (Okuno et al., 1998).

As *PPARG* is expressed at low levels in muscle and macrophages, conditional deletion studies have also been performed to elucidate its role in development and pathology in these tissues. *PPARG* knockout using muscle creatine kinase (MCK-Cre) results in insulin resistance in muscle, and can induce secondary effects in whole-body metabolism including hypertriglyceridemia (Hevener et al., 2003). While *PPARG* is normally expressed at very low levels in hepatocytes, PPARγ protein levels increase in livers of high-fat diet treated mice, and hepatocyte-specific *PPARG* knockout reduces lipid accumulation in this model (Morán-Salvador et al., 2011). *PPARG* expression is also much lower in macrophages than in adipose tissue, yet it plays an important function in regulating lipid uptake and the activation of anti-inflammatory pathways (Chawla et al., 2001a; Lefterova et al., 2010; Nelson et al., 2018). In an injury model of cardiac hypertrophy, PPARγ was shown to be involved in fatty acid uptake and the regulation of glycerolipid biosynthesis genes within cardiomyocytes (Krishnan et al., 2009). These data from mouse models support a role for PPARγ in the regulation of lipid metabolism in adipocytes as well as other tissues (e.g., liver, macrophages), particularly during conditions of metabolic disease and related pathologies.

1.1.b Roles of PPARγ in cancer

PPARγ has been traditionally described as having tumor suppressive functions in a variety of mouse models of cancer, although studies suggest that this is highly dependent on cell/tissue of origin, as well as the specific genetic and carcinogenic drivers of each subtype. Heterozygous deletion of *PPARG* in chemically-induced models of colorectal and breast cancer increases tumorigenesis and decreases survival time compared to wildtype controls (Girnun et al., 2002; Nicol et al., 2004). However, two other studies in an $Apc^{Min/+}$ driven model demonstrated that troglitazone and rosiglitazone (TZD) treatment increased the frequency and

size of polyps, suggesting oncogenic functions for *PPARG* in this background (Lefebvre et al., 1998; Saez et al., 1998).

Due to the potency of TZDs in inducing terminal adipocyte differentiation (accompanied by cell cycle arrest), it was hypothesized that these drugs could be useful in halting cancer cell growth. Indeed, anti-proliferative effects of TZDs were particularly pronounced in liposarcomas, tumors which are derived from a cell-of-origin in the mesenchymal lineage and express levels of PPARγ nearly equivalent to adipocytes (Tontonoz et al., 1997). However, most *in vitro* studies examining the relationship between TZDs and cancer proliferation involve doses in the micromolar range, concentrations associated with "off-target" effects on cellular processes including inhibition of the p38 MAPK pathway and inhibiting the anti-apoptotic functions of Bcl-2 and Bcl-xL independently of PPARγ (Fujita et al., 2011; Shiau et al., 2005). TZDs were reportedly effective in reducing xenograft tumor growth of lung adenocarcinoma cells, yet endogenous levels of PPARγ in lung adenocarcinoma cells were not demonstrated in that publication (Srivastava et al., 2014). A careful analysis of PPARγ protein abundance and expression patterns throughout the course of disease progression will be a useful first step in determining whether it provides oncogenic or tumor suppressor functions in a given cancer model.

To that end, our curated data from publicly available sources suggest that PPARγ might play an important biological role in other cancer subtypes where it is expressed appreciably. For example, analyses of mRNA expression patterns and sensitivity of cancer cell lines to *PPARG* CRISPR knockout show that pancreatic cancer cell lines have the highest expression of the gene among all cell lines profiled (**Figure 3.1E**) and that these cell lines may be sensitive to its inhibition (**Figure 3.4E**). Based on these data, we speculate that pancreatic adenocarcinoma may be another cancer dependent on PPARγ signaling for growth, although this remains to be determined experimentally.

1.2 Introduction to clear cell renal cell carcinoma (ccRCC)

Kidney cancer is the 8th most prevalent cancer diagnosed each year in the United States, with an estimated 64,000 new cases in 2017 (Institute, 2018). The median age at diagnosis for both sexes is 64, and total overall incidence rate has been increasing over the past decade. Clear cell renal cell carcinoma (ccRCC) accounts for 70-80% of kidney cancer diagnoses, and represents the most aggressive subtype of this disease (Rini et al., 2009). Risk factors for ccRCC include smoking, obesity, von Hippel-Lindau (VHL) disease (defined below), and hypertension. If disease is detected early and still localized within the kidney, surgical resection or nephrectomy is performed with a 5-year survival rate of ~92%. However, if the tumor has spread locally or systemically, 5-year survival rates drop to 67% or 12%, respectively, due to limitations in current standard-of-care therapies for metastatic disease (Institute, 2018).

A defining morphological hallmark of ccRCC is robust lipid and glycogen accumulation in the cytoplasm of tumor cells, giving rise to the name “clear cell”. Widespread metabolic reprogramming in glucose, lipid, and amino acid metabolism broadly contributes to the clear cell phenotype (Wettersten et al., 2017), although the advantages conferred unto tumor cells harboring these adaptations are incompletely understood. Compared with other solid tumors driven by loss of classical tumor suppressors or activation of oncogenes (e.g., those encoding p53 and K-Ras), ccRCC has been labeled as a “metabolic disease” supported by alterations in myriad bioenergetic pathways (Hakimi et al., 2013b; Linehan et al., 2010). Genetic hallmarks include biallelic inactivation of the *VHL* tumor suppressor gene, the negative regulator of hypoxia-inducible factor (HIF) proteins, as well as copy number alterations of chromosome 3p, 5q, and 14q genes, and high frequency of mutation in chromatin modifying enzymes (e.g., *PBRM1*, *SETD2*, and *BAP1*). Here, we discuss recent advances in ccRCC research related to elucidating the underlying genetic drivers of human disease, progress on obtaining an autochthonous, genetically engineered mouse model (GEMM) for pre-clinical studies, metabolic reprogramming, and therapeutic strategies moving forward.

1.2.a Genetics of ccRCC

VHL loss and HIF-α stabilization

The most common genetic event of ccRCC is copy number deletion, inactivating mutation, and/or epigenetic silencing of *VHL* (encoding pVHL), the recognition component of an E3-ubiquitin ligase complex responsible for targeting HIF-1α and HIF-2α for proteasomal degradation under normoxic conditions (**Figure 1.1**). VHL disease is a familial disorder marked by increased propensity for ccRCC, retinal and cerebellar hemangioblastoma, and pheochromocytoma development. In hereditary disease, patients inherit only one functional copy of the *VHL* gene, and subsequent loss of heterozygosity (LOH) results in disease (Kaelin Jr, 2007). pVHL loss results in constitutive stabilization of HIF-α subunits even under oxygen-replete conditions, which translocate to the nucleus and heterodimerize with HIF-1β (ARNT) (Keith et al., 2012). HIFs transcriptionally activate numerous genes involved in cellular processes including glycolysis, angiogenesis, and metastasis of cancer cells (Mucaj et al., 2012). Notably, while *VHL* inactivation occurs in upwards of 90% of all patients, its loss alone is insufficient to generate ccRCC tumors (Mandriota et al., 2002; Nickerson et al., 2008). Characterization of HIF-α protein accumulation in ccRCC has revealed distinct patterns; ~10% retain wildtype *VHL* and express neither HIF-1α nor HIF-2α, ~60% of tumors express both HIF-1α and HIF-2α, and ~30% express HIF-2α alone (Gordan et al., 2008). This can occur as a result of loss of chromosome 14q as disease advances, on which the *HIF1A* gene resides (Kaku et al., 2004; Shen et al., 2011). Indeed, HIF-1α has been linked with tumor suppressive functions in ccRCC (Shen et al., 2011), (Zhang et al., 2007), while HIF-2α has been established as a dominant oncogenic driver of disease progression (Gordan et al., 2007; Kondo et al., 2003; Kondo et al., 2002; Raval et al., 2005). These observations have supported efforts to develop small molecule antagonists of HIF-2α, which are currently being tested in clinical trials for the treatment of metastatic ccRCC (Martínez-Sáez et al., 2017), and will be discussed later.

Copy number and single nucleotide variation

Recent sequencing studies involving large cohorts of ccRCC patients have revealed signatures of copy number amplification and deletion across the tumor genome (Beroukhim et al., 2009), (Dondeti et al., 2012). A 43 megabase region of chromosome 3p contains multiple *bona fide* or putative tumor suppressor genes including *VHL*, *PBRM1*, *BAP1*, and *SETD2* (discussed below) (Peña-Llopis et al., 2013). Mechanistically, this gene inactivation occurs on one allele through intergenic point mutation, and on the second allele through LOH (Gerlinger et al., 2012) (Gerlinger et al., 2014). On a genome-wide scale, copy number variation of the following regions are most abundant in ccRCC tumors: chromosome 3p loss (91%), 5q gain (67%), and 14q loss (49%) (Network, 2013).

While chromosome 3p and 14q genes are generally associated with having tumor suppressive functions in ccRCC, copy number amplification of a ~60 gene region of chromosome 5q35 harbors candidate oncogenes (Dondeti et al., 2012; Network, 2013). *SQSTM1*, which encodes the p62 protein involved in activation of NRF2 and resistance to oxidative stress, was shown to be a chromosome 5q gene frequently amplified in ccRCC patient samples and cell lines (Li et al., 2013). Suppression of p62 decreased resistance to redox stress and soft agar colony formation *in vitro* and xenograft tumor growth *in vivo*. Additionally, siRNA-mediated suppression of *SQSTM1* reduced mechanistic target of rapamycin (mTOR) signaling, a key nutrient sensing pathway involved in the regulation of cell proliferation, protein synthesis, and autophagy, suggesting multiple mechanisms by which p62 promotes ccRCC progression (Duran et al., 2011). Other work has implicated the chromosome 5q genes *EZH2*, *STC2*, and *VCAN*, which were all copy number gained and overexpressed at the mRNA level, as having oncogenic functions in ccRCC (Dondeti et al., 2012), (Liu et al., 2016). These data suggest that the chromosome 5q hotspot of gene duplication may contain several clinically relevant targets.

Genome-wide association studies (GWAS) have also been conducted in ccRCC patients to illuminate single nucleotide variants predisposing individuals to the disease. A 2017 study identified seven new susceptibility loci, including a single nucleotide polymorphism (SNP) within a

predicted intronic enhancer of *DPF3*, a histone acetylation and methylation reader protein of the BRG1-associated factor (BAF) 180 and polybromo-BAF (PBAF) chromatin remodeling complexes (Scelo et al., 2017). Interestingly, the location of this SNP (14q24) is deleted in one quarter to half of patients (Scelo et al., 2014), and dysregulation of other components of BAF and PBAF complexes are common features of ccRCC. The same group also identified *BHLHE41*, a gene encoding a basic helix-loop-helix protein located in the 12p12.1 susceptibility locus, from GWAS (Bigot et al., 2016). The ccRCC risk allele associated with this gene increased its expression, and the authors provided functional evidence that ectopic expression of *BHLHE41* increased xenograft tumor growth.

An earlier GWAS identified two SNPs associated with RCC susceptibility within a 4.2 kb region of the first intron of *EPAS1* (encoding HIF-2α) as well as another at 11q13.3, which is not localized intergenically but flanks *MYEOV* and *CCND1* (encoding cyclin D1) (Purdue et al., 2011). Additional work demonstrated that the risk SNP at this *CCND1* enhancer promoted HIF-2α binding, thereby increasing the mRNA expression of this oncogenic cell cycle regulator (Schödel et al., 2012). The variants within *EPAS1* are also notable as HIF-2α inhibition has been repeatedly demonstrated to reduce ccRCC growth (Kondo et al., 2003; Kondo et al., 2002; Qiu et al., 2015). However, the functional relationship between intronic *EPAS1* SNPs and its mRNA expression was not determined. A study of familial renal cell carcinoma identified mutations in the *CDKN2B* gene through exon sequencing as predisposing individuals to tumor development (Jafri et al., 2015). *CDKN2B* encodes the $p15^{INK4B}$ protein, which normally functions as a tumor suppressor by binding and inhibiting cyclin-dependent kinases 4 and 6 to prevent cell cycle progression (Roussel, 1999). These mutations, which germline-inactivated *CDKN2B* in 5% of patients, were predicted to destabilize the interaction between $p15^{INK4B}$ and the CDKs. Furthermore, expression of wildtype $p15^{INK4B}$ *in vitro* was shown to suppress colony formation relative to the mutant isoforms, providing support for its ability to act as a tumor suppressor in ccRCC.

Perhaps not unexpectedly, subclonal heterogeneity is a common feature within ccRCC tumors (Gerlinger et al., 2014). Such variation manifests as spatially separated mutational patterns and chromosomal imbalances, which create a range of intratumoral phenotypes. For example, gene expression patterns associated with both good and poor prognoses can be found within the same tumor, and roughly 2/3rd of all somatic mutations are not detectable in every sequenced region (Gerlinger et al., 2012). The degree to which clonal heterogeneity affects disease progression and informs treatment strategies will be an important consideration for both researchers and clinicians moving forward. Nevertheless, additional studies on copy number and single nucleotide variation may help elucidate the etiology of ccRCC, as well as identify new therapeutic targets of interest.

Histone and chromatin modifying enzyme mutations

After mutation of *VHL* (53% of patients), *PBRM1*, *SETD2,* and *BAP1* are the most commonly mutated genes in ccRCC at 40%, 13%, and 10% of patients, respectively (Turajlic et al., 2015). *PBRM1* encodes BAF180, which is the defining subunit of the PBAF switch/sucrose non-fermentable (SWI/SNF) chromatin remodeling complex which uses ATP for nucleosome repositioning (Varela et al., 2011). Varela, *et al.* demonstrated that suppression of *PBRM1* through siRNA resulted in enhanced proliferation, colony formation, and migration of several ccRCC cell lines *in vitro*, consistent with a tumor suppressive function in renal carcinoma (Varela et al., 2011). Interestingly, Gao, *et al.* did not recapitulate these *in vitro* findings, but found that *PBRM1* suppression by CRISPR did promote subcutaneous tumor growth in an on-target fashion (Gao et al., 2017). Inactivating or truncating mutations in *JARID1C* (also known as *KDM5C*), a histone H3 lysine 4 demethylase, and *UTX* (KMD6A) a histone H3 lysine 27 demethylase were identified in another study as positively selected for in ccRCC compared to other cancers (Dalgliesh et al., 2010; Van Haaften et al., 2009). Depletion of SETD2, the histone H3 lysine 36 tri-methyltransferase catalyzing methylation at sites of active transcription, was associated with DNA replication stress and reduced loading of nucleosome components onto chromatin (Kanu et

al., 2015). The authors speculated that *SETD2* loss of function during disease progression could be a source of genomic instability and heterogeneity within ccRCC. *BAP1*, a deubiquitinating enzyme involved in transcriptional repression of genes as a polycomb-group protein, exhibits mutations that are largely mutually exclusive with *PBRM1* (Guo et al., 2012). How hypermethylation of enhancer and promoter CpG regions affects ccRCC progression is an ongoing area of investigation in the field (Shenoy et al., 2015).

1.2.b Genetic mouse models of renal cell carcinoma

Tumor suppressor deletion

As *VHL* deletion is insufficient to drive ccRCC tumorigenesis (Rankin et al., 2006), conditional knockout mice have been generated in several laboratories combining deletion of candidate tumor suppressor genes based on large-scale patient sequencing data (Network, 2013; Sato et al., 2013). A recent report combined *Vhl* and *Pbrm1* deletion throughout renal tubules, collecting ducts, and thick ascending limbs using *Ksp*-Cre (Shao et al., 2002), and found that 67% of these mice first developed polycystic kidney disease (PKD) within 10-14 months of age (Nargund et al., 2017). While deletion of either gene alone did not result in PKD or ccRCC, 50% of the double knockout ($Vhl^{-/-}$, $Pbrm1^{-/-}$) mice showed signs of tumor incidence after 10 months of age, with clear cell morphology, activated mTOR signaling, and reduction in oxidative phosphorylation gene signatures reported. Notably, while the primary tumors were orthotopically transplantable into NSG mice, metastatic tumor burden was not detected in $Vhl^{-/-}$, $Pbrm1^{-/-}$ mice.

Though *TP53* deletion or mutation is relatively uncommon in human ccRCC tumors, another study examined the effect of conditional *Vhl*, *Trp53*, and *Rb1* loss in the renal epithelium (utilizing *Ksp*-Cre), as changes in regulators of the p53 pathway and the G1/S cell cycle transition are frequently copy number modified according to The Cancer Genome Atlas (TCGA) data (Harlander et al., 2017). The authors found evidence of tumor onset as early as 7.5 months following triple knockout in a subset of mice, which were characterized by HIF-α and mTORC1 pathway activation by carbonic anhydrase 9 and phospho-4E-BP1 immunostaining, respectively.

Further analyses of a larger cohort suggested 82% of *Vhl*$^{-/-}$, *Trp53*$^{-/-}$, *Rb1*$^{-/-}$ mice developed tumors within 15 months of gene deletion, the majority of which were classified as grade 3 or 4 tumors growing in acinar or pseudo-papillary patterns. These renal tumors had clear or weakly stained cytoplasm, and displayed gene expression and mutational signatures similar to human ccRCC. While some *Vhl*$^{-/-}$, *Trp53*$^{-/-}$, *Rb1*$^{-/-}$ tumors were sensitive to 1st and 2nd line chemotherapies sunitinib and everolimus, nearly all were resistant to 3rd line treatment with acriflavine, the pan-HIF-α inhibitor (Lee et al., 2009). These results mimic the variability in drug responsiveness typical of the human disease. Similar to *Vhl* and *Pbrm1* co-deletion, *Vhl*$^{-/-}$, *Trp53*$^{-/-}$, *Rb1*$^{-/-}$ mice developed tumors which remained localized within the kidney.

Consistent with chromosome 3p genes displaying tumor suppressive functions in ccRCC, the effect of *Bap1* deletion in combination with either *Vhl* or *Pbrm1* loss has been examined in several publications from the Brugarolas group. Under the control of *Six2*-Cre driver, which is expressed in multipotent nephron progenitor cells of the kidney during development, the authors first generated *Vhl*$^{-/-}$, *Bap*$^{+/-}$ mice (deletion of both alleles of *Vhl* and one of *Bap1*) (Wang et al., 2014). These mice developed kidneys with atypical cysts and neoplasia resembling those of patients with VHL syndrome. Some of the lesions observed were similar to early-stage ccRCC tumors by cytoplasmic clearing, Ki67 expression, and phospho-S6 positivity as a marker of mTOR activity, yet tumors remained small overall. Again, tumors from this mouse model did not metastasize, and *Vhl*$^{-/-}$, *Bap1*$^{+/-}$ mice died after 8 months from renal failure, suggesting that additional events are required for ccRCC progression.

A more recent study from this group used additional Cre drivers to modulate *Pbrm1* and *Bap1* levels in different lineages within the kidney. *Pax8*-Cre was used to delete *Vhl* and *Bap1* or *Pbrm1* within the proximal and distal renal tubules, loops of Henle, collecting ducts, and parietal cells of the Bowman capsule (Gu et al., 2017). *Sglt2*- and *Villin*-Cre were also used for more specific deletion within proximal tubule epithelial cells. Tumors generated with *Pax8*-Cre were larger than those generated with the *Six2*-Cre model investigated previously. Interestingly, deletion of both alleles of *Vhl* along with a single allele of either *Pbrm1* or *Bap1* using *Sglt2*- and

Villin-Cre drivers did not result in ccRCC formation. Based on these data, the authors speculated that ccRCC may be derived from the parietal epithelial cells of the Bowman capsule, rather than proximal tubule cells, as previous histologic and gene expression data would suggest (Chen et al., 2016a; Yoshida et al., 1986). The authors also found that activation of mTORC1 signaling through inactivation of one allele of *Tsc2* caused the formation of higher grade ccRCC specifically in *Pbrm1*-deficient kidneys. Notably, patients with *PBRM1* and *BAP1* mutations have distinct gene expression patterns and clinical outcomes, and these alterations are largely mutually exclusive (Kapur et al., 2013). While *BAP1*-deficient tumors are higher in grade and portend worse prognosis than *PBRM1*-deficient tumors, it is believed that *BAP1* mutations are secondary to *PBRM1* loss in the pathogenesis of ccRCC (Hakimi et al., 2013a; Peña-Llopis et al., 2012).

Oncogene activation

An early mouse model of ccRCC was generated using a constitutively active mutant of HIF-1α, termed TRACK (transgenic model of cancer of the kidney) (Fu et al., 2011). HIF-1α protein is found in *VHL*-deficient renal epithelial cells and in early tubular lesions, cysts, and ccRCC, suggesting it is important for carcinogenesis (Rankin et al., 2006). TRACK mice expressed a triple-mutant HIF-1α, which was insensitive to hydroxylation and therefore degradation by the PHD/pVHL system, under the control of the γ-glutamyl transferase (*GGT*) proximal tubule-specific promoter. Phenotypes included abnormal vascularization, renal cysts, cleared cells, and high carbonic anhydrase 9 staining. A small percentage of cleared cells accumulated γH2AX, a marker of DNA double-strand breaks, although the mechanism by which HIF-1α led to genomic instability was not described. Even though HIF-1α exerts tumor suppressive functions in established ccRCC, this study demonstrates it is a critical downstream mediator of *VHL* loss early in disease progression. Accordingly, neither late-stage nor metastatic disease was detected in TRACK mice.

Another two studies investigated the role of MYC overexpression in the kidney and its role in promoting renal tumorigenesis. According to TCGA data, genomic amplification of *MYC*

only occurs in about 5-10% of patients, however, the MYC/MAX transcriptional network has been predicted to promote glycolysis, de-differentiation, and growth in a majority of ccRCC (Tang et al., 2009). MYC pathway activation is also associated with a hereditary RCC characterized by translocation of chromosomes 3 and 8 (Drabkin et al., 1985). Conditional overexpression of *MYC*, but not *KRAS*, under the *GGT* gene promoter gave rise to a highly aggressive RCC that most resembled collecting-duct carcinoma (Shroff et al., 2015). Combined gene expression and metabolite analysis, along with small molecule inhibition of glutaminase, revealed a dependency on glutamine for sustained growth of these tumors, similar to the human disease.

In another report, the combination of MYC overexpression along with further deletion of *Vhl* and/or *Cdkn2a* (encoding Ink4/Arf) was investigated for the ability to induce papillary or clear cell renal cell carcinoma (Bailey et al., 2017). This study utilized the *Ksp* promoter to drive expression of a doxycycline-inducible Myc transgene. When MYC was overexpressed without deletion of either *Vhl* or *Cdkn2a*, the mice developed tumors histologically consistent with papillary RCC. However, *Vhl* deletion in combination with MYC overexpression ("VM") mice generated tumors more similar to ccRCC based on cytoplasmic clearing, necrosis, and hemorrhage. Addition of *Cdkn2a* deletion to this model ("VIM") further potentiated ccRCC formation compared with *Vhl* deletion alone, increasing tumor volume and decreasing median survival time. VIM mice had a median survival of 29.5 weeks following gene inactivation/induction, whereas, VM mice had a median survival of 57 weeks. Importantly, 2 out of 6 VIM mice developed metastasis to the liver, and *in vitro* characterization of a cell line derived from this mouse model showed increased expression of epithelial-mesenchymal transition genes as well as increased matrigel invasion relative to a VM line.

ccRCC research is currently limited by the lack of a GEMM that accurately represents the complete spectrum of phenotypes characteristic of human disease. As evidenced by the publications described above, the various methods used to either delete tumor suppressors and/or express oncogenes in distinct kidney lineages result in different propensities for ccRCC development. Furthermore, the long latency of tumor formation in GEMMs currently available, as

well as lack of metastatic spread typical of human ccRCC, poses challenges for researchers studying the molecular mechanisms governing these events. In the meantime, identification of subpopulations of established patient-derived cell lines having metastatic capacity (Vanharanta et al., 2013) and incorporation of patient-derived xenografts will allow the field to investigate these phenomena in greater detail. Additional GEMMs mimicking the initiation and progression of ccRCC will ultimately be beneficial for the pre-clinical study of targeted therapy. A deeper understanding of the genetic, epigenetic, and metabolic changes that synergize with *VHL* loss to generate ccRCC, and the order in which they occur, will ultimately facilitate the development of such tools.

1.2.c Metabolic reprogramming in ccRCC

Glucose utilization

Aerobic glycolysis, commonly known as the "Warburg effect," is a hallmark of many cancers regardless of cell-of-origin (Pavlova and Thompson, 2016), and this phenomenon is amplified in *VHL*-deficient ccRCC due to HIF activation. A primary consequence of constitutive HIF activation is decreased pyruvate entry into the TCA cycle and increased glycolytic flux towards lactate due to the actions of pyruvate dehydrogenase kinase 1 (PDK1) and lactate dehydrogenase (LDHA), respectively (Wettersten et al., 2017). It is believed that enhanced glycolysis benefits tumors through several mechanisms, one being the generation of building blocks for nucleotides, proteins, and lipids through pathways branching from glycolytic intermediates (Ward and Thompson, 2012). The pentose phosphate pathway, beginning with glucose-6-phosphate and generating NADPH and ribose 5-phosphate, is important for lipid and nucleotide production. Additionally, NADPH produced from these reactions can be used to reduce oxidized glutathione, helping to maintain antioxidant capacity in rapidly proliferating cells. The hexosamine pathway, beginning with fructose 6-phosphate, is important for the generation of precursors used in *N*-glycosylation of proteins. These modifications are important for the proper folding of growth factor and nutrient receptors, which feeds back to regulate cellular metabolism

more broadly (Wellen and Thompson, 2012). Although an inefficient means of ATP generation relative to oxidative phosphorylation, aerobic glycolysis in cancer cells occurs at a rate much higher than in non-proliferative cells (Liberti and Locasale, 2016). An equivalent rate of ATP synthesis along with the additional generation of anabolic precursors and reducing equivalents is a proposed explanation for why tumors rewire metabolism to promote the Warburg effect.

In addition to their canonical, catalytic functions, several reports demonstrate that certain glucose metabolic enzymes exhibit dual functions through physical association with HIFs (Luo et al., 2011), (Xie and Simon, 2017). The HIF-1α target gene pyruvate kinase (*PKM*) encodes isoforms PKM1 and PKM2, of which PKM2 is a key regulator of glycolytic flux. The Semenza group showed that in addition to its catalytic function, PKM2 can bind to HIF-1α as a co-activator and enhance p300 recruitment and localization to hypoxia response elements (Luo et al., 2011). Additionally, our group demonstrated that the gene encoding the gluconeogenic enzyme fructose-1,6-bisphosphatase 1, FBP1, is uniformly silenced or deleted in ccRCC patients (Li et al., 2014). Loss of FBP1 promotes ccRCC progression by two distinct mechanisms; first, by promoting glycolytic flux in renal epithelial cells, and secondly, by dissociation with the HIF-α inhibitory domain, facilitating constitutive HIF activity at the chromatin-level. Further research exploring the relationship between HIFs and their cell type-specific transcriptional targets will provide insight into the complex regulation of metabolism in ccRCC.

PI3K-Akt-mTOR pathway

The phosphoinositide 3-kinase (PI3K) signaling pathway is activated by copy number variation or mutation of its positive effectors *PIK3CA*, *MTOR*, and negative regulators *PTEN* and *TSC1/2* in 28% of patients in ccRCC (Network, 2013; Turajlic et al., 2015). PI3K activation activates Akt, also known as protein kinase B, by phosphorylation at the cell surface. One of the major downstream targets of activated Akt is mTORC1, which increases anabolic pathways such as protein, lipid, and nucleotide synthesis (Dibble and Manning, 2013). Inactivation of the negative regulators of mTORC1, TSC1 and TSC2, has been associated with increased risk of

ccRCC development, which presents at an earlier age than sporadic disease (Bjornsson et al., 1996). Collectively, these effects render the pathway constitutively active even in the absence of growth factors. The effects of altered glucose and amino acid metabolism on ccRCC pathogenesis was comprehensively reviewed in 2017 (Wettersten et al., 2017), as such, we will focus on reprogrammed lipid metabolism in the remainder of this section.

Lipid metabolism

As renal proximal tubule epithelial cells (RPTEC) transition into ccRCC, they undergo dramatic rewiring of various metabolic pathways including lipid utilization, synthesis, and storage (**Figure 1.2**). Healthy RPTEC are characterized by high rates of beta-oxidation to fuel their primary role in ion exchange and secretion (Kang et al., 2015). Beta-oxidation is the process by which lipids are broken down into acetyl-CoA, generating the reducing equivalents NADH and $FADH_2$ to produce ATP through oxidative phosphorylation. Compared to RPTEC, ccRCC have reduced mitochondrial content and defective mitochondrial structure and activity (Meierhofer et al., 2004), (Nilsson et al., 2015). At the gene expression level, transcriptional regulators of mitochondrial homeostasis and oxidative phosphorylation are uniformly suppressed in ccRCC relative to adjacent healthy kidney tissue (Tun et al., 2010). These adaptations are largely due to constitutive HIF signaling, although additional factors regulating these pathways remain to be explored. One study examined the relationship between HIF-α and PGC-1α, a peroxisome proliferator-activated receptor gamma (PPARγ) transcriptional co-activator involved in the process of mitochondrial biogenesis and respiration (Puigserver et al., 1998). *VHL*-deficient ccRCC cells exhibit elevated levels of Dec1, a transcriptional repressor and HIF-α target gene, which blocks expression of PGC-1α (LaGory et al., 2015). Ectopic expression of PGC-1α increased oxidative stress and slowed tumor growth in a subcutaneous xenograft model. Furthermore, lower levels of *PPARGC1A* (PGC-1α) mRNA were correlated with worse patient survival, and total mitochondrial content was correlated inversely with tumor grade (Simonnet et al., 2002), consistent with its role as a tumor suppressor in ccRCC.

Transcriptional repression of carnitine palmitoyltransferase (*CPT1A*), the rate limiting enzyme involved in fatty acid transport into the mitochondria for beta-oxidation, also occurs in ccRCC via a HIF-α dependent mechanism (Du et al., 2017). A recent report found that pVHL reconstitution in several ccRCC cell lines reduced lipid droplet (LD) accumulation in a CPT1A dependent manner (i.e., knockdown of *CPT1A* in pVHL-reconstituted cells partially increased lipid accumulation). Interestingly, pVHL status had no effect on lipid uptake rates, as measured through the uptake of BODIPY, an unsaturated, fluorescently labeled fatty acid molecule. Ectopic expression of CPT1A increased oxygen consumption rate, decreased LD abundance, and decreased xenograft tumor growth. Clinically, CPT1A levels and activity are reduced in ccRCC compared with healthy kidney tissue, and patients with reduced *CPT1A* expression have worse prognosis.

Concomitant with decreased beta-oxidation in ccRCC tumors is increased lipid synthesis and storage. Fatty acid synthesis occurs when cytosolic citrate is cleaved by the enzyme ATP citrate lyase, or ACLY, to produce acetyl-CoA. Carboxylation of acetyl-CoA to malonyl-CoA by acetyl-CoA carboxylase (ACC) generates the building blocks for long-chain fatty acid formation which can go on to be desaturated and further modified to produce more complex lipid species. Two key enzymes in this process are fatty acid synthase (FASN), which produces palmitic acid (C16:0), and stearoyl-CoA desaturase 1 (SCD1), which primarily produces oleic acid (C18:1) from the desaturation of stearic acid. In ccRCC, metabolism of glutamine-derived α-ketoglutarate to citrate by reductive carboxylation fuels lipid synthesis rather than glucose-derived citrate generated by oxidation (Gameiro et al., 2013; Metallo et al., 2012). In addition to increasing anabolic lipid metabolism for the production of membranes needed during rapid cell proliferation, new evidence suggests additional roles for *de novo* lipogenesis (DNL) and lipid uptake in carcinogenesis. FASN levels correlate positively with tumor aggressiveness and poor survival in ccRCC (Hakimi et al., 2016; Horiguchi et al., 2008), and genetic and pharmacologic inhibition of SCD1 induces apoptosis in ccRCC cell lines both *in vitro* and *in vivo* (Von Roemeling et al., 2013). Treatment with ACC inhibitor reduces total phospholipid and triglyceride content, as

predicted, and also increases sensitivity to oxidative stress-induced cell death (Rysman et al., 2010). Other work has demonstrated that lipid uptake protects against endoplasmic reticulum (ER) stress in ccRCC and other cancers, particularly under hypoxia when cells cannot desaturate fatty acids due to the inactivation of SCD1 (Kamphorst et al., 2013; Young et al., 2013).

The protective effect of LD accumulation in cancer cells is incompletely understood, although recent studies suggest several mechanisms by which LDs can enhance tumorigenesis and cell viability. LDs consist of a core of neutral lipids including triglyceride and cholesterol esters surrounded by a monolayer of membrane from the endoplasmic reticulum and coat proteins including the perilipin family (Walther and Farese Jr, 2012). Inhibition of the LD coat protein perilipin 2 in ccRCC, a highly-expressed HIF-2α target gene, reduced neutral lipid accumulation, tumor growth, and increased ER stress both *in vitro* and *in vivo* (Qiu et al., 2015). In glioblastoma and breast cancer, it was recently demonstrated that lipid accumulation following hypoxia-reoxygenation protects cells from reactive oxygen species (ROS)-induced cytotoxicity (Bensaad et al., 2014). In another hypoxic microenvironment, the *Drosophila* neural stem cell niche, LDs that form during oxidative stress reduce ROS levels and inhibit the oxidation of polyunsaturated fatty acids (PUFA) (Bailey et al., 2015). When PUFA are stored in LDs rather than in membranes, they are less vulnerable to peroxidation, which inhibits proliferation through damaging macromolecules. In theory, these responses are even more critical to maintain in ccRCC, where lipid accumulation is a defining molecular and morphological hallmark of disease. Taken together, these results suggest pathways involving anabolic lipid metabolism could one day be targeted for therapeutic benefit in ccRCC.

In a recently published lipidomic analysis of 49 patients (Saito et al., 2016), elevated levels of ether-type phospholipids, cholesterol esters, and triacylglycerols were reported in ccRCC, consistent with previously published metabolomic analyses (Gebhard et al., 1987; Hoffmann et al., 2005; Yoshimura et al., 2012). These metabolic changes were also correlated with gene expression levels of lipogenic genes. While it is clear that suppression of either HIF-1α or HIF-2α markedly reduces LD formation in ccRCC (Du et al., 2017; Qiu et al., 2015; Sundelin et al., 2012),

the target genes and mechanisms responsible for the clear cell phenotype have not been completely defined. Additionally, the role of other lipogenic transcription factors such as sterol regulatory element-binding protein 1 or 2 (SREBP1/2) and carbohydrate-responsive element-binding protein (ChREBP) remain to be fully elucidated in ccRCC.

1.2.d Therapeutic strategies for ccRCC

Anti-angiogenics and mTOR inhibitors

Anti-angiogenic therapy targeting receptor tyrosine kinases (RTKs) such as vascular endothelial growth factor receptor (sunitinib, sorafenib, etc) or VEGF ligand by monoclonal antibody (bevacizumab) has traditionally been a first-line standard-of-care for ccRCC patients (Ricketts et al., 2016) (a graphical representation of the therapies reviewed in this section is presented in **Figure 1.3**). Although these agents are being investigated for several malignancies including colorectal and lung cancers, anti-angiogenics are theoretically well-suited for the treatment of ccRCC due to constitutive HIF activity and exceedingly high VEGF accumulation. However, clinical trials indicate that at least as single-therapy, anti-angiogenic drugs are only modestly effective for the treatment of metastatic ccRCC. In a randomized, double-blind trial of bevacizumab, the probability of being progression-free after eight months was significantly extended by 30% (high-dose), 14% (low-dose), and 5% (placebo) (Yang et al., 2003). However, there was no significant difference in overall survival between placebo, low, or high-dose bevacizumab. A phase III study of sunitinib in patients with high risk of tumor recurrence after nephrectomy revealed that 64.9% of patients were disease-free at three years after adjuvant treatment with sunitinib compared with 59.5% in the placebo group (Ravaud et al., 2016). At five years, the proportions fell to 59.3% (sunitinib) and 51.3% (placebo). Side effects from sunitinib treatment included diarrhea, hypertension, fatigue, and nausea.

Rapamycin analogs, or rapalogs (everolimus, temsirolimus), are used for the treatment of advanced ccRCC after patients have been treated with a RTK inhibitor. A phase III study in patients whose disease progressed after receiving either RTK- or VEGF-targeted therapy found

that everolimus was effective in prolonging progression-free survival compared with placebo control (Motzer et al., 2008). Side effects from everolimus included hyperglycemia, hyperlipidemia, and hypercholesterolemia due to effects on mTOR-regulated glucose and lipid metabolism, as well as diarrhea and rash. Yet overall, the risk of severe effects was low and no detrimental effects on health-related quality-of-life was observed in everolimus treated individuals compared with placebo. The clinical trials reported above led to FDA approval for angiogenesis and mTOR inhibitors nearly a decade ago, and current investigation has now shifted toward targeted therapy of HIF-2α as well as immune checkpoint blocade.

Targeting HIF-2α

HIF-2α is the primary oncogenic driver of ccRCC progression downstream of *VHL* loss. Pre-clinical work from several labs has examined the efficacy of a HIF-2α inhibitors utilizing a panel of ccRCC cell lines in orthotopic xenograft assays as well as patient-derived xenografts grown subcutaneously (Chen et al., 2016b; Cho et al., 2016; Wallace et al., 2016). PT2399 blocks the interaction between HIF-2α and HIF-1β/ARNT by binding to a pocket within the PAS-B domain of HIF-2α, thereby eliminating DNA binding. Importantly, PT2399 reduces HIF-2α target gene expression without affecting HIF-1α targets (Cho et al., 2016). When tested alongside sunitinib, PT2399 decreased tumorgraft growth by 60% across all samples tested compared with 40% for sunitinib treatment, without causing a reduction in body weight as seen with the latter drug (Chen et al., 2016b). Resistance mechanisms were observed in tumors initially sensitive to PT2399, which were characterized by increased tumor vascularity and VEGF production despite dissociation between HIF-2α and ARNT. However, they took nearly double the amount of time to develop as tumors treated with sunitinib. Based on these results, a derivative of PT2399, PT2385, is currently being tested in clinical trials for ccRCC (Medicine, 2018).

Targeting glutaminase

Since being reviewed by Wettersten, *et al.*, two phase II clinical trials have been initiated to examine the effect of CB-839, a small molecule inhibitor of glutaminase, along with either cabozantinib, everolimus, or placebo, on patients with advanced or metastatic RCC (Tannir et al., 2018). Additionally, a pre-clinical report on the role of glutamine addiction in ccRCC further supports the possibility of therapeutically targeting this axis in kidney cancer (Aboud et al., 2017). Aboud, *et al.* demonstrate that ccRCC tumors grown orthotopically show increased uptake of ^{18}F-(2*S*,4*R*)4-fluoroglutamine relative to adjacent healthy kidney tissue and are sensitive to glutaminase inhibition by CB-839. These results suggest that PET imaging could be useful to identify ccRCC patients likely to respond to glutaminase inhibition clinically.

Immunotherapy

Immune checkpoint blockade represents a promising strategy for the treatment of many cancer subtypes including ccRCC. Such therapies remove the “brakes” from a patient’s immune system, allowing T-cells to recognize and destroy cancer cells. While ccRCC does not harbor as many somatic mutations per megabase as melanoma or non-small cell lung cancer, which creates a higher neo-antigen load and is thought to predict response to immunotherapy, positive immune responses can be achieved in a subset of patients (De Velasco et al., 2016; Schumacher and Schreiber, 2015). One method of achieving this effect is to antagonize programmed cell death-1 receptor (PD-1), which is found on activated T-cells and interacts with PD-L1 or PD-L2 on tumor cells. This interaction normally allows tumor cells to evade the immune response, but when inhibited restores antitumor immunity (Parikh and Lara, 2017). Clinical work comparing nivolumab, a monoclonal antibody targeting PD-1, to everolimus, found that nivolumab extended median survival to 25 months compared with 19.6 months for everolimus treatment in patients with advanced ccRCC (Motzer et al., 2015). However, durable effects were only seen in 20-25% of patients (De Velasco et al., 2016). Current investigations across cancer subtypes are geared toward defining mechanisms that underlie positive and lasting responses to immune checkpoint blockade. A recent study identified signatures of response to checkpoint therapies in ccRCC

(Miao et al., 2018). Through whole exome sequencing of 35 tumors of patients with metastatic ccRCC, it was determined that biallelic *PBRM1* loss was associated with significantly longer overall survival than patients with *PBRM1* intact. It was hypothesized that *PBRM1* loss-of-function and subsequent alterations in SWI/SNF signaling networks may underlie this effect. It is the hope that through these analyses, specific patient populations can be identified which would respond best to immunotherapy based on the genetic and mutational landscape of their tumors.

1.3 Introduction to bladder urothelial carcinoma (UC)

Bladder urothelial carcinoma (UC) is the 4th most prevalent form of cancer diagnosed in men in the United States, and is most commonly detected in patients over the age of 65. While men have a 3 to 4-fold higher risk of bladder cancer incidence compared to women, women typically are diagnosed at later stages and have a poorer prognosis (Berdik, 2017). The majority of bladder cancers are derived from an epithelial layer known as the urothelium, or transitional epithelium, which comprises the innermost lining of the bladder, ureters, and renal pelvis. Bladder cancers arising from non-urothelial layers (i.e., sarcomas, squamous and small-cell carcinomas, and adenocarcinomas) only account for 10% of all cases (Sanli et al., 2017).

Top risk factors for UC include smoking (linked with 65% of cases in men and 30% in women) and occupational exposure to carcinogens such as paint, rubber, petroleum products, and dyes (Berdik, 2017), although occupational carcinogen exposure only accounts for 8% of total cases worldwide (Purdue et al., 2015). Genetic background likely plays a large role in disease susceptibility, although predispositions to UC development have been less studied until recently. One study found that women with a history of smoking and either null mutations in the *N*-acetyltransferase carcinogen-detoxification gene *GSTM1* or polymorphisms in *NAT2* (resulting in “slow-acetylator” phenotype) are at increased risk of developing UC compared to smoking women with wildtype gene function (García-Closas et al., 2005). Genome wide association studies have implicated polymorphisms in the urea transporter gene *SLC14A1* to UC development, which modulates concentrations of carcinogens in the urine (Rafnar et al., 2011),

as well as variants near 8q24.21. These polymorphisms map to a region near *MYC* which have also been identified in GWAS of colorectal, breast, and pancreatic cancers (Rothman et al., 2010).

Clinical stratification, disease subtypes and biomarkers

Clinically, UC is stratified into two types of disease: non-muscle-invasive bladder cancer (NIMBC) and muscle-invasive bladder cancer (MIBC). NIMBC is the most frequently diagnosed form of UC, accounting for 75% of cases each year in the United States. NIMBC represents Stage 0 (T0) papillary tumors as well as Stage I carcinoma *in situ* (CIS), which is more aggressive and likely to spread. Twenty-five percent of patients are initially diagnosed with MIBC, tumors which have invaded through the lamina propria and into the outer muscle and fat layers of the bladder (Stage II-IV) (Choi et al., 2014b). The most frequent sites of UC metastasis include lymph nodes (69% of patients), bone (47% of patients), and lung (37% of patients) (Shinagare et al., 2011).

Over the past three decades, the percentage of patients surviving 5 years after diagnosis has been unchanged, compared to improvements seen in prostate, kidney, and breast cancer survival rates (Berdik, 2017). This is largely due to limited targeted therapeutic options and a standard of care regimen which has been constant during the same time period (discussed below). In order to identify common transcriptional signatures that may provide insight into rational therapeutic options, three different groups have independently classified MIBC tumors into subcategories based on RNA-sequencing. Specific demarcations are as follows: University of North Carolina (UNC): basal and luminal (Damrauer et al., 2014). MD Anderson Cancer Center (MDA): Basal, p53-like, luminal (Choi et al., 2014b). TCGA: Clusters I and II (enriched with breast cancer luminal markers), Clusters III and IV (enriched with breast cancer basal markers) (Network, 2014). Basal tumors are characterized by squamous histology and are generally more aggressive, yet also highly sensitive to cisplatin-based combinatorial chemotherapy. Luminal

tumors are characterized by papillary histology and are slower growing, but also more chemo-resistant (Choi et al., 2014b).

Major biomarkers of the luminal subtype of UC include PPARγ, estrogen receptor 1 (ESR1), receptor tyrosine kinase ERBB2 (also known as HER2/neu), and fibroblast growth factor receptor 3 (FGFR3). The differentiation status of luminal MIBC tumors can also be assessed by the presence of uroplakins, proteins which form plaques on the apical surface of the urothelium to act as a permeability barrier (Wu et al., 2009). Biomarkers of the basal subtype include TP63 (p63), STAT3, HIF-1α, and epidermal growth factor receptor (EGFR) (Damrauer et al., 2014). Keratin proteins (KRT5, KRT6, and KRT14) are enriched in basal MIBCs as well as a lethal squamous cell carcinoma subtype, and are important for the invasive properties of these cancers (Sjödahl et al., 2012).

Mouse models of UC

As there is no uniform molecular driver of UC pathogenesis as in other urinary system cancers (i.e., ccRCC, loss of the tumor suppressor gene *VHL*), generation of MIBC in mice requires the deletion of multiple tumor suppressor genes such as *Trp53*, *Rb1*, or *Pten* in the urothelium. A commonly used model for the generation of UC in mice is *Upk2*-Cre, where the uroplakin 2 gene promoter drives the expression of Cre-recombinase in urothelial cells (de la Peña et al., 2011). Notably, *Upk2*-mediated expression of a dominant-negative p53 mutant alone in the urothelium is insufficient to generate UC, as these mice do not develop urothelial hyperplasia until at least 10 months of age (Gao et al., 2004). This result is surprising given that nearly 50% of MIBC harbor inactivating mutations in *TP53* (Hurst et al., 2018). In the combinatorial models, CIS lesions develop first, followed by high-grade MIBC with features common to human disease including *ERBB2* and PI3K pathway upregulation (Gao et al., 2004; Puzio-Kuter et al., 2009; Zhang et al., 1999).

Carcinogen-induced UC typically involves oral administration of N-butyl-N-(4-hydroxybutyl) nitrosamine (BBN) in rodents, which also generates tumors with morphological

features reminiscent of human UC (FUKUSHIMA et al., 1976; Grubbs et al., 1977). However, latency and incomplete incidence of tumors are two limitations of this model. For example, administration of 150 mg BBN by oral gavage twice weekly for 8 weeks will result in UC in 48% of rats, detectable 10 months after administration (Lubet et al., 2008). In C57BL/6 mice, continuous dosage of 35 mg/kg/day BBN in the drinking water results in UC after 190 days and males and 253 days in females, with metastatic spread detectable in 13 out of 100 mice. Interestingly, this sex difference in tumor onset can be abolished either through castration of males or treating females with testosterone (Bertram and Craig, 1972). While the BBN model may be more comparable to environmental carcinogen exposure affecting human disease, the latency of tumor initiation and low incidence of metastasis are important considerations to performing pre-clinical studies using this reagent.

1.3.a Therapeutic strategies for UC

NIMBC is treated by a procedure called transurethral resection of bladder tumor (TURBT), which can also be followed by adjuvant intravesical therapies. The most common intravesical therapy is the delivery of a substrain of *Mycobacterium bovis* named Bacillus Calmette-Guerin (BCG), which is related to tuberculosis and used to stimulate an immune reaction within the bladder (Brandau and Suttmann, 2007). Alternatively, chemotherapy such as mitomycin, gemcitabine, or valrubicin can be delivered directly to the bladder via a catheter, yet BCG immunotherapy is superior to intravesical chemotherapy in preventing bladder cancer recurrence (Böhle et al., 2003).

Treatment of MIBC or recurrent NIMBC is much more invasive, typically involving radical cystectomy. This “gold-standard” intervention not only includes removal of the entire bladder, but other reproductive organs such as the prostate and seminal vesicles for men and the uterus, ovaries, and part of the vagina for women (Sanli et al., 2017). Radical cystectomy is followed by construction of a “neobladder” using a portion of the intestines, or the creation of a urostomy to divert urine to an external bag. The 10-year recurrence-free survival following radical cystectomy

is 86% for T0 tumors and 76% for T1-T3, but drops to 34% when disease has metastasized to lymph nodes (Stein et al., 2001). While intravenous delivery of neoadjuvant chemotherapy (prior to cystectomy) has only been associated with small increases in disease-free survival at 5 years (~5%), adjuvant chemotherapy cocktails including methotrexate, vinblastine, adriamycin, cisplatin (MVAC) or gemcitabine with cisplatin produces a pathological complete response in 30-40% of patients (Sternberg et al., 2013). In the coming decades, the combination of immunotherapy and/or possible targeted therapies based on "druggable" biomarkers associated with basal or luminal subcategories of MIBC will hopefully reduce the need for invasive surgical procedures and improve UC survival.

1.4 Main hypothesis and objectives

The focus of my thesis research has been elucidating the role of PPARγ in ccRCC and UC. Since PPARγ is expressed in a subset of both ccRCC and UC tumors at levels higher than their adjacent epithelium/cell-of-origin (Collet et al., 2011; Network, 2014), our general hypothesis was that PPARγ has pro-oncogenic functions in both tumor types. The questions that have guided these investigations have been: 1) How does PPARγ-RXR genomic occupancy differ between lineages? 2) Does PPARγ primarily regulate genes involved in lipid and glucose metabolism in these cancer subtypes, or are there unique targets that contribute to the cell-type specific functions of this nuclear receptor? 3) Does inhibiting PPARγ activity, either pharmacologically or genetically, affect tumor growth of ccRCC and UC? If so, what are the molecular mechanisms responsible for this dependency? To answer these questions, I used multiple human cell lines derived from each tumor type in various *in vitro* and *in vivo* assays of tumor progression. I also employed genome-wide techniques including ChIP-seq and RNA-seq to investigate PPARγ-RXR genomic occupancy and its effects on gene expression in these cancer models. In Chapters 2 and 3, I explore these questions in ccRCC and UC, respectively. In Chapter 4, I summarize the findings of my thesis research and address several remaining questions related to this work.

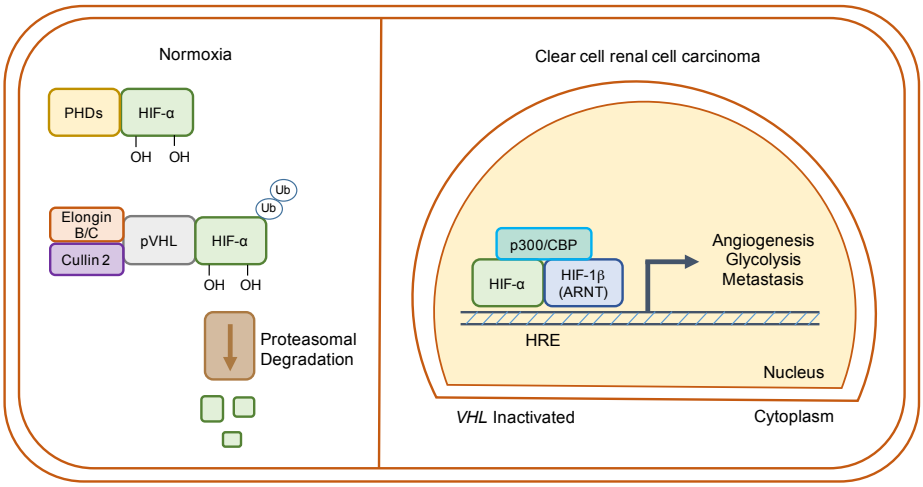

Figure 1.1: Regulation of hypoxia-inducible factor (HIF) signaling by the von Hippel-Lindau (VHL) tumor suppressor
Under oxygen-replete conditions, HIF-α subunits are hydroxylated by prolyl hydroxylases (PHDs) and then ubiquitinated by an E3-ubiquitin ligase complex containing pVHL, tagging them for proteasomal degradation. In hypoxia, or when *VHL* is inactivated (such as in ccRCC), HIF-α subunits escape degradation, translocate to the nucleus, and heterodimerize with HIF-1β (ARNT). HIFs generally promote a transcriptional program favoring increased angiogenesis, glycolysis, and metastatic capabilities of ccRCC tumors. HRE = hypoxia response element.

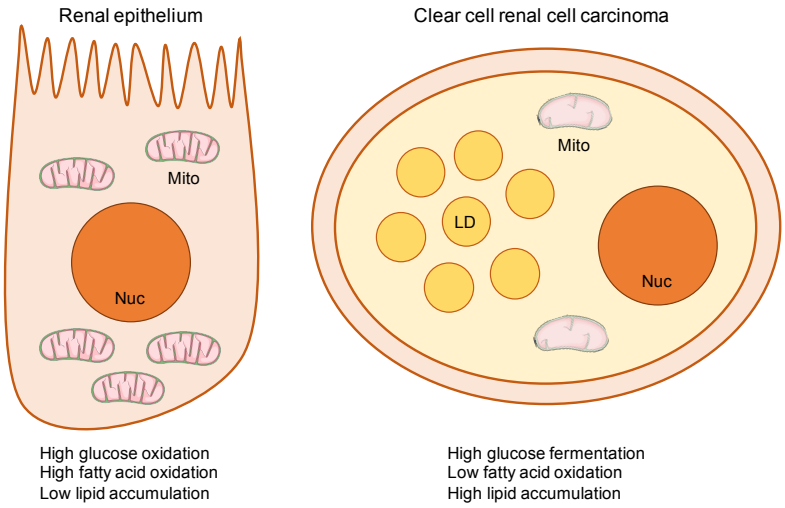

Figure 1.2: Comparison of the metabolic state of renal epithelium and clear cell renal cell carcinoma (ccRCC)
Renal epithelial cells (of the proximal tubule, a proposed cell-of-origin of ccRCC) are characterized by high levels of glucose and fatty acid oxidation to serve their energetic needs. As these cells transition into ccRCC, they begin to store triglyceride and cholesterol ester in cytoplasmic lipid droplets. Furthermore, ccRCC have low levels of fatty acid oxidation and compromised mitochondrial architecture relative to healthy renal epithelium. Nuc = nucleus. Mito = mitochondria. LD = lipid droplet.

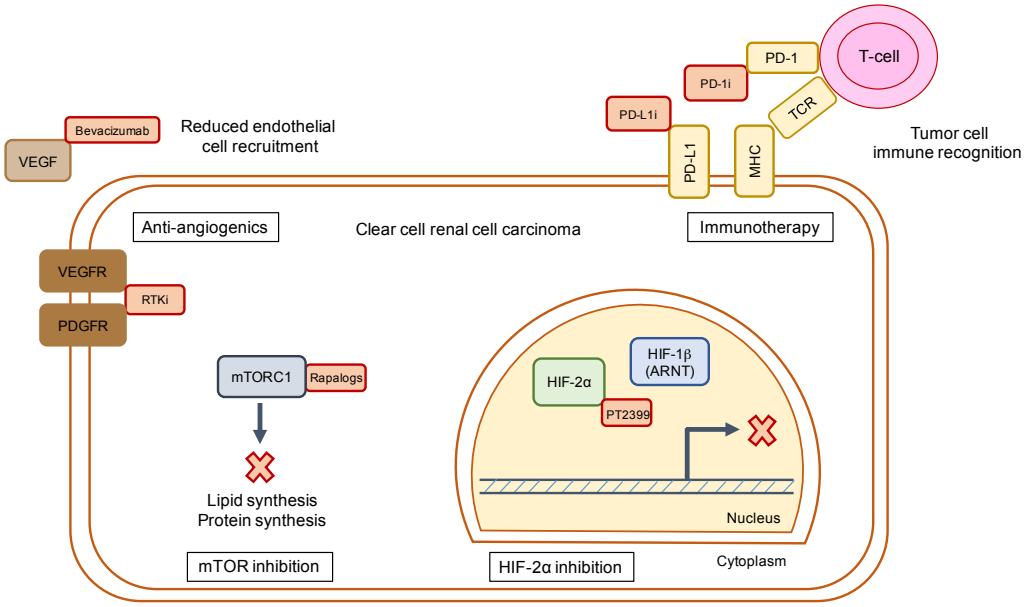

Figure 1.3: Select pharmacological approaches for the treatment of metastatic ccRCC
Current and future therapeutic strategies for ccRCC include inhibition (denoted by red boxes) of mTOR signaling, angiogenesis, HIF-2α signaling, and immune checkpoint blockade. RTKi = receptor tyrosine kinase inhibitors. Rapalogs = rapamycin analogs. PD-1i = PD-1 inhibitor. PD-L1i = PD-L1 inhibitor.

Chapter 2: PPARγ is dispensable for clear cell renal cell carcinoma progression

This chapter has been adapted with modifications from: Sanchez, DJ, Steger, DJ, Skuli, N, Bansal, A, Simon, MC. PPARγ is dispensable for clear cell renal cell carcinoma progression. *Mol Metab*. 2018 Aug;14:139-149. doi: 10.1016/j.molmet.2018.05.013.

Acknowledgments: We thank John Tobias for bioinformatics assistance, Raymond Soccio for guidance with ChIP experiments, and Jeff Ishibashi for technical assistance. We also thank Karin Eisinger and Mitch Lazar for their critical comments on the manuscript. This work was supported by grants T32 HD083185 and F31 CA206381 (to Danielle J. Sanchez), R01 DK098542 (to David J. Steger) and P01 CA104838 to M. Celeste Simon.

2.1 Abstract

Clear cell renal cell carcinoma (ccRCC) is a subtype of kidney cancer defined by robust lipid accumulation, which prior studies have indicated plays an important role in tumor progression. We hypothesized that the peroxisome proliferator-activated receptor gamma (PPARγ), detected in both ccRCC tumors and cell lines, promotes lipid storage in ccRCC and contributes to tumorigenesis in this setting. PPARγ transcriptionally regulates a number of genes involved in lipid and glucose metabolism in adipocytes, yet its role in ccRCC has not been described. The objective of this study was to elucidate endogenous PPARγ function in ccRCC cells. Using chromatin immunoprecipitation followed by deep sequencing (ChIP-seq), we found that PPARγ and its heterodimer RXR occupy the canonical DR1 PPAR binding motif at approximately 1000 locations throughout the genome that can be subdivided into adipose-shared and ccRCC-specific sites. CRISPR-Cas9 mediated, loss-of-function studies determined that PPARγ is dispensable for viability, proliferation, and migration of ccRCC cells *in vitro* and *in vivo*. Also, surprisingly, PPARγ deletion had little effect on the robust lipid accumulation that typifies the "clear cell" phenotype of kidney cancer. Our results suggest that PPARγ plays neither a tumor suppressive nor oncogenic role in advanced ccRCC, and thus single-agent therapeutics targeting PPARγ are unlikely to be effective for the treatment of this disease. The unique cistrome of PPARγ in ccRCC cells demonstrates the importance of cell type in determining the functions of PPARγ.

2.2 Introduction

Kidney cancer is the 8th most prevalent form of cancer diagnosed each year in the United States, with approximately 64,000 new diagnoses and 14,400 deaths annually (Institute, 2018). While localized disease can be treated by surgical resection, 30% of patients initially present in the clinic with metastatic disease, which carries a poor prognosis due to limited efficacy of current standard-of-care therapies (Rydzanicz et al., 2013). As such, a significant clinical need remains for therapeutics targeting unique genetic and metabolic vulnerabilities within this tumor type.

Clear cell renal cell carcinoma (ccRCC), the most common subtype of kidney cancer, is defined by constitutive hypoxia-inducible factor signaling as well as widespread changes in cellular metabolism of glucose, amino acids, and lipids (Wettersten et al., 2017). Phenotypically, ccRCC is characterized by robust intracellular lipid and glycogen accumulation, resulting in "cleared" cytoplasm when prepared for common histologic analyses. Rather than simply reflecting a byproduct of increased anabolic metabolism, recent studies suggest that maintaining the integrity of neutral lipid droplets as well as abundant lipid uptake is critical to maintain ccRCC cell viability (Qiu et al., 2015), particularly when oxygen is limiting in the tumor microenvironment (Young et al., 2013). However, factors imparting a lipogenic quality to ccRCC tumors remain to be fully elucidated.

The peroxisome proliferator-activated receptor gamma (PPARγ) along with its heterodimeric DNA-binding partner retinoid X receptor (RXR) promote the transcription of genes broadly important for lipid, glucose, and hormone metabolism, most notably in the context of adipose tissue (Ahmadian et al., 2013). PPARγ, the master regulator of adipogenesis, is both necessary and sufficient for this process *in vitro* and *in vivo* (Tontonoz et al., 1994; Wang et al., 2013). Additionally, in non-adipose contexts including ischemic, diseased cardiomyocytes (Krishnan et al., 2009) and macrophages (Chawla et al., 2001a), PPARγ contributes to the regulation of genes involved in lipid metabolism. In a mouse model of high fat diet (HFD)-induced hepatosteatosis, PPARγ protein expression is elevated in the livers of mice fed HFD relative to controls (Morán-Salvador et al., 2011), although the absolute level remains far below those

observed in adipose tissues. Interestingly, conditional deletion of *Pparg* within hepatocytes abrogated liver steatosis, suggesting a link between PPARγ and lipid uptake, synthesis, and/or storage in this model.

Previous reports indicate that PPARγ is functionally expressed (Collet et al., 2011) in ccRCC and that increased PPARγ abundance correlates with reduced patient survival (Zhu et al., 2015), suggesting a possible oncogenic function. *In vitro* studies investigating the role of PPARγ in ccRCC and other cancers have largely employed natural and synthetic activating ligands including the insulin-sensitizing thiazolidinediones, yet many used super-physiologic concentrations which can cause off-target effects and confound interpretation of results (Fujita et al., 2011; Shiau et al., 2005). In this study, our goal was to investigate endogenous PPARγ function through ChIP-seq and a number of *in vitro* and *in vivo* assays of tumor progression using loss-of-function models in established ccRCC cell lines.

2.3 Materials and Methods

Primary Patient Samples and Gene Expression Data

Matched tumor/normal samples were obtained from the Cooperative Human Tissue Network (CHTN). Tumors were homogenized in TRIzol (see quantitative real-time PCR) or whole cell elution buffer (see Western blot) and analyzed for *PPARG* mRNA and protein expression. Gumz, *et al.* microarray dataset was downloaded from Oncomine. RNA-seq data for 480 ccRCC and 69 normal kidney samples were downloaded from TCGA on April 2, 2013. Differential gene expression analysis of tumor and normal samples was performed using DeSeq (Bioconductor Version 2.12). TCGA mutation and copy number data for 418 sequenced patients/cases were downloaded from cBioPortal for Cancer Genomics (Network, 2013).

Cell Culture, Plasmids, Lentiviral Production, and Viral Transduction

Human ccRCC cell lines (RCC10, UMRC2, Caki2, 786-O, A498, 769-P) were obtained from the American Type Culture Collection (ATCC) and were cultured in DMEM (ThermoFisher Scientific, cat. 11965092) supplemented with 10% FBS (Gemini Bio-Products, cat. 900-108). Immortalized renal epithelial cells (HK2) obtained from ATCC and cultured in Keratinocyte Serum Free Media with appropriate supplements (ThermoFisher Scientific, cat. 17005042). Human single-guide RNAs (sgRNA) targeting *PPARG* #1 (ctccgtggatctctccgtaa) and #3 (cattacgaagacattccatt) along with control gRNA targeting mouse *Rosa26* locus (aagatgggcgggagtcttct) were cloned into LentiCRISPRv2 plasmid (Sanjana et al., 2014). Mature antisense human *PPARG* shRNA #3 sequence (clone ID: TRCN0000001673) along with scrambled (SCR) control were cloned into a doxycycline-inducible pLKO lentiviral plasmid (AddGene, cat. 21915, (Wiederschain et al., 2009)). Lentivirus was prepared by co-transfection of 293T cells with shRNA or CRISPR plasmid of interest along with packaging plasmids pVSVg (AddGene, cat. 8454), psPAX2 (AddGene, cat. 12260) and Fugene6 transfection reagent (Promega). Lentivirus-containing media was collected from plates at 24 and 48 hours post-transfection, filtered using a 0.45 μm filter, and stored at -80°C. For viral transduction, cells were

incubated with lentivirus-containing medium and 8 μg/mL polybrene for 24 hours. Cells were allowed to recover for another 24 hours before selection with puromycin. All experiments were performed with cells that survived puromycin selection and displayed knockdown/knockout of *PPARG* as assayed by Western blot.

Quantitative Real-Time PCR (qRT-PCR)

Total RNA was isolated using TRIzol reagent (ThermoFisher Scientific, cat. 15596026) and RNeasy mini kit (Qiagen, cat. 74104). Reverse transcription was performed using High-Capacity RNA-to-cDNA (Applied Biosystems, cat. 4387406). qRT-PCR was performed using ViiA7 Real-Time PCR system (Applied Biosystems) with TaqMan master mix (Life Technologies). TaqMan probes were used to quantitate expression of *PPARG* (cat. Hs01115513_m1), *FABP4* (cat. Hs01086177_m1), *CD36* (cat. Hs01567185_m1) *SLC38A4* (Hs00394339_m1), and normalized to housekeeping genes *HPRT1* (cat. Hs02800695_m1) and *TBP* (Hs00427620_m1).

Western Blot

Cells were washed with PBS prior to lysis in whole cell elution buffer (150 mM NaCl, 10 mM Tris pH 7.6, 0.1% SDS, and 5 mM EDTA) containing Roche ULTRA protease inhibitor cocktail (cat. 05892791001). Proteins were resolved by SDS-PAGE, transferred to nitrocellulose membranes, and immunoblotting was performed by incubating with primary antibodies overnight at 4°C. The next day, membranes were incubated with secondary antibody and Western Lightning Plus-ECL, Enhanced Chemiluminescence Substrate (PerkinElmer, cat. NEL103E001EA) was used to visualize proteins. All primary antibodies were diluted of 1:1000 in 5% w/v nonfat milk (except GAPDH, 1:10,000), and secondary antibodies were diluted 1:2000 in 5% w/v nonfat milk. PPARγ (cat. 2435), FASN (cat. 3180), GAPDH (cat. 2118), anti-Rabbit IgG, HRP-linked (cat. 7074), anti-Mouse IgG, HRP-linked (cat. 7076) were purchased from Cell Signaling Technology. SREBP1 (cat. 13551) was purchased from Santa Cruz Biotechnology. SCD (cat. 19862) was purchased from Abcam.

Chromatin Immunoprecipitation (ChIP) and ChIP-seq

ChIP was performed with whole cell extracts isolated from UMRC2 PPARγ WT and PPARγ KD cell lines using 10 μg PPARγ (Santa Cruz, cat. sc-7196) or 10 μg RXRα/β/γ (Santa Cruz, cat. sc-774) antibodies for immunoprecipitation (IP). Briefly, confluent 10 cm dishes of cells were prepared by crosslinking with 1% formaldehyde for 15 minutes at room temperature, and quenched with 125 mM glycine for 5 min at room temperature. Cells were harvested by scraping and pellets were resuspended in 200 μl SDS lysis buffer (50 mM HEPES/NaOH pH 7.5, 1% SDS, 10 mM EDTA, 1 mM PMSF, and Roche ULTRA protease inhibitor cocktail (cat. 05892791001)) on ice for 10 minutes. Sonication was performed using Bioruptor Pico (Diagenode, cat. B01060010) on high setting for 30 seconds, followed by centrifugation of lysates to remove cellular debris. 100 μl of sheared chromatin from each tube was then diluted 10X, with 5% saved as Input DNA and the rest prepared for either PPARγ or RXR IP.

PPARγ WT, PPARγ KD, RXR, and Input libraries were prepared in duplicate from two independent biological replicates. For ChIP-seq, sequencing data was mapped to the human genome (GRCh38) using STAR (Dobin et al., 2013) with parameters appropriate for ungapped alignments. Peaks were called for each sample with input samples as background by HOMER (Heinz et al., 2010). HOMER was also used for differential peak calling (PPARγ WT vs. KD and RXR WT vs. KD) and to annotate peaks to proximal genes as described in Ensembl v85 (http://www.ensembl.org/index.html). For bioinformatics analyses displayed in Figure 2C - 2F, 1031 “high-confidence sites” were defined by the following criteria: peak score ≥ 10 (≥ 1 read per million), fold change (PPARγ WT vs. KD) ≥ 2, RXR peak called with strict overlap. Motif enrichment analysis was performed on this filtered peak list (1031 peaks) using HOMER against the standard list of known motifs; *de novo* motif discovery included consideration of lengths 8,10,12,15,18 bp.

Annexin V-PI Apoptosis Assay

30,000 cells of each cell line were plated in triplicate on 6-well plates. Four days later, cells were prepared using the FITC–Annexin V, PI Kit (BD Biosciences, cat. 556547) according to the manufacturer's instructions. Flow cytometry was performed using the BD Accuri C6 instrument, with viable cells represented as the double-negative population.

2D and 3D Proliferation Assays

For 2D proliferation assays, 30,000 cells of each cell line were plated in triplicate on 6-well plates. The following day (represented as Day 0), cells were trypsinized and counted using the Countess Automated Cell Counter (Invitrogen, cat. C10281), as per the manufacturer's instructions with Trypan blue. Cells were then counted again at the indicated timepoints. For 3D proliferation assays, 3,000 cells of each cell line were plated in 24 wells of a Corning Costar 96-well Ultra-low attachment round bottom plate (Sigma-Aldrich, cat. CLS7007) (Vinci et al., 2012). Cells were mixed with Matrigel (BD Biosciences, cat. 356234) at a final concentration of 2.5%, and plates were centrifuged at 1800 rpm for 10 minutes to form spheroids. The following day (represented as Day 0), spheroids were imaged using the Invitrogen EVOS FL Auto Cell Imaging System, and were imaged again at the indicated timepoints over the course of two weeks. Spheroid volume was calculated using a previously published ImageJ macro (Ivanov et al., 2014).

Subcutaneous Xenograft

Experiments were approved by the Animal Care and Use Committee at the University of Pennsylvania. Six female NIH-III nude mice (Charles River Laboratories, 4-6 weeks old) were injected in each flank with $5x10^6$ UMRC2 control or *PPARG* KO cells. Cells were resuspended in ice-cold PBS and were mixed 1:1 with Matrigel (BD Biosciences, cat. 356234) in a final volume of 200 μL per injection. Tumor volumes were recorded at the indicated timepoints using caliper measurements, calculated by the formula $V=(\pi/6)(L)(W^2)$, where L was the longer measurement and W was the shorter measurement. At Day 75 post-injection, mice were sacrificed by CO_2 inhalation and tumors were dissected for further analyses.

Immunohistochemistry

Xenograft tumors were dehydrated, embedded in paraffin, and sectioned for staining. Immunohistochemistry was performed as previously described (Qiu et al., 2015) using 1:200 PPARγ (Cell Signaling Technology, cat. 2435), 1:100 Ki67 (Abcam, cat. Ab15580), and 1:400 Cleaved Caspase-3 (Cell Signaling Technology, cat. 9661).

Oil Red O Staining

Oil Red O powder (350 mg) was dissolved in 100 mL 100% isopropanol as a stock solution. Working solutions were prepared by mixing 60% stock with 40% H_2O, vortexing, and resting for 30 minutes at room temperature before filtering through a 0.2 μm filter. Cells were washed twice in PBS, fixed in 4% paraformaldehyde for 15 minutes, and then incubated with the Oil Red O working solution for 30 minutes at room temperature. Three more PBS washes were performed before cells were counterstained with hematoxylin and coverslipped for imaging.

BODIPY (493/503) Staining

50,000 cells of each cell line were plated in triplicate on 6-well plates. Three days later, live cells were washed twice in PBS and incubated in 2 μg/mL BODIPY 493/503 (Life Technologies, cat. D3922) in PBS for 15 minutes at 37°C. After staining and trypsinization, cells were washed twice in PBS and fixed in 2% paraformaldehyde for 15 minutes in the dark. Fixed cells were washed and resuspended in PBS, passed through a cell strainer, and flow cytometry was performed on a BD Accuri C6 instrument under FL-1.

Triglyceride Measurement

Xenograft tumors were homogenized in complete lysis buffer (50 mM Tris pH 7.4, 140 mM NaCl, 0.1% Triton X-100, 1 mM PMSF) containing Roche ULTRA protease inhibitor cocktail (cat. 05892791001) using a Tissue-Tearor (BioSpec Products, cat. 985370). Triglyceride content

was measured using the LiquiColor Triglycerides kit (Stanbio Laboratory, cat. 2100) according to the manufacturer's instructions and data were normalized to weight of each sample.

In Vitro Migration (Scratch) Assay

UMRC2 and A498 control and *PPARG* KO cell lines were plated to reach confluence the following day. Scratches were made on the plates using a pipette tip and immediately imaged (represented as 0 hr). 16 hours later, the scratched wells were imaged once again. For both timepoints, wound area was determined using ImageJ, and data are expressed as scratch area remaining at 16 hr relative to 0 hr timepoint.

Soft Agar Colony Formation Assay

UMRC2 and A498 control and *PPARG* KO cell lines were plated at a density of 6,000 cells per well (in 6-well plates) in complete DMEM containing 0.3% agarose (low-melt 2-hydroxyethylagarose, Sigma Aldrich A4018), onto underlays composed of DMEM containing 0.6% agarose. Additional media was added to the cultures once per week, and after three weeks of growth the colonies were quantified.

Statistics

Statistical analyses were performed using GraphPad Prism version 7 software, using unpaired t-test with Welch's correction. Data are presented as mean ± SEM of at least three independent experiments. Statistical significance was defined as *** ($p < 0.001$), ** ($p < 0.01$), * ($p < 0.05$), n.s. = not significant.

2.4 Results

2.4.a PPARγ expression in ccRCC patient samples and cell lines

A 43 megabase region of chromosome 3p harbors *bona fide* and putative tumor suppressor genes in ccRCC (Peña-Llopis et al., 2013) including von Hippel-Lindau (*VHL*), the most commonly mutated gene in ccRCC and initiating tumorigenic event (Mandriota et al., 2002). Unlike tumor suppressor genes located in this region, such as *VHL*, *SETD2*, *PBRM1,* and *BAP1*, *PPARG* is free from mutations which could render the protein non-functional or functional as a dominant-negative factor, and retains wildtype sequence in 96% of ccRCC tumors (**Figure 2.1A**). *PPARG* mRNA expression is elevated in early-stage ccRCC relative to matched healthy kidney tissue (**Figure 2.1B**) (Gumz et al., 2007; Tun et al., 2010). The Cancer Genome Atlas (TCGA) RNA-seq data stratified according to tumor stage confirmed a significant increase in *PPARG* transcripts in stage I and II patients, with non-significant changes in stages III and IV relative to normal kidney tissue (**Figure 2.1C**). To verify *PPARG* mRNA and protein expression in ccRCC, we examined matched tumor/normal pairs by RT-qPCR and Western blot. *PPARG* mRNA (**Figure 2.1D**) and protein (**Figure 2.1E**) abundances were variable between tumor/normal samples, yet a subset of samples displayed elevated PPARγ expression relative to adjacent healthy kidney tissue. PPARγ expression in the kidney is highest in medullary collecting ducts (Guan et al., 2005; Guan et al., 1997) and is not expressed significantly in renal proximal tubule epithelial cells (RPTEC), a proposed cell-of-origin for ccRCC (Chen et al., 2016a; Yoshida et al., 1986). This may explain the heterogeneity observed across the kidney lysates sampled. We further examined PPARγ expression in a panel of ccRCC cell lines relative to immortalized (HK2) and purified primary (RPTEC) cells (**Figure 2.1F-G**), and found elevated mRNA and protein abundance in ccRCC relative to control in 4 out of 6 lines tested.

2.4.b Genome-wide analysis of PPARγ-RXR binding in ccRCC

To understand the functional role of PPARγ in kidney cancer, we sought to characterize the PPARγ-RXR cistrome in the context of ccRCC and determine the relatedness of genomic

occupancy to that found in adipocytes. ChIP-qPCR interrogating a number of adipocyte sites (Soccio et al., 2011) in the UMRC2 cell line revealed coordinated occupancy for PPARγ and its heterodimeric binding partner RXR at *PDK4* and *PLIN1* (**Figure 2.2A**). To examine occupancy across the entire genome, we performed chromatin immunoprecipitation followed by deep sequencing (ChIP-seq) for PPARγ and RXR. We identified 1031 binding sites based on the following criteria: peak score greater than or equal to 10, wildtype vs. knockdown fold change greater than or equal to 2 (validation of PPARγ protein knockdown in **Figure 2.3A**), and RXR peak called with strict overlap (**Figure 2.2B**). We validated PPARγ binding at eight of the top sites called in our data set based on peak score using control and *PPARG* KO cells (**Figure 2.4A-C, Table 1**). Additionally, we addressed the functionality of PPARγ binding in ccRCC cells through an shRNA-resistant cDNA rescue experiment. Ectopic expression of PPARγ increased the expression of *SLC38A4*, a gene with two PPARγ-RXR binding sites within 10 kb of the transcriptional start site (**Figure 2.4D**). When cells were treated with shRNA targeting *PPARG*, *SLC38A4* expression was diminished, but not when cells also contained the resistant cDNA (**Figure 2.4E-F**). These data suggest that *SLC38A4* is a direct transcriptional target of PPARγ in ccRCC and provide evidence that endogenous PPARγ activity regulates gene expression in our cell culture models.

Through *de novo* motif analysis we found that the canonical nuclear receptor direct repeat 1 (DR1) motif is most highly enriched under PPARγ-RXR bound DNA in ccRCC, present at 60.3% of sites (**Figure 2.2C**). Other transcription factor motifs represented include RAR-related orphan receptor alpha (RORA) at 17.3% of sites and the hepatocyte nuclear factors alpha (HNF1A, 16.3% of sites) and gamma (HNF4G, 5.7% of sites). Interestingly, the C/EBP motif, which is found at 91% of PPARγ-binding regions in adipocytes (Lefterova et al., 2008), is only found at 4.6% of PPARγ-RXR-bound regions in ccRCC. Consistent with previously published ChIP-seq data sets in tissues including adipocytes and macrophages (Lefterova et al., 2010) (Schmidt et al., 2011), PPARγ-RXR is bound most frequently at intergenic (37.2%) and intronic (47.1%) regions of the genome in ccRCC, rather than at promoter-transcriptional start sites

(10.4%) (**Figure 2.2D**). We then annotated peaks to the nearest gene and performed gene ontology analysis to determine putative PPARγ-regulated pathways in ccRCC. Annotation of "adipose-shared" genes include "metabolism of lipids and lipoproteins", "organic acid metabolic process", and "lipid localization" (**Figure 2.2E**), whereas "ccRCC-specific" genes belonged to cellular processes broadly important in cancer cell biology, including signal transduction and regulation of cell shape and size (**Figure 2.2F**).

2.4.c PPARγ is dispensable for ccRCC viability and proliferation *in vitro*

As PPARγ was shown to bind near genes associated with regulation of protein serine/threonine kinase activity and G2/M transition of mitotic cell cycle in ccRCC (**Figure 2.2F**), we hypothesized that its loss would affect cell growth over time. Upon confirming effective knockout of PPARγ using CRISPR-Cas9 (**Figure 2.3B**, **Figure 2.5A**), we subjected UMRC2 and A498 ccRCC cell lines to a variety of *in vitro* assays to determine the functional consequence of PPARγ loss. *PPARG* KO did not affect the viability (**Figure 2.5B-C**) or proliferation rate (**Figure 2.5D-E**) of either cell line when cells were grown in replete conditions (21% O_2, 25 mM glucose and 10% FBS). Since oxygen and nutrient limitation can profoundly influence cancer cell growth, we embedded control and *PPARG* KO cells in Matrigel and allowed tumor spheroids to proliferate over the course of two weeks. *PPARG* KO did not affect spheroid volume during the assay (**Figure 2.5F-H**).

Additional "ccRCC-specific" PPARγ bound genes included those involved in "regulation of cell shape" and "regulation of locomotion", which we hypothesized could affect migratory capacity. We plated UMRC2 and A498 cells to confluency and performed an *in vitro* scratch assay to measure migration over the course of 16 hours, a timepoint chosen based on the nearly complete recovery of the wound prior to the doubling time. We found no significant difference in the percentage of wound healing that occurred between control and *PPARG* KO cells (**Figure 2.6A-B**). We also found that PPARγ depletion only modestly affected anchorage-independent growth of UMRC2 and A498 ccRCC cells (**Figure 2.6C-D**).

2.4d PPARγ is dispensable for ccRCC xenograft tumor growth *in vivo*

To assess the function of PPARγ in ccRCC tumor growth *in vivo*, we implanted UMRC2 control and *PPARG* KO cells subcutaneously into opposing flanks of NIH-III nude mice. Analysis of tumor volume (**Figure 2.7A**) over the course of the experiment and tumor weights at day 75 post-injection (**Figure 2.7B**) revealed no significant difference in the growth of *PPARG* KO tumors relative to control. Additionally, control and *PPARG* KO tumors were sectioned and immunohistochemistry was performed for markers of proliferation (Ki67) and apoptosis (cleaved caspase-3), as well as to confirm PPARγ loss over the duration of the assay (**Figure 2.7C**). Quantitation of these markers revealed no significant difference between control and *PPARG* KO tumors, suggesting that PPARγ is dispensable for ccRCC cell growth *in vivo* (**Figure 2.7D-E**).

2.4.e Lipid storage and triglyceride synthesis occur independently of PPARγ in ccRCC

As PPARγ is responsible for promoting lipid uptake and storage in adipocytes, and is bound near lipid metabolism related genes in our model (**Figure 2.2E**), we hypothesized that its loss in ccRCC would reduce neutral lipid content. Surprisingly, we found that loss of PPARγ did not affect lipid accumulation in either ccRCC cell line tested *in vitro* by Oil Red O (**Figure 2.8A**) or BODIPY 493/503 (**Figure 2.8B**) staining. In agreement with this, expression of a number of proteins involved in *de novo* lipogenesis that are reduced following hepatocyte-specific deletion of PPARγ (Morán-Salvador et al., 2011), including sterol regulatory element-binding protein 1 (SREBP1), fatty acid synthase (FASN), and stearoyl-CoA desaturase 1 (SCD), did not change substantially following PPARγ loss in our models (**Figure 2.8C**). Additionally, we measured triglyceride levels in control and *PPARG* KO xenograft tumors to determine whether exposure to oxygen and nutrient depletion *in vivo* would affect the ability of the cells to store triglyceride. Consistent with our *in vitro* results, we found no significant difference in triglyceride content between control and *PPARG* KO tumors (**Figure 2.8D**). These data indicate that PPARγ is

dispensable for the “clear cell” phenotype of renal cancer with regard to triglyceride synthesis and storage.

2.5 Discussion

“Druggability” of nuclear receptors via small molecule agonists or antagonists make them appealing therapeutic targets to treat diseases like diabetes and cancer. Across various tumor types, studies have revealed both oncogenic and tumor suppressive roles for PPARγ (Tontonoz and Spiegelman, 2008). Heterozygous deletion of PPARγ in mice has demonstrated that it primarily acts as a tumor suppressor in chemically-induced models of colon (Girnun et al., 2002), breast, ovarian and skin cancers (Nicol et al., 2004), whereas newly uncovered oncogenic functions for PPARγ have been reported in bladder cancer using *in vitro* cell culture models (Goldstein et al., 2017; Halstead et al., 2017). We hypothesized that PPARγ would promote ccRCC tumorigenesis due to the fact that its lipid-laden phenotype is tightly linked to cell viability and proliferation. Our lab previously reported that suppression of the lipid droplet coat protein perilipin 2 in ccRCC reduces neutral lipid accumulation, engaging the endoplasmic reticulum stress response and causing tumor regression (Qiu et al., 2015). Additionally, cells defined by constitutive mTORC1 signaling such as ccRCC (Network, 2013) (Turajlic et al., 2015) require import of exogenous unsaturated fatty acids during hypoxia to maintain membrane homeostasis and prevent cell death (Kamphorst et al., 2013; Young et al., 2013). However, our current understanding of the molecular mediators of lipid uptake and storage in ccRCC is limited.

In this study, we performed loss-of-function experiments to elucidate PPARγ’s role in ccRCC in established cell lines both *in vitro* and *in vivo*. PPARγ deletion in two ccRCC cell lines affected neither viability, proliferation, migratory capacity *in vitro*, nor tumor growth in a subcutaneous xenograft model. Surprisingly, we also show that PPARγ is dispensable for lipid storage and maintenance of total triglyceride levels in ccRCC cells grown both *in vitro* and *in vivo*. While our data collectively suggest that PPARγ is not required for ccRCC progression, we cannot exclude a potential role for this nuclear receptor in tumor initiation. The stage-specific

upregulation of *PPARG* transcripts in stage I and II kidney tumors (**Figure 2.1B-C**) is consistent with PPARγ protein expression patterns in human prostate cancer (Nakamura et al., 2009). Functionally, this may reflect a role for PPARγ in epithelial-to-mesenchymal transition of renal epithelium to ccRCC, although this remains to be explored. *PPARG* expression may also be inversely related to the differentiation status of tumors, as previously reported in liposarcoma (Demetri et al., 1999; Tontonoz et al., 1997).

One factor that may influence PPARγ's function in regulating ccRCC gene expression is cooperative transcription factor binding. For example, CCAAT-enhancer-binding proteins (C/EBPs) have been shown to be required for robust PPARγ target gene expression in adipocytes (Lefterova et al., 2008), yet the C/EBP motif only appeared under ~5% of the binding sites called in ccRCC (**Figure 2.2C**). Lack of PPARγ/C/EBP cooperativity may underlie the lack of "classic" PPARγ target gene expression including *CD36*, *FABP4*, and other genes broadly important in lipid and glucose metabolism (**Figure 2.3C**) and demonstrate distinct PPARγ action in ccRCC vs. adipose tissue. Additionally, *de novo* motif analysis revealed that the retinoic acid receptor-related orphan receptor alpha (RORα) motif is the second most commonly enriched motif under PPARγ-RXR-bound DNA in ccRCC (**Figure 2.2C**). A recent report demonstrated that RORα reduces PPARγ transcriptional activity via the recruitment of histone deacetylase 3 to PPARγ target gene promoters in the livers of mice fed HFD (Kim et al., 2017). PPARγ-RORα co-localization in ccRCC and negative regulation of lipid metabolism-related genes would be consistent with the phenotypes observed in our experiments, as PPARγ depletion did not reduce triglyceride content or significantly alter expression of *de novo* lipogenesis enzymes (**Figure 2.8**).

We considered that compensatory up-regulation of other PPAR family members may underlie the lack of phenotypes observed in our experiments, however, we determined that *PPARG* KO cells do not increase expression of *PPARA* or *PPARD* (**Figure 2.3D**). Indeed, expression of *PPARA, PPARGC1A,* and additional genes involved in beta-oxidation of lipids are highly suppressed in ccRCC relative to healthy renal tubule epithelium (Kang et al., 2015). Ectopic expression of such factors in ccRCC reduces tumor growth (LaGory et al., 2015), further

illustrating the importance of reprogramming lipid metabolism from an oxidative to anabolic state in this tumor type. In conclusion, our investigation of PPARγ in ccRCC led to a novel PPARγ-RXR cistrome, which shares both similarities and differences with published cistromes in tissues such as adipocytes and macrophages. Of note, our dataset will be beneficial to researchers studying cell type-specific functions of PPARγ in cancer as well as the role of other subfamily 1 nuclear receptors that heterodimerize with RXR in ccRCC. Finally, while PPARγ is expressed in ccRCC tumors, it does not appear to be necessary for tumor maintenance based on our assays.

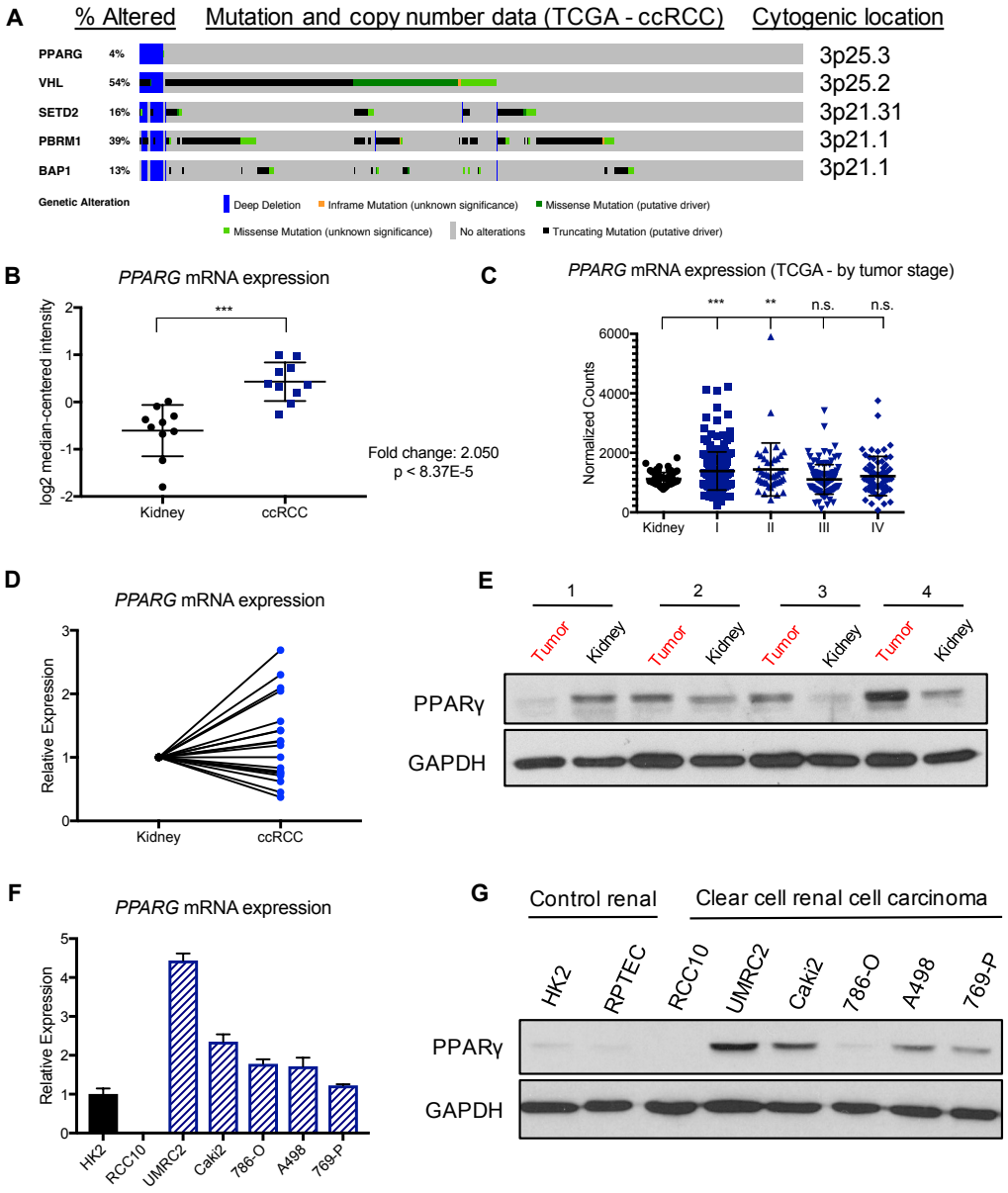

Figure 2.1: PPARγ expression in ccRCC patient samples and cell lines
(**A**) Frequency of select chromosome 3p gene alterations in ccRCC tumors (cBioPortal). n = 448 patients. (**B**) *PPARG* mRNA expression in ccRCC and adjacent healthy kidney tissue from Gumz Renal microarray dataset. *** ($p < 0.001$). (**C**) *PPARG* mRNA expression in ccRCC and adjacent healthy kidney tissue from TCGA data set, stratified according to tumor stage. *** ($p < 0.001$), ** ($p < 0.01$), n.s. = not significant. (**D**) RT-qPCR for *PPARG* expression in eighteen tumor-normal paired samples. (**E**) Western blot for PPARγ expression in four tumor-normal paired samples. (**F**) *PPARG* mRNA expression in control renal cell line (HK2, black bar) and ccRCC cell lines (RCC10 through 769-P, blue bars). (**G**) PPARγ protein expression in control renal cell lines (HK2, RPTEC), ccRCC cell lines (RCC10 through 769-P).

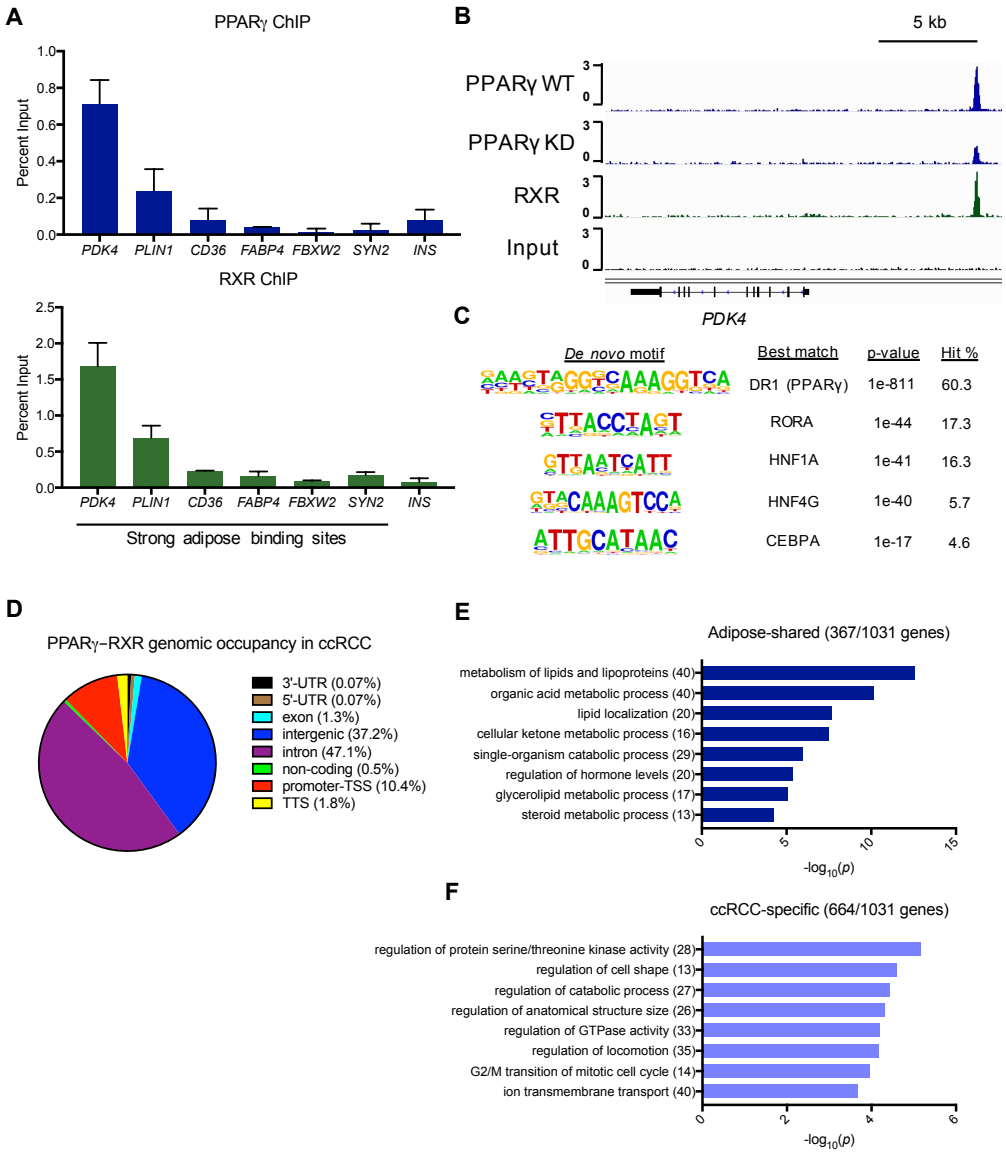

Figure 2.2: Genome-wide analysis of PPARγ-RXR binding in ccRCC
(**A**) PPARγ and RXR enrichment at a subset of strong adipocyte binding sites in UMRC2 ccRCC cells (*INS*, negative control) assayed by ChIP-qPCR. (**B**) ChIP-seq tracks of PPARγ WT, PPARγ KD, RXR and Input, showing binding to enhancer site -12 kb from *PDK4*. (**C**) *De novo* motif analysis of PPARγ and RXR binding sites. For bioinformatics analyses displayed in C-F, 1031 "high-confidence sites" were defined by the following criteria: peak score ≥ 10 (≥ 1 read per million), fold change (WT vs. KD) ≥ 2, RXR peak called with strict overlap. (**D**) Frequency of PPARγ-RXR heterodimer occupancy at various genomic locations, defined by HOMER annotate peaks. (**E**) Gene ontology of PPARγ and RXR binding sites, annotated to nearest gene. 367/1031 genes (36%) were directly shared with human adipose. Data were compared to published PPARγ ChIP-seq from an adipocyte cell line (Soccio et al., 2011). Numbers in parenthesis indicate number of genes per category. (**F**) Gene ontology of PPARγ and RXR binding sites, annotated to nearest gene. 664/1031 genes (64%) were unique to ccRCC. Data were compared to published PPARγ ChIP-seq from an adipocyte cell line (Soccio et al., 2011). Numbers in parenthesis indicate number of genes per category.

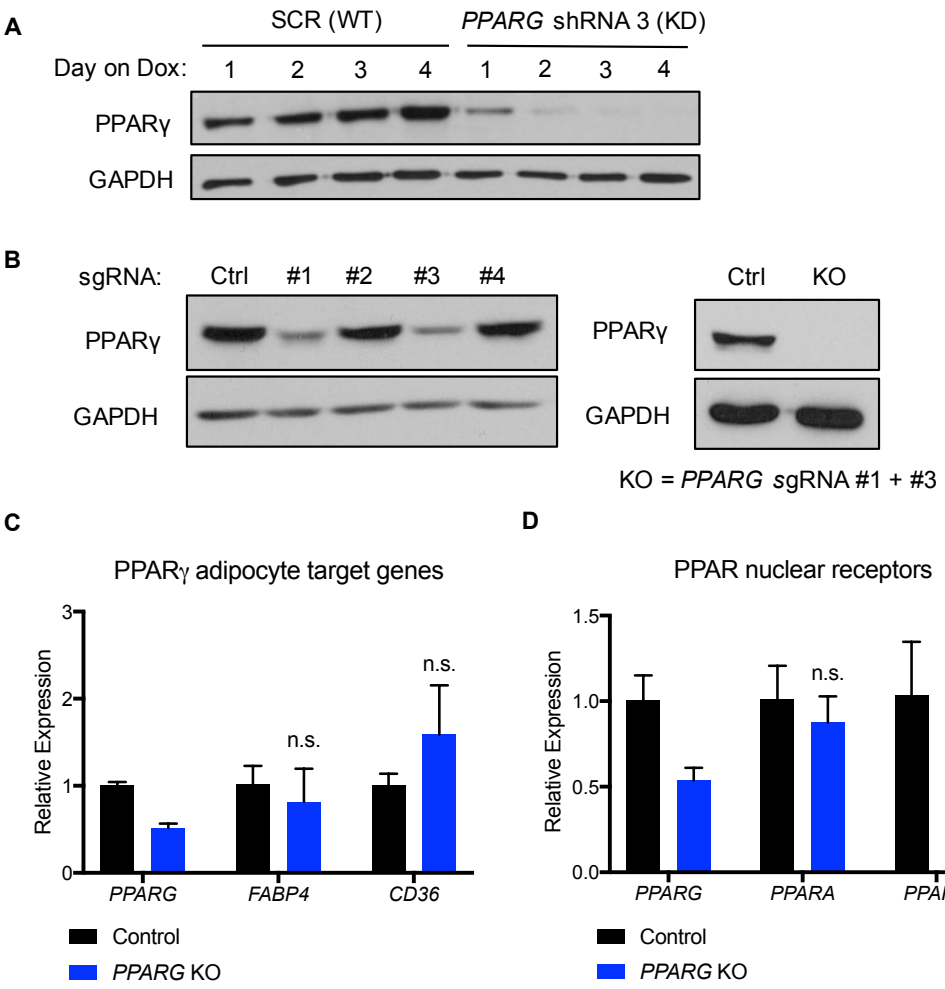

Figure 2.3: Validation of *PPARG* suppression strategies by shRNA and CRISPR-Cas9
(**A**) Validation of doxycycline-inducible shRNA system in UMRC2 cells. PPARγ protein levels are rapidly decreased following addition of doxycycline to media at 1 ug/mL. Doxycycline-inducible SCR (WT) and *PPARG* shRNA #3 (KD) cells were collected at the Day 2 timepoint for ChIP-seq experiment. (**B**) (Left) Western blot of PPARγ levels following lentiviral infection of UMRC2 cells with several gRNAs (#1-4) targeting *PPARG*. (Right) *PPARG* protein levels following combined lentiviral infection of UMRC2 cells with gRNAs #1 and #3. Addition of both gRNAs generates nearly complete knockout as assessed by Western blot, and is referred to throughout the manuscript as "*PPARG* KO". (**C**) Expression of PPARγ adipocyte target genes *FABP4* and *CD36* following *PPARG* KO in UMRC2 cells. (**D**) Expression of PPAR family members *PPARA* and *PPARD* following *PPARG* KO in UMRC2 cells.

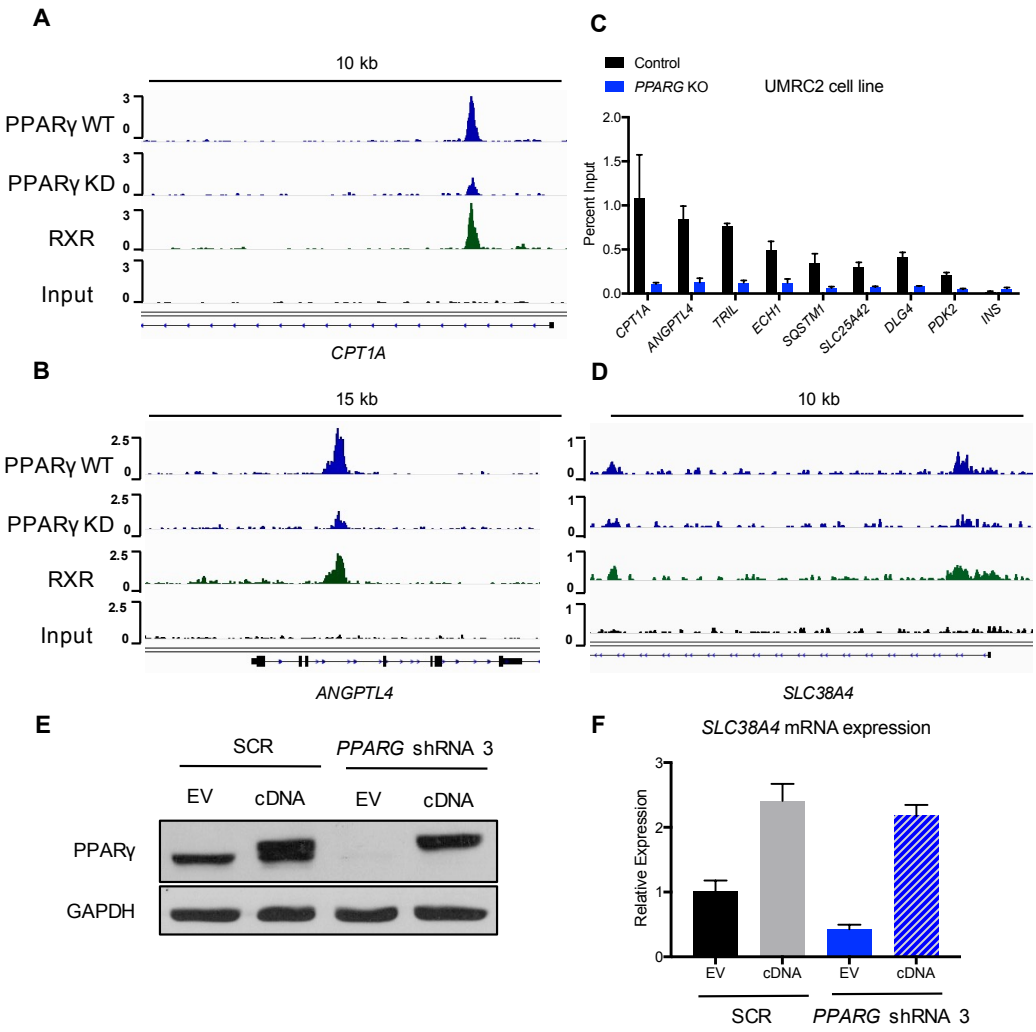

Figure 2.4: Validation of ChIP-seq dataset and functional PPARγ binding
(**A**) ChIP-seq tracks of PPARγ WT, PPARγ KD, RXR and Input, showing binding to intronic enhancer site upstream of *CPT1A* transcriptional start site. (**B**) ChIP-seq tracks of PPARγ WT, PPARγ KD, RXR and Input, showing binding to intronic enhancer site upstream of *ANGPTL4* transcriptional start site. (**C**) PPARγ enrichment at a subset of binding sites in UMRC2 ccRCC cells identified from ChIP-seq (*INS*, negative control) assayed by ChIP-qPCR. (**D**) ChIP-seq tracks of PPARγ WT, PPARγ KD, RXR and Input, showing binding sites downstream of *SLC38A4* transcriptional start site. (**E**) Western blot of PPARγ levels in UMRC2 cells following addition of empty vector (EV) or *PPARG* shRNA-resistant cDNA (FLAG-tagged) and expression of either SCR or *PPARG* shRNA #3. (**F**) qPCR for PPARγ target gene *SLC38A4* in UMRC2 cells following addition of *PPARG* shRNA-resistant cDNA (FLAG-tagged) and expression of either SCR or *PPARG* shRNA #3.

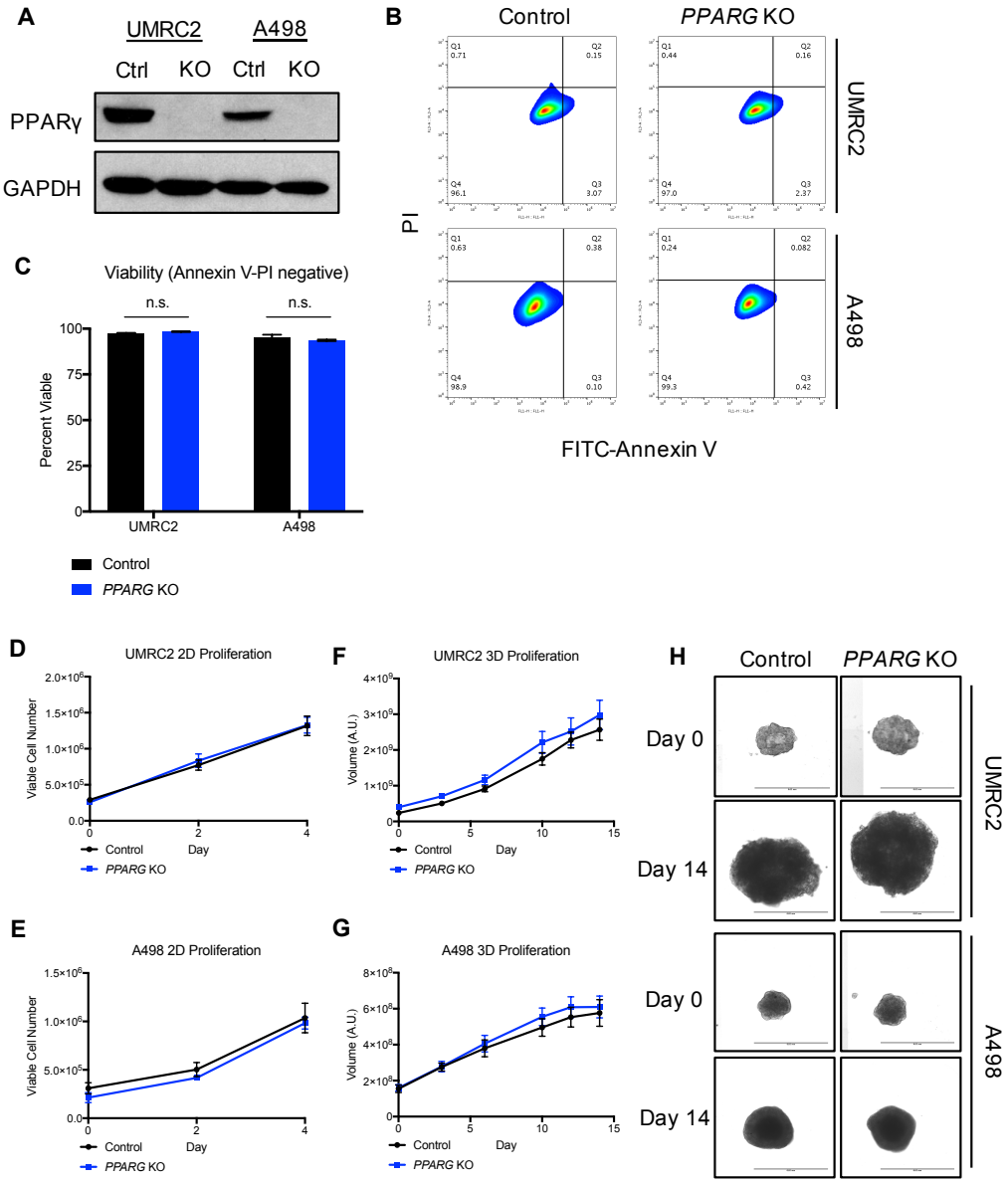

Figure 2.5: PPARγ is dispensable for ccRCC viability and proliferation *in vitro*
(**A**) Western blot of PPARγ levels in UMRC2 and A498 cells following *PPARG* KO. (**B**) Annexin V–PI flow cytometry plots for UMRC2 and A498 control and *PPARG* KO cells. (**C**) Quantification of Annexin V–PI double-negative population (lower left quadrant) for UMRC2 and A498 control and *PPARG* KO cells. (**D**) Growth curve of UMRC2 cell line measuring proliferation rate of control and *PPARG* KO cells over the course of four days. n.s. = not significant. (**E**) Growth curve of A498 cell line measuring proliferation rate of control and *PPARG* KO cells over the course of four days. (**F**) Growth curve of UMRC2 tumor spheroids measuring proliferation rate of control and *PPARG* KO cells over the course of two weeks. (**G**) Growth curve of A498 tumor spheroids measuring proliferation rate of control and *PPARG* KO cells over the course of two weeks. (**H**) Representative images of UMRC2 and A498 control and *PPARG* KO spheroids at indicated timepoints. Scale bar = 100 μm.

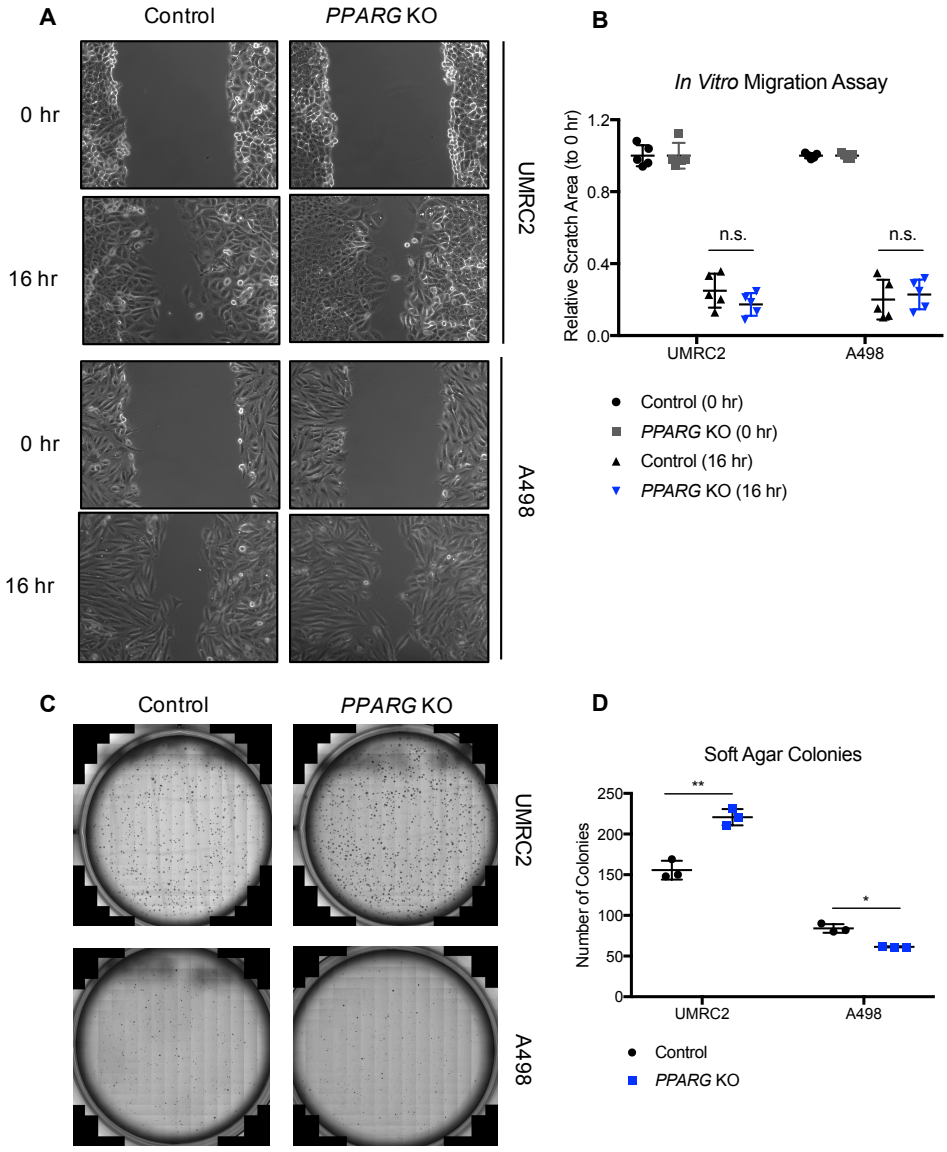

Figure 2.6: PPARγ is dispensable for migration and anchorage-independent growth of ccRCC cells *in vitro*

(**A**) Representative images of UMRC2 and A498 control and *PPARG* KO cell lines at indicated timepoints during migration assay. (**B**) Quantification of scratch area remaining in UMRC2 and A498 control and *PPARG* KO cell lines at indicated timepoints. n.s. = not significant. (**C**) Representative images of UMRC2 and A498 control and *PPARG* KO cells grown in soft agar colony formation assay. (**D**) Quantification of soft agar colony formation in UMRC2 and A498 control and *PPARG* KO cell lines. ** ($p < 0.01$), * ($p < 0.05$).

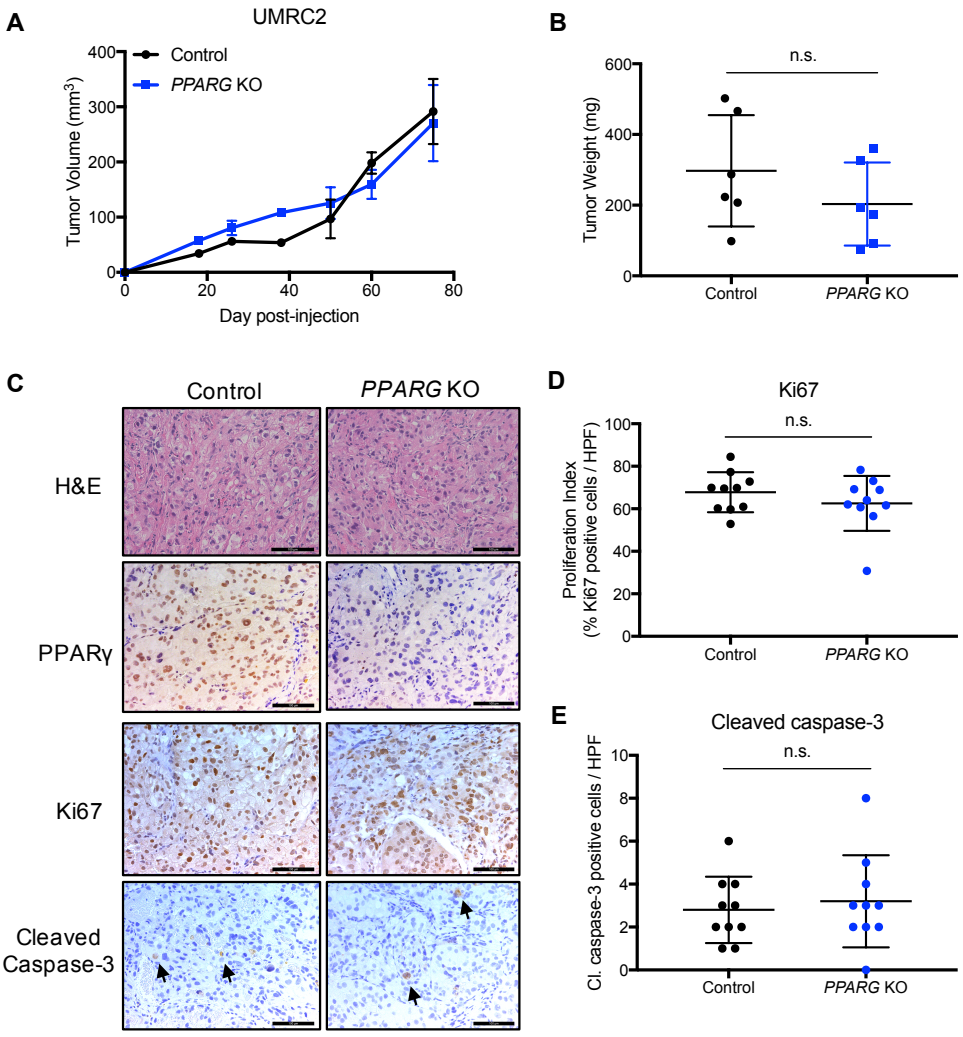

Figure 2.7: PPARγ is dispensable for ccRCC xenograft tumor growth *in vivo*
(**A**) Tumor volume measurements for UMRC2 control and *PPARG* KO subcutaneous xenografts at indicated timepoints. (**B**) Tumor weight measurements for UMRC2 control and *PPARG* KO subcutaneous xenografts at day 75 post-injection. n.s. = not significant. (**C**) Representative images of hematoxylin and eosin (H&E) staining and PPARγ, Ki67 and cleaved caspase-3 immunohistochemistry from UMRC2 control and *PPARG* KO subcutaneous xenograft tumors. Scale bar = 100 μm. (**D**) Quantification of Ki67-positivity shown in Figure 4C. n.s. = not significant. (**E**) Quantification of cleaved caspase-3-positivity shown in Figure 4C. n.s. = not significant.

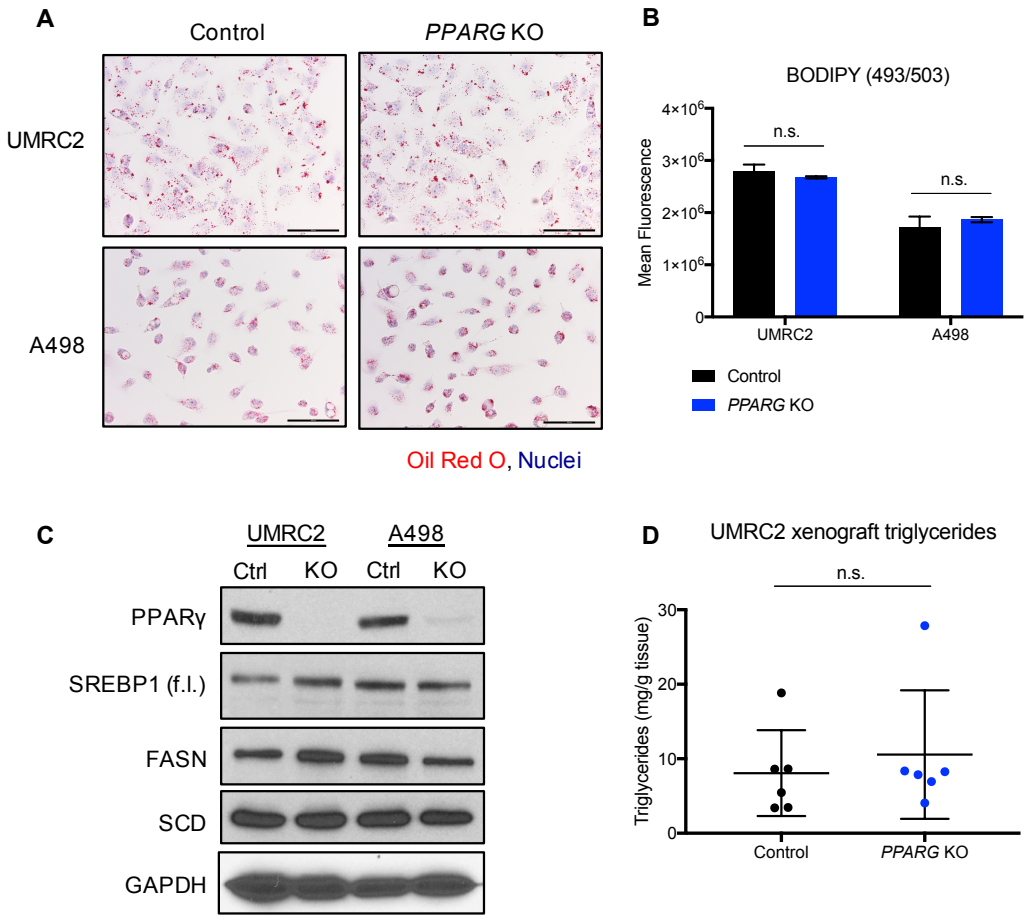

Figure 2.8: Lipid storage and triglyceride synthesis occur independently of PPARγ in ccRCC

(**A**) Representative images of UMRC2 and A498 control and *PPARG* KO cells stained with Oil Red O and counterstained with hematoxylin to visualize nuclei. Scale bar = 100 μm. (**B**) Quantification of BODIPY (493/503) staining of UMRC2 and A498 control and *PPARG* KO cell lines. n.s. = not significant. (**C**) Western blot of PPARγ, SREBP1 (f.l. = full length), FASN, and SCD in UMRC2 and A498 control and *PPARG* KO cell lines. (**D**) Triglyceride content of UMRC2 control and *PPARG* KO subcutaneous xenograft tumors. n.s. = not significant.

Chapter 3: Cell-intrinsic tumorigenic functions of PPARγ in bladder urothelial carcinoma

This chapter is in preparation for submission: Sanchez, DJ, Missiaen, R, Skuli, N, Steger, DJ, Simon, MC. Cell-intrinsic tumorigenic functions of PPARγ in bladder urothelial carcinoma. *Manuscript in preparation*.

Acknowledgments: We thank John Tobias for bioinformatics assistance with ChIP-seq and RNA-seq datasets. This work was supported by grants T32 HD083185 and F31 CA206381 (to Danielle J. Sanchez), R01 DK098542 (to David J. Steger) and P01 CA104838 to M. Celeste Simon.

3.1 Abstract

The role of peroxisome proliferator-activated receptor gamma (PPARγ) has been well characterized in the developmental process of adipogenesis, yet its aberrant expression patterns and functions in cancer subtypes are less understood. While PPARγ has been recently demonstrated to play non-cell-autonomous roles in promoting bladder urothelial carcinoma (UC) progression, its cell-intrinsic, oncogenic functions remain to be fully described. Here, we report robust expression and nuclear accumulation of PPARγ in 47% of UC patient samples by immunohistochemistry, exceeding mRNA expression patterns published by The Cancer Genome Atlas. We use several established human cell lines in *in vitro* assays to determine the functional consequence of pharmacological and genetic inhibition of PPARγ in UC. Loss of PPARγ transcriptional activity reduces proliferation of multiple UC cell lines, most strongly in those characterized by *PPARG* genomic amplification or activating mutation of *RXRA*, the obligate heterodimer of PPARγ. We show that treatment of UC cells with PPARγ inverse-agonist or *PPARG* knockout by CRISPR-Cas9 induces cell cycle arrest in G_1 phase. Through genome-wide approaches including ChIP- and RNA-seq, we define a candidate set of PPARγ-regulated genes in UC. Collectively, our data indicate that PPARγ promotes UC progression in a subset of patients, at least in part, through cell-autonomous mechanisms.

3.2 Introduction

Bladder urothelial carcinoma (UC) is the 9th leading cause of cancer worldwide, with an estimated ~81,000 new cases in 2018 and ~17,000 annual deaths per year in the United States alone (Siegel Rebecca et al., 2018). Clinically, UC is stratified into non-muscle invasive bladder cancer (NMIBC) and muscle-invasive bladder cancer (MIBC), both contributing to disease morbidity and mortality (Robertson et al., 2017). MIBC is currently treated by radical cystectomy preceded or followed by chemotherapy including methotrexate, vinblastine, doxorubicin, and cisplatin (Sanli et al., 2017). Recently, large-scale genomic sequencing of hundreds of primary patient samples has revealed distinct clusters of MIBC, most broadly stratified into luminal and basal subcategories based on common transcriptional features (Choi et al., 2014a; Sanli et al., 2017). The identification of molecular signatures and drivers of these programs will pave the way for improved, targeted therapies, of which there are currently few to treat localized and metastatic UC.

One transcription factor reported to be a hallmark of luminal MIBC is the peroxisome proliferator-activated receptor gamma (PPARγ) (Rochel et al., 2019). PPARγ is a member of the nuclear receptor family of transcription factors, which act as molecular sensors to regulate gene expression based on environmental and metabolic cues (Ahmadian et al., 2013). PPARγ binds DNA as a heterodimeric pair with retinoid X receptor (RXR), and exists in complex with co-repressor or co-activator proteins depending on activation state. Associations with co-activator or co-repressor proteins facilitates chromatin remodeling and target gene activation or repression, respectively (McKenna and O'Malley, 2002). During development, PPARγ and C/EBP transcription factors induce adipogenesis from mesenchymal progenitor cells (Tontonoz et al., 1994). In differentiated, post-mitotic adipocytes it regulates the expression of genes involved in lipid and glucose metabolism, and the expression of endocrine “adipokine” factors which affect whole-body energy homeostasis (Shapira and Seale, 2019).

Long-term use of certain thiazolidinediones, synthetic agonists of PPARγ used to manage blood glucose levels in type 2 diabetics, has been associated with increased risk of

bladder cancer development. Pioglitazone, but not rosiglitazone, has been associated with bladder cancer risk in some, but not all, population-based cohort studies (Lewis et al., 2011; Neumann et al., 2012; Tuccori et al., 2016). In a pre-clinical study employing a carcinogen-induced model of bladder cancer, rosiglitazone treatment increased incidence and size of UC in rats in a dose-dependent manner (Lubet et al., 2008). However, rosiglitazone treatment alone did not induce UC tumors in this study, suggesting a potential synergistic relationship between PPARγ activation and carcinogen exposure in UC development *in vivo*. Nevertheless, these observations have led our group and others to speculate that PPARγ might be an important factor in UC development and progression in a subset of patients. Indeed, a number of recent studies link PPARγ activity to UC, describing its ability to promote disease progression in both cell-autonomous (Biton et al., 2014; Goldstein et al., 2017; Halstead et al., 2017; Rochel et al., 2019) and non-cell-autonomous fashions (Korpal et al., 2017). However, the direct molecular mechanisms by which PPARγ inhibition reduces tumor growth have not been described, nor have the downstream mediators of PPARγ-RXR transcriptional activity been defined. In this study, our objective was to further elucidate the cell-intrinsic role of PPARγ signaling in UC and identify candidate target genes responsible for UC progression based on genome-wide approaches.

3.3 Materials and Methods

Primary Patient Samples and Genomics Data

Bladder urothelial carcinoma tissue array containing 60 cases of urothelial carcinoma plus adjacent normal bladder tissue was purchased from US Biomax, Inc. (cat. BC12011c). TCGA datasets (Network, 2014; Robertson et al., 2017) were analyzed for *PPARG* and *RXRA* mutational burden, copy number variation, mRNA upregulation, and co-expression patterns using cBioPortal for Cancer Genomics (Cerami et al., 2012; Gao et al., 2013). The CERES dependency score (**Figure 3.4E**) is based on data from a cell depletion assay. A lower score indicates a higher likelihood that the gene of interest is essential in a given cell line. A score of 0 indicates a gene is not essential; correspondingly -1 is comparable to the median of all pan-essential genes (Meyers et al., 2017).

Cell Culture, Plasmids, Lentiviral Production and Transduction

Human UC cell lines (5637, HT-1197, HT-1376, TCCSUP, T24) were purchased from the American Type Culture Collection (ATCC), with the exception of Cal29 (DSMZ, cat. ACC-515). All cell lines were cultured in RPMI 1640 medium containing L-glutamine (ThermoFisher Scientific, cat. 11875-085) supplemented with 10% FBS (Gemini Bio-Products, cat. 900-108). Human single-guide RNAs (sgRNA) targeting *PPARG* #6 (cattacgaagacattccatt) and #9 (caactttgggatcagctccg) along with control gRNA targeting mouse *Rosa26* locus (aagatgggcgggagtcttct) were cloned into LentiCRISPRv2 plasmid (Sanjana et al., 2014). Mature antisense human *PPARG* shRNA #2 sequence (clone ID: TRCN0000001672) along with scrambled (SCR) control were cloned into a pLKO lentiviral plasmid. Lentivirus was prepared and cells were transduced as previously described (Sanchez et al., 2018). All experiments were performed with cells that survived puromycin selection and displayed knockdown/knockout of *PPARG* as assayed by Western blot.

PPARγ Agonists and Inhibitors

Rosiglitazone (Sigma-Aldrich, cat. R2408) was resuspended in DMSO to create a 1 mM stock solution and was used at a final concentration of 100 nM in all experiments. The PPARγ inverse-agonist T0070907 (Santa Cruz Biotechnology, cat. sc-203287) was resuspended in DMSO to create a 1 mM stock solution and was used at a final concentration of 100 nM in all experiments. An equivalent volume of DMSO was used as a control for all experiments involving PPARγ pharmacological agents.

Quantitative Real-Time PCR (qRT-PCR)

Total RNA was isolated using TRIzol reagent (ThermoFisher Scientific, cat. 15596026) and RNeasy mini kit (Qiagen, cat. 74104). Reverse transcription was performed using High-Capacity RNA-to-cDNA (Applied Biosystems, cat. 4387406). qRT-PCR was performed using ViiA7 Real-Time PCR system (Applied Biosystems) with TaqMan master mix (Life Technologies). TaqMan probes were used to quantitate expression of *PPARG* (cat. Hs01115513_m1), *FABP4* (cat. Hs01086177_m1), *PLIN2* (cat. Hs00605340_m1), SCD (cat. Hs01682761_m1), LPL (cat. Hs00173425_m1), PPARA (cat. Hs00947536_m1) and normalized to housekeeping gene *TBP* (Hs00427620_m1).

Western Blot and Immunohistochemistry

Western blot was performed as previously described (Sanchez et al., 2018). Primary antibodies were diluted 1:1000 in 5% w/v nonfat milk (except GAPDH, 1:10,000), and secondary antibodies were diluted 1:2000 in 5% w/v nonfat milk. PPARγ (cat. 2435), GAPDH (cat. 2118), and anti-Rabbit IgG, HRP-linked (cat. 7074) antibodies were purchased from Cell Signaling Technology.

Human bladder cancer tissue array was processed for immunohistochemistry by baking the slide in a dry oven for 20 minutes at 55°C. Slide was then deparaffinized by incubation in 100% xylene for 15 min, 2X, followed by rehydration in a series of washes from 100% ethanol (EtOH), 95% EtOH, 70% EtOH, 100% dH_2O for 5 min each. Slide was then boiled in antigen

unmasking solution (1M sodium citrate solution, pH 6.0) for 20 min, left to cool on bench for 20 min, and incubated in dH_2O for 20 min for further cooling. Endogenous peroxidase activity was blocked by transferring slide to 1% H_2O_2 solution for 30 minutes. Slide was washed in 1X TT buffer for 5 min, 3X, sample area was outlined with hydrophobic pen, and samples were incubated in blocking buffer (5% BSA, 2% goat serum diluted in 1X TT buffer) for 1 hr at RT. Samples were incubated overnight in PPARγ antibody diluted 1:200 in blocking buffer overnight at 4°C. The following day, slide was washed in 1X TT buffer for 5 min, 3X, and incubated in secondary antibody (1:200 biotinylated goat anti-Rabbit, diluted in 1X TT) for 1 hr at RT. Slide was further processed using Vectastain Elite ABC kit (Fisher Scientific, cat. PK6100) according to the manufacturer's instructions, and staining was visualized with DAB peroxidase substrate kit (Vector Laboratories, cat. SK4100). Slide was counterstained with hematoxylin and dehydrated before coverslipping and imaging.

Chromatin Immunoprecipitation (ChIP) and ChIP-seq

ChIP was performed with whole cell extracts isolated from 5637 parental cells using 2.5 μg PPARγ (Santa Cruz, cat. sc-7196), 2.5 μg RXRα/β/γ (Santa Cruz, cat. sc-774), or 2.5 μg Normal Rabbit IgG (Cell Signaling Technology, cat. 2729) antibodies for immunoprecipitation (IP). Briefly, confluent 10 cm dishes of cells were prepared by crosslinking with 1% formaldehyde for 15 minutes at room temperature (RT), and quenched with 125 mM glycine for 5 min at room temperature. Cells were harvested by scraping and pellets were resuspended in 200 μl SDS lysis buffer (50 mM HEPES/NaOH pH 7.5, 1% SDS, 10 mM EDTA, 1 mM PMSF, and Roche ULTRA protease inhibitor cocktail (cat. 05892791001)) on ice for 10 minutes. Sonication was performed using Bioruptor Pico (Diagenode, cat. B01060010) on high setting for 4 cycles of 30 seconds on, 30 seconds off, followed by centrifugation of lysates to remove cellular debris. 66 μl of sheared chromatin from each tube was then diluted 10X, with 5% saved as Input DNA and the rest prepared for either PPARγ, RXR, or IgG IP.

PPARγ IP, RXR IP, IgG IP and Input libraries were prepared in duplicate from two independent biological replicates. For ChIP-seq, sequencing data was mapped to the human genome (GRCh38) using STAR (Dobin et al., 2013) with parameters appropriate for ungapped alignments. Peaks were called for each sample with input samples as background by HOMER (Heinz et al., 2010). HOMER was also used for differential peak calling (PPARγ vs. Input and RXR vs. Input) and to annotate peaks to proximal genes as described in Ensembl v85 (http://www.ensembl.org/index.html). Motif enrichment analysis was performed using HOMER against the standard list of known motifs; *de novo* motif discovery included consideration of lengths 8,10,12,15,18 bp. For bioinformatics analyses displayed in Figure 3.6C-D, "high-confidence sites" were defined by the following criteria: peak score ≥ 10 (≥ 1 read per million) and RXR peak called with strict overlap. Gene ontology was performed using Metascape (metascape.org).

RNA-seq

Total RNA was isolated from four technical replicates of 5637 control, 100 nM T0070907-treated, *PPARG* sgRNA 6, and *PPARG* sgRNA 9 cell lines as described above. NEBNext Ultra II RNA Library Prep Kit for Ilumina was used for preparing ~250-300 bp insert cDNA, non-directional libraries according to manufacturer's instructions at Novogene Corporation (Sacramento, CA). Libraries were sequenced using the Ilumina platform with paired-end 150 bp sequencing at 20M raw reads/sample at Novogene. Raw sequence files (fastq) for 16 samples were mapped using Salmon (Patro et al., 2017) against the human transcripts described in GENCODE (version 28, built on the human genome GRCh38.p12). Transcript counts were summarized to the gene level using tximport (Soneson et al., 2015), and normalized and tested for differential expression using DESeq2 (Love et al., 2014). Statistics for each contrast of interest were exported for further analysis. Genes used for gene ontology met the following criteria: significantly up- or down-regulated by inverse-agonist or CRISPR treatment at least 1.5-fold with padj < 0.05. Gene ontology was performed using Metascape (metascape.org).

Annexin V-PI Apoptosis Assay

5,000 cells of each cell line were plated in triplicate on 6-well plates. Cells were treated for 8 days with media containing DMSO or 100 nM T0070907, and then prepared using the FITC–Annexin V, PI Kit (BD Biosciences, cat. 556547) according to the manufacturer's instructions. Flow cytometry was performed using the BD Accuri C6 instrument, with viable cells represented as the double-negative population.

Proliferation Assay

25,000 cells of control gRNA, *PPARG* sgRNA #6, or *PPARG* sgRNA #9 UC cell lines were plated in triplicate on 6-well plates. The following day (represented as Day 0), cells were trypsinized and counted using the Countess Automated Cell Counter (Invitrogen, cat. C10281), as per the manufacturer's instructions with Trypan blue. Cells were then counted again at the indicated timepoints, and fresh media was added every two days.

Clonogenic Growth Assay

5,000 cells of each cell line were plated in triplicate on 6-well plates. The next day, media containing either 100 nM T0070907 or an equivalent volume of DMSO was added to the wells in triplicate. UC cells were treated with DMSO or T0070907 for 9 days (with the exception of T24, 5 days) with fresh medium supplied every 2 days. At the end of the experiment, cells were washed in PBS and stained with crystal violet solution (0.5% crystal violet in 20% methanol) for 10 minutes. Plates were then washed twice with PBS and allowed to dry before imaging. Quantitation was performed by adding 500 μL methanol to dry wells and incubating at RT with rocking for 20 minutes. Absorbance was read using a spectrophotometer at 570 nm, and data are represented as fold change relative to DMSO readings.

Cell Cycle Analysis

5,000 cells of the 5637 cell line were plated on 6-well plates. The following day, cells were serum starved for 24 hours to synchronize the population, after which media containing DMSO and 100 nM T0070907 were added to triplicate wells. Cells were harvested after 5 days of drug treatment, fixed using ice-cold 70% ethanol, and stored at -20°C for 2 hours. Following centrifugation and removal of ethanol, cells were washed twice in FACS buffer (PBS containing 2% FBS and 1 mM EDTA). For dual Ki67/PI staining to determine non-proliferative (G_0 population): samples were resuspended in 200 μL FACS buffer and stained for 30 minutes at RT in the dark with Ki67-FITC monoclonal antibody (SolA15) (Life Technologies, cat. 11-5698-82) at 1:100. Cells were then washed twice with FACS buffer and resuspended in 500 μL PI staining solution (PBS containing 50 μg/mL PI, 100 μg/mL RNAse A and 2 mM $MgCl_2$). Cells were strained through 40 μm filters and incubated at RT in the dark for 20 minutes before analysis by flow cytometry. For analysis of the cell cycle phases, cells were stained with PI antibody only.

Adipogenesis Assay

250,000 NIH-3T3 cells (ATCC) were infected with MSCV-retroviral empty vector or vector containing *PPARG* cDNA resistant to shRNA #2 on 10 cm dishes. When cells were confluent, induction medium was added to the plates for 48 hours (DMEM containing 10% FBS supplemented with 125 nM indomethacin, 0.5 mM isobutylmethylxanthine (IBMX), 1 mM dexamethasone, 20 nM insulin, and 1 μM rosiglitazone). After 48 hours, medium was changed to DMEM containing 10% FBS supplemented with 20 nM insulin and 1 μM rosiglitazone. Medium was changed every 2 days until plates were harvested on day 10 after induction and stained with oil red o to visualize adipogenesis. Oil red o staining was performed as previously described (Sanchez et al., 2018).

Statistics

Statistical analyses were performed in Microsoft Excel using Student's two-tailed, unpaired t-test. Data are presented as mean ± SD of at least three independent experiments.

Statistical significance was defined as *** ($p < 0.001$), ** ($p < 0.01$), * ($p < 0.05$), n.s. = not significant.

3.4 Results

3.4.a Characterization of PPARγ expression in bladder urothelial carcinoma

Genomic sequencing data available from The Cancer Genome Atlas (TCGA) revealed that 21% of UC tumors have genomic amplification and/or mRNA upregulation of *PPARG*, and that 11-14% display genomic amplification and/or activating mutation in *RXRA*, the obligate heterodimer of PPARγ, in a largely mutually-exclusive pattern (**Figure 3.1A**). To validate that the effects on *PPARG* mRNA abundance translated to protein expression, we performed immunohistochemistry for PPARγ on 60 independent UC patient samples from a commercially available tissue array (**Figure 3.1B**). Surprisingly, our analysis revealed that nearly 50% of UC tissues stained positive for PPARγ nuclear accumulation, while normal bladder epithelium was entirely negative (**Figure 3.1C-D**). Consistent with the pattern observed in primary patient samples, analysis of Cancer Cell Line Encyclopedia (CCLE) data demonstrated that across all tumor types, *PPARG* mRNA expression was significantly elevated in human cancer cell lines derived from the urinary tract (**Figure 3.1E**).

3.4.b Pharmacological inhibition of PPARγ reduces growth of a subset of bladder urothelial carcinoma cell lines *in vitro*

In agreement with previously published data (Biton et al., 2014; Goldstein et al., 2017), treatment of a number of human UC cell lines with the PPARγ inverse agonist, T0070907, decreased clonogenic growth over the course of six to ten days (**Figure 3.2A-B**). We confirmed that treatment with T0070907 affected gene expression at the concentration administered by assessing the expression of two PPARγ target genes, *PLIN2* and *FABP4*, by qPCR in the 5637 cell line (**Figure 3.3A**). The cell lines which displayed the largest decrease in proliferation, 5637 and HT-1197, are notable in that they display *PPARG* genomic amplification and a RXRα

p.S427F predicted activating mutation (Halstead et al., 2017), respectively. We next performed flow cytometry-based, Annexin V-propidium iodide (PI) staining to determine the effect of the PPARγ inverse-agonist on cell viability. Long-term treatment of six UC cell lines with T0070907 did not decrease viability of cells relative to control (**Figure 3.2C**), suggesting that reduced cell number following pharmacological inhibition of PPARγ may result from cell cycle arrest rather than induction of cell death (Biton et al., 2014). To test this, we performed PI staining on 5637 cells treated with T0070907 for 5 days to analyze the percentage of cells within each phase of the cell cycle. Treatment with PPARγ inverse-agonist significantly increased the percentage of cells in G_1 phase and reduced the G_2/M phase population relative to control (**Figure 3.2D, Figure 3.3B**). Additionally, we determined that T0070907 increased the percentage of cells in G_0 phase relative to control 4-fold (**Figure 3.2E**) after seven days of treatment. These results suggest that pharmacological inhibition of PPARγ reduces cell cycle progression in a subset of UC.

3.4.c Genetic inhibition of PPARγ reduces growth of several bladder urothelial carcinoma cell lines *in vitro*

To validate the effects observed by pharmacological inhibition of PPARγ, we next depleted PPARγ protein from the panel of sensitive UC cell lines using two independent sgRNA using the CRISPR-Cas9 gene editing system. PPARγ depletion via CRISPR also inhibited the proliferation of these UC cell lines *in vitro* (**Figure 3.4A-B**, **Figure 3.5A**), in a similar manner to that observed through pharmacological PPARγ inhibition. Indeed, *PPARG* KO also resulted in a block in cell cycle progression in the 5637 cell line (**Figure 3.4C-D**), increasing the percentage of cells in G_1 and lowering the G_2/M phase population relative to control knockout. Furthermore, we employed an shRNA-resistant *PPARG* cDNA to validate the effects of PPARγ depletion on cell growth in UC (**Figure 3.5B-C**), and we confirmed functionality of the shRNA-resistant *PPARG* cDNA by its ability to induce adipogenesis in NIH-3T3 cells when cultured in the presence of adipogenic stimuli (**Figure 3.5D**). These data confirm the sensitivity of a subset of urinary tract-

derived tumors to *PPARG* knockdown *in vitro*, as predicted from CCLE Achilles heel shRNA and CRISPR screens (**Figure 3.4E**) (Barretina et al., 2012; Meyers et al., 2017).

3.4.d Genome-wide analysis of PPARγ-RXR binding and gene regulation in UC

To investigate PPARγ occupancy genome-wide in UC, we performed chromatin immunoprecipitation followed by deep sequencing (ChIP-seq) in the 5637 cell line for PPARγ, RXR, and IgG and Input controls (**Figure 3.6A,** pre-sequencing ChIP validation shown in **Figure 3.7A**). Additionally, we confirmed PPARγ and RXR binding at several strong binding sites by ChIP-qPCR (**Figure 3.7B-C, Table 1**). *De novo* motif analysis revealed that the majority of PPARγ-RXR binding in UC cells occurs at the direct repeat 1 (DR1) nuclear receptor motif (**Figure 3.6B**), consistent with binding patterns in other cell types including adipocytes, macrophages (Lefterova et al., 2010), lung adenocarcinoma (Srivastava et al., 2014), and clear cell renal cell carcinoma (ccRCC) (Sanchez et al., 2018). A previous report demonstrated that the transcription factors FOXA1, GATA3, and PPARγ are major molecular drivers of the luminal subtype of UC (Warrick et al., 2016), but did not investigate whether these proteins work coordinately based on proximal DNA binding to promote a luminal vs. basal state. Our data indicate that FOXA1, GATA3, and PPARγ likely regulate distinct genes in UC, based on the fact that neither FOXA1 nor GATA3 motifs were enriched at PPARγ-RXR binding sites (**Figure 3.6B**). In agreement with this, the DR1 motif was not enriched under FOXA1 occupied regions in the luminal RT4 bladder cancer cell line (Warrick et al., 2016). PPARγ-RXR heterodimers were predominantly located in intergenic and intronic regions of the genome at 46.08% of sites and 42.37% of sites, respectively (**Figure 3.6C**). To begin to elucidate the transcriptional programs regulated by PPARγ in UC, we annotated PPARγ-RXR binding sites to the nearest gene and performed gene ontology (GO) for 2581 genes. We found that GO pathways involved in migration, adhesion, and regulation of transmembrane receptor tyrosine kinase signaling were most highly represented among this gene set (**Figure 3.6D**).

To determine the effects of PPARγ inhibition on gene expression, we performed RNA-seq in the 5637 cell line with four experimental conditions involving either inverse-agonist treatment or gene knockout by two *PPARG* sgRNA (**Figure 3.6E**). As the knockout of *PPARG* was incomplete at the protein level for sgRNA 9 (**Figure 3.6E**), we proceeded to narrow our targets of interest based on overlap between inhibitor treatment and *PPARG* KO by sgRNA 6. Significantly altered genes by both *PPARG* CRISPR knockout and inhibitor were enriched in pathways related to inflammatory response (**Figure 3.6F**), including leukocyte chemotaxis, response to tumor necrosis factor, and response to lipopolysaccharide. Importantly, we confirmed that six chemokines whose expression increased following PPARγ inhibition (**Figure 3.8A**) did not have PPARγ-RXR binding sites within 200 kb of the TSS (data not shown). These results suggest that the inflammatory response inhibited by active PPARγ signaling is likely mediated by an independent transcriptional program such as NF-κB in UC. However, this is unlikely to occur through direct transrepression of NF-κB targets by PPARγ, as was previously suggested (Korpal et al., 2017).

We predict that PPARγ targets of interest in regulating UC proliferation fall into a list of 30 protein-coding genes significantly downregulated at least 1.5-fold (padj < 0.05) by both inhibitor treatment and *PPARG* KO by sgRNA 6 (**Figure 3.9C**). Of the 30 genes, 7 had a significant positive association with *PPARG* expression in RNA-seq data from 126 primary bladder urothelial carcinoma samples (Network, 2014; Robertson et al., 2017). One of the most downregulated genes among all groups in our dataset was sonic hedgehog (*SHH*), a regulator of embryonic development and maintenance of tissue polarity (Rimkus et al., 2016; Villavicencio et al., 2000) (**Figure 3.8B**). PPARγ-RXR heterodimers bind several locations up and downstream of SHH within a 200 kb window (**Figure 3.8C**). Functionally, *SHH*-expressing cells were shown to give rise to MIBC in a carcinogen-induced mouse model (Shin et al., 2014a), but its connection to PPARγ signaling has not yet been described. Another gene of interest is proline-rich 15 (*PRR15*), also significantly downregulated following PPARγ inhibition in all three experimental conditions with two PPARγ-RXR binding sites within a 200 kb window of the gene (**Figure 3.8D-E**).

Importantly, *PRR15* exhibited a strong positive correlation with *PPARG* expression in primary patient samples according to TCGA data (**Figure 3.8F**). Although PRR15 function is currently unknown, high mRNA expression was observed in murine and human colorectal carcinoma samples bearing mutations in the *APC* gene (Meunier et al., 2011). *PRR15* expression in tumors from $Apc^{Min/+}$ mice co-localized with Ki67 and histone H3 positivity, and elevated levels were associated with advanced tumor stage in human colorectal cancer. Furthermore, another recent study demonstrated that PRR15 is required for ovine and human trophoblast viability and survival (Gates et al., 2017). These data lead us to speculate that genes such as *SHH* and *PRR15* are associated with PPARγ-dependent proliferation and cell cycle progression in bladder urothelial carcinoma.

3.5 Discussion

Active PPARγ-RXR signaling has been implicated as a molecular signature of luminal MIBC, yet the cell-autonomous mechanisms by which PPARγ contributes to UC growth are incompletely understood. In this study, we confirmed that treatment of UC cell lines with PPARγ inverse-agonist T0070907 reduced growth *in vitro* as previously reported (Goldstein et al., 2017), and demonstrated that pharmacological inhibition of PPARγ results in reduced cell cycle progression rather than induction of apoptosis. The block in the G_1 phase of the cell cycle observed following treatment with inverse-agonist was also replicated by genetic knockout of *PPARG* by CRISPR-Cas9. To further elucidate the effects of genetic and pharmacological inhibition of PPARγ signaling in UC, we performed ChIP- and RNA-seq to identify commonly deregulated pathways. Our findings corroborate recently published data showing an inverse correlation between PPARγ activity and immune infiltration in UC (Korpal et al., 2017), and also reveal novel PPARγ-RXR transcriptional targets which may be responsible for promoting growth in UC.

Interestingly, lipid and glucose metabolism-related pathways were not among the most highly enriched pathways in our ChIP-seq dataset, suggesting that the PPARγ-RXR cistrome is

distinct in UC relative to other cell types including adipocytes and ccRCC (Lefterova et al., 2008; Sanchez et al., 2018). However, analyses of downregulated genes comparing control to either PPARγ inhibitor-treated or *PPARG* sgRNA 6-treated cells suggest that some "canonical" targets are affected in UC, as evidenced by downregulation of several targets within the KEGG hsa03320: PPAR signaling pathway (*FABP5*, *PLIN2*, *LPL*, *SCD*) by both manipulations (**Figure 3.9C**). The absence of widespread alterations in gene expression involved in lipid and glucose metabolism pathways may be explained by the lack of C/EBP transcription factor co-occupancy with PPARγ in this cistrome. We hypothesize that the targets most important for UC proliferation are related to extracellular matrix organization (matrisome associated), adhesion, and cytokine-mediated signaling pathways (**Figure 3.6D-F**). Future studies performing ChIP-seq in primary urothelial carcinoma tissue would be beneficial to validate the genomic occupancy patterns observed in the 5637 cell line, and to further correlate genomic binding with PPARγ-responsive genes *in vivo*.

Based on our ChIP- and RNA-seq data, we propose *SHH* as a novel target gene of PPARγ in UC. Briefly, SHH is a signaling effector that binds extracellularly to the transmembrane receptor Patched (PTCH). The PTCH-SHH interaction inactivates the 7-pass transmembrane receptor Smoothened, which allows for the transcription factor GLI1 to translocate to the nucleus and regulate genes involved in proliferation and stem cell self-renewal (Rimkus et al., 2016). *SHH* expression has a weak, yet statistically significant positive association with *PPARG* expression in primary patient samples according to TCGA data, and treatment of the 5637 cell line with the PPARγ agonist rosiglitazone increased expression of this gene 4-fold relative to control. Our gain- and loss-of-function experiments suggest that *SHH* is a direct target gene of PPARγ in the 5637 *in vitro* cell culture model of UC (**Figure 3.9A-B**). The varied levels of natural endogenous ligands of PPARγ *in vitro* and *in vivo* certainly affect gene expression, and is an important consideration when trying to identify targets likely to be most relevant to the human disease. Functionally, *SHH* has been implicated in normal bladder development and in the maintenance of bladder cancer stemness (Syed et al., 2016). SHH positivity is also associated with the luminal-papillary subclass

of MIBC, the same as PPARγ (Robertson et al., 2017). However, the role of the SHH pathway in UC is controversial, with reports indicating both pro- (Islam et al., 2016; Nedjadi et al., 2018) and anti-tumorigenic (Shin et al., 2014b) roles in UC initiation and progression. The relationship between PPARγ signaling, *SHH* expression, and UC proliferation remains to be further clarified.

Another putative PPARγ target of interest based on our ChIP-seq, RNA-seq, and gene expression data from primary samples is *PRR15*. *PRR15* knockdown reduced the expression of a number of pro-proliferative cell cycle genes including *CCND1* and *CDK6* and increased the expression of anti-proliferative genes *CCNG2* and *CDKN1A* in a human trophoblast cell line (Gates et al., 2017). However, its role and expression patterns in UC have not been previously described. In conclusion, our study supports a cell-autonomous, pro-oncogenic role for PPARγ signaling in luminal bladder urothelial carcinoma and provides a candidate list of target genes responsible for these phenotypes from the intersection of *in vitro* genome-wide approaches and *in vivo* primary patient sequencing data.

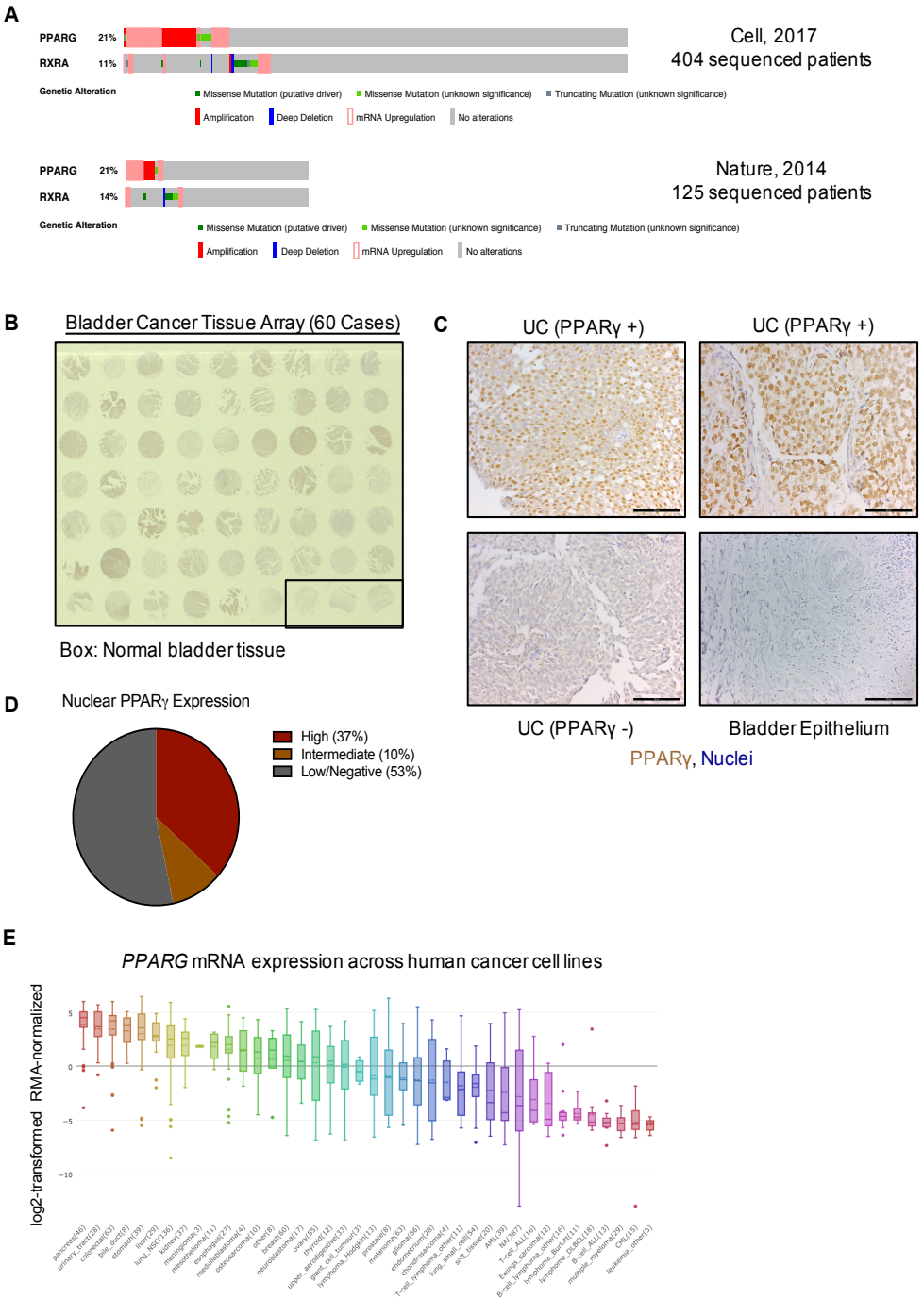

Figure 3.1 – Characterization of PPARγ expression in bladder urothelial carcinoma (UC)
(A) Frequency of copy number, mutational, and gene expression alterations in *PPARG* and *RXRA* from primary UC tumors. n = 529 patients (cBioPortal). **(B)** Immunostaining of PPARγ in tissue array of 60 primary UC tumors and healthy bladder tissue. **(C)** High-magnification images of PPARγ staining in primary UC tumors and healthy bladder tissue. Scale bar = 100 μm. **(D)** Quantification of PPARγ nuclear expression in primary UC tumors. **(E)** *PPARG* mRNA expression patterns across human cancer cell lines documented by the Cancer Cell Line Encyclopedia (CCLE).

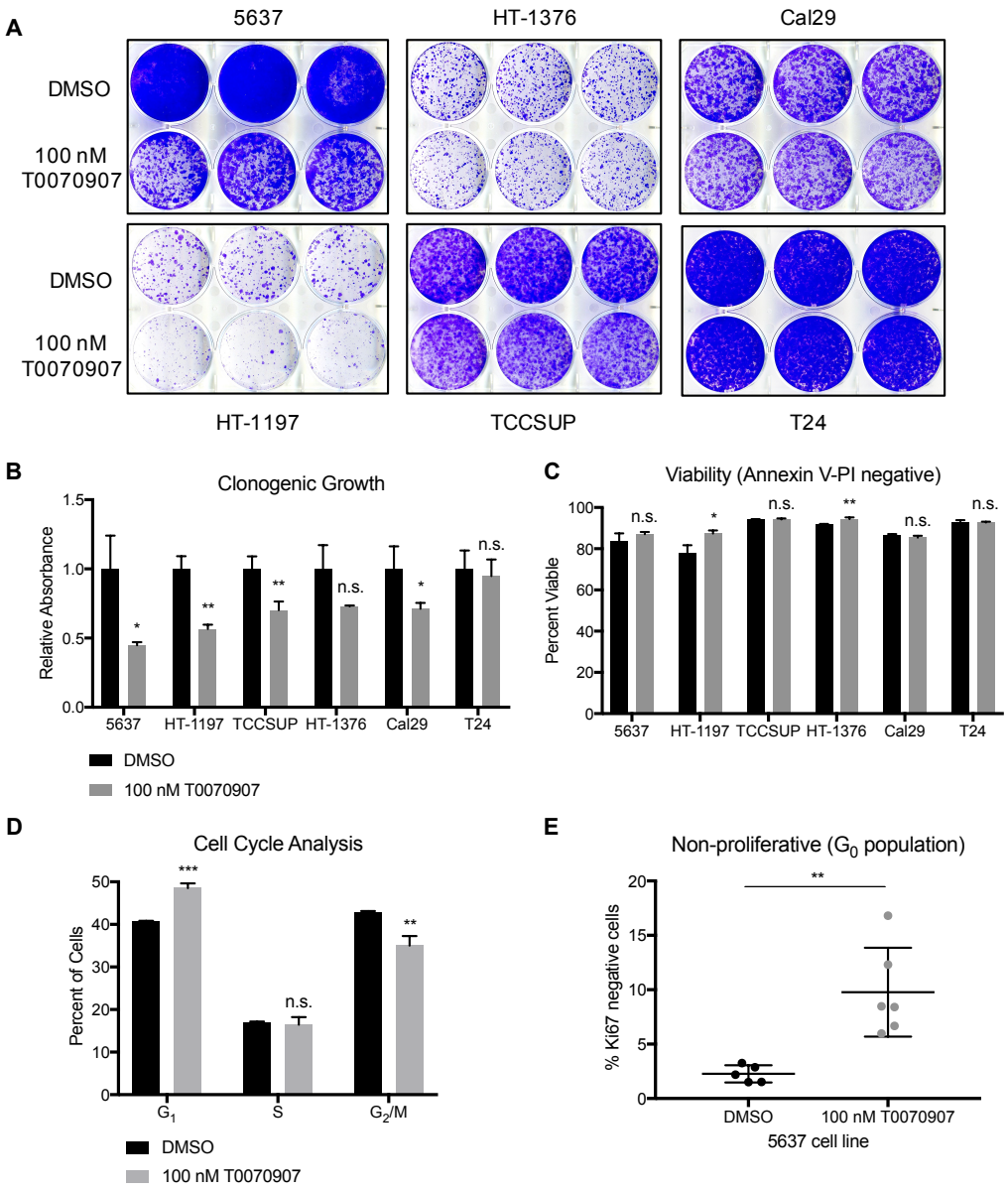

Figure 3.2 – Pharmacological inhibition of PPARγ reduces growth of a subset of UC cell lines *in vitro*

(A) Clonogenic growth of UC cell lines treated with DMSO or 100 nM T0070907 in long-term culture assayed by crystal violet staining. **(B)** Quantification of crystal violet staining in panel (A), depicted as relative absorbance compared to DMSO. ** ($p < 0.01$), * ($p < 0.05$), n.s. = not significant. **(C)** Annexin V–PI double-negative population of UC cell lines treated with DMSO or 100 nM T0070907 in long-term culture, determined by flow cytometry. ** ($p < 0.01$), * ($p < 0.05$), n.s. = not significant. **(D)** Percentage of 5637 cells in each phase of the cell cycle following DMSO or 100 nM T0070907 treatment, determined by flow cytometry staining of propidium iodide. *** ($p < 0.001$), ** ($p < 0.01$), n.s. = not significant. **(E)** Percentage of $Ki67^{-}/PI^{+}$ 5637 cells following DMSO or 100 nM T0070907 treatment, determined by flow cytometry. ** ($p < 0.01$).

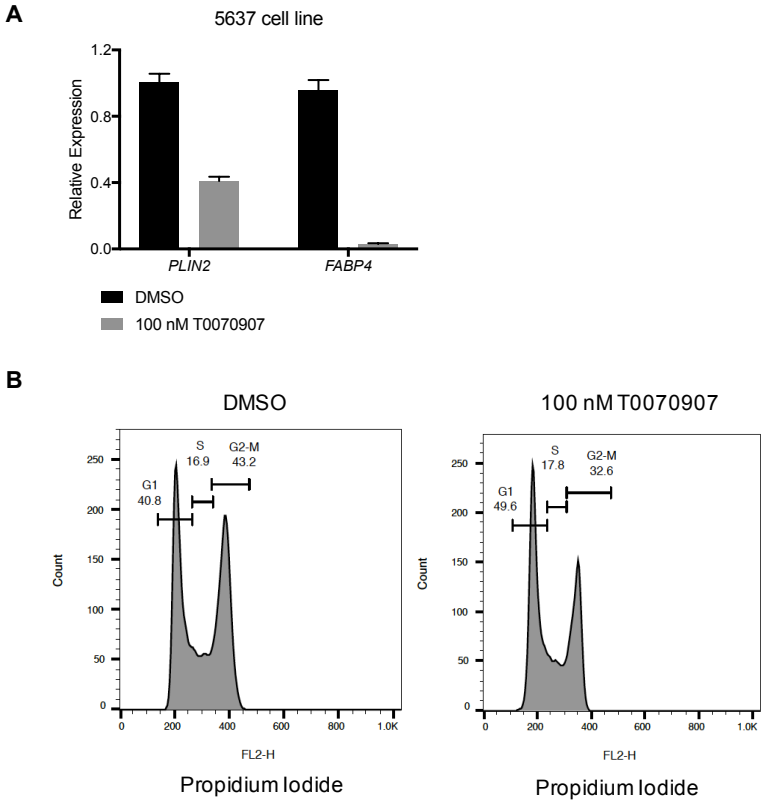

Figure 3.3 Effect of pharmacological PPARγ inhibition on gene expression and cell cycle progression
(A) qPCR for PPARγ target genes *PLIN2* and *FABP4* following 48 hrs of DMSO or 100 nM T0070907 treatment in 5637 cells. **(B)** Representative flow cytometry plots of data displayed in Figure 3.2D.

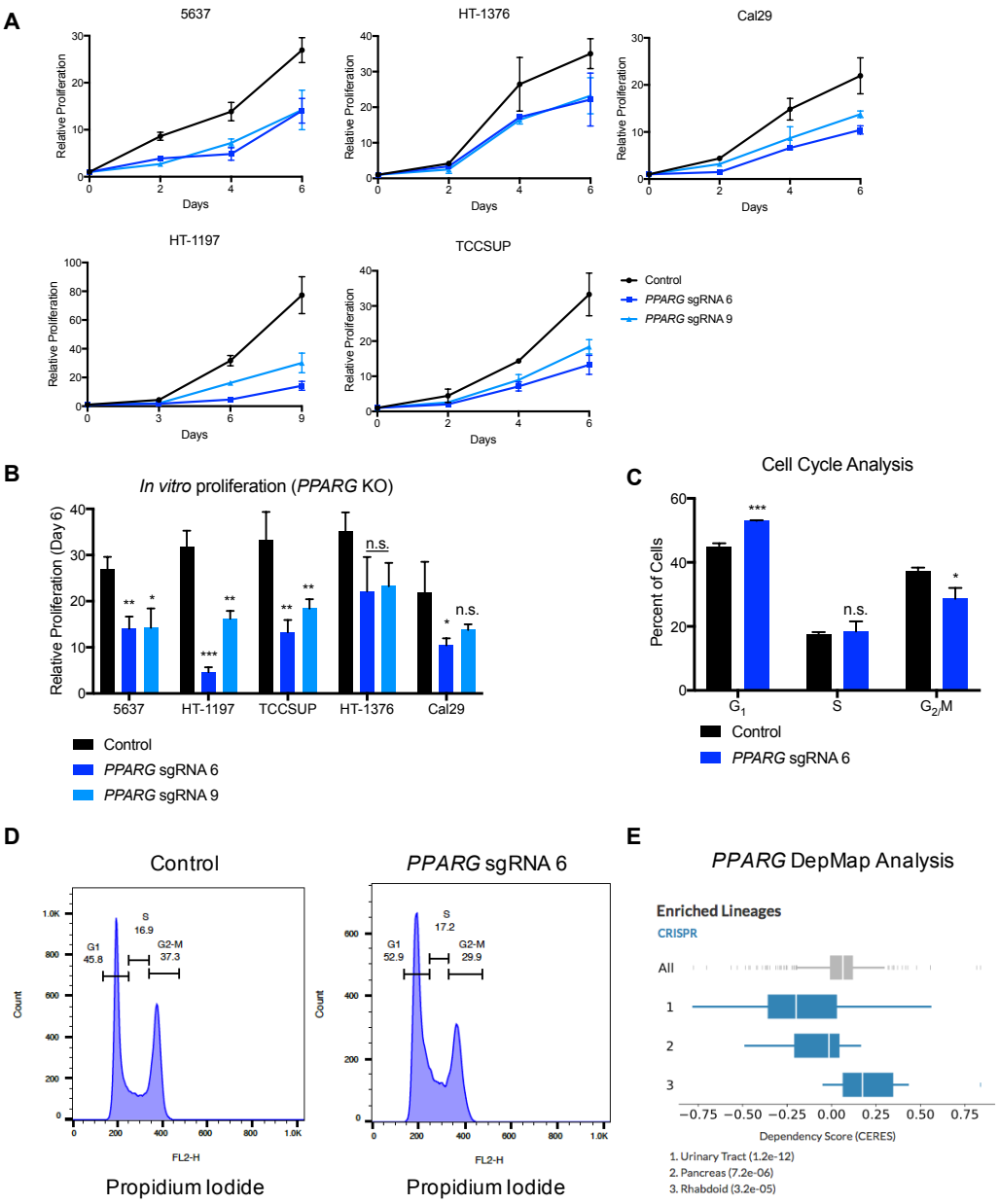

Figure 3.4 – Genetic inhibition of PPARγ reduces growth of several UC cell lines *in vitro*
(A) Growth curves of control, *PPARG* sgRNA 6, and *PPARG* sgRNA 9 (*PPARG KO*) UC cell lines over the course of 6-9 days. Values are normalized to cell count of each line at the Day 0 timepoint. **(B)** Relative proliferation of *PPARG* KO to control cell lines at day 6 of the growth curves from panel (A). *** ($p < 0.001$), ** ($p < 0.01$), * ($p < 0.05$), n.s. = not significant. **(C)** Percentage of control and *PPARG* KO 5637 cells in each phase of the cell cycle, determined by flow cytometry staining of propidium iodide. *** ($p < 0.001$), * ($p < 0.05$), n.s. = not significant. **(D)** Representative flow cytometry plots of data displayed in panel (C). **(E)** DepMap analysis of *PPARG* CRISPR knockout in CCLE cell lines. A lower CERES score indicates that a given lineage is more sensitive to *PPARG* depletion.

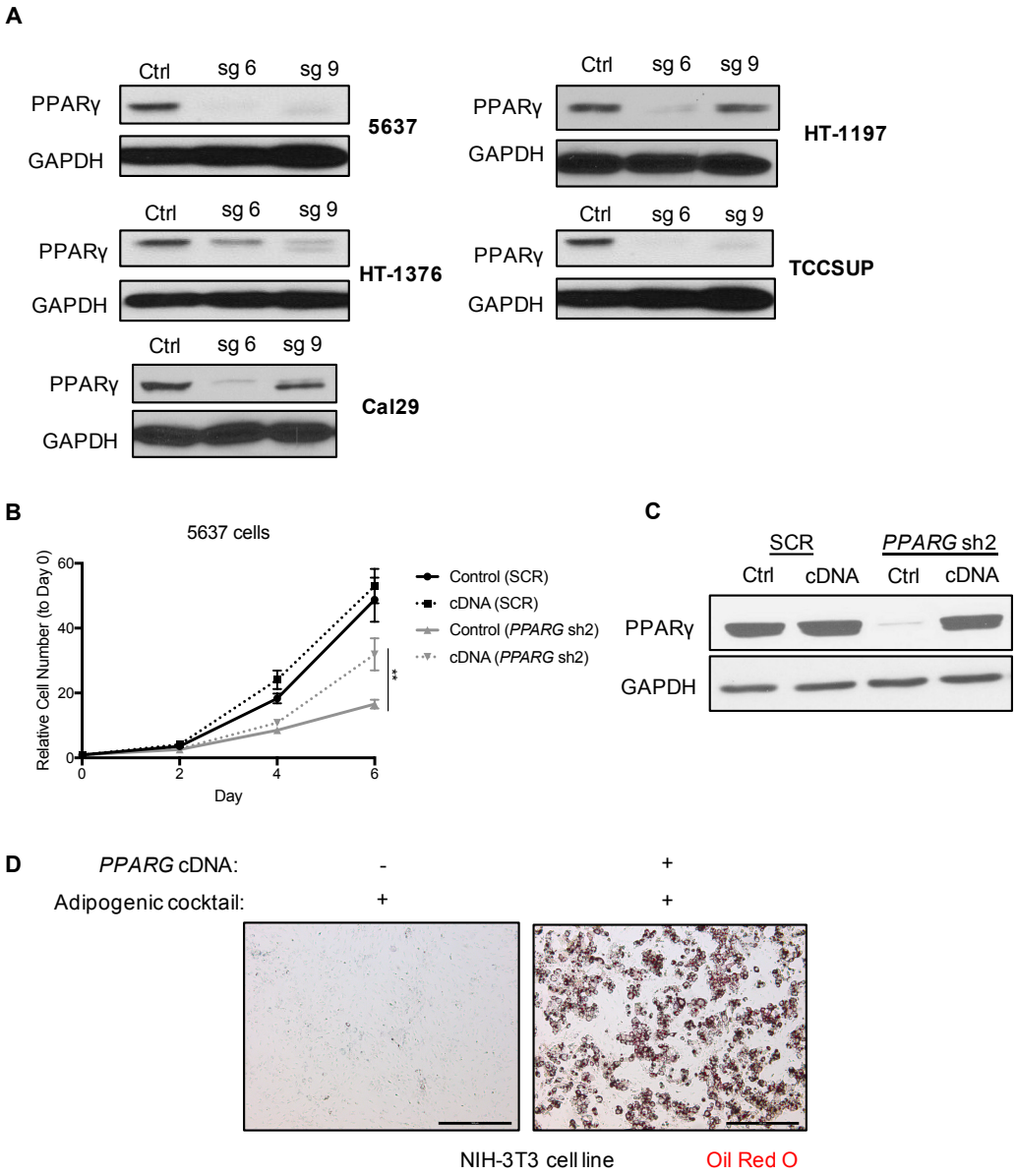

Figure 3.5 – Validation of *PPARG* CRISPR knockout and shRNA rescue experiment
(A) Western blot for PPARγ expression in control, *PPARG* sgRNA 6 and *PPARG* sgRNA 9 UC cell lines. **(B)** Growth curve of *PPARG* shRNA rescue experiment in 5637 cells. **(C)** Western blot of PPARγ levels in 5637 cells following addition of empty vector (control) or *PPARG* shRNA-resistant cDNA (cDNA) and expression of either SCR or *PPARG* shRNA #2. **(D)** Oil red o staining of NIH-3T3 cells expressing either empty vector or *PPARG* shRNA-resistant cDNA and treated with adipogenic cocktail.

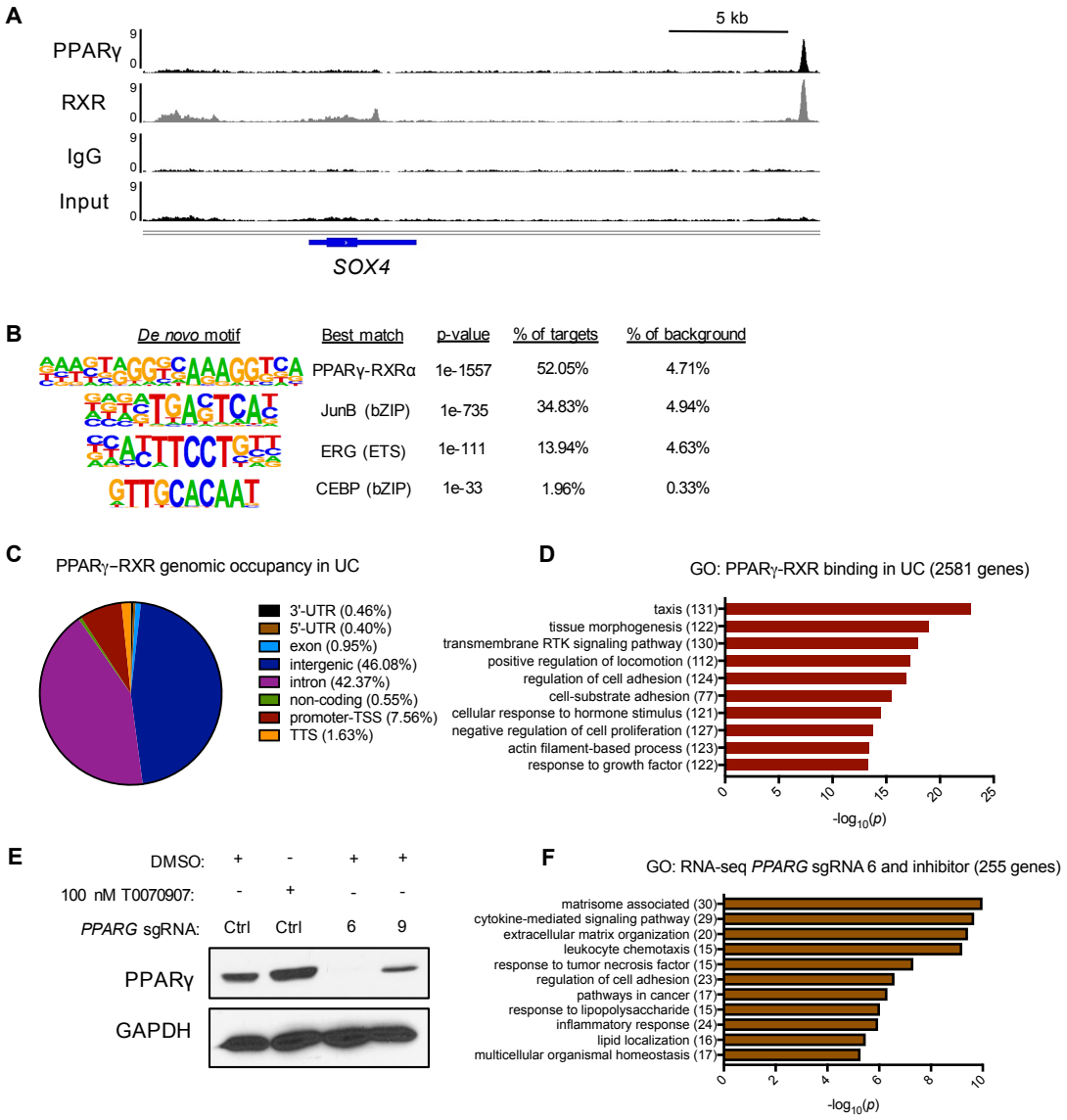

Figure 3.6 – Genome-wide analysis of PPARγ-RXR binding and gene regulation in UC
(A) ChIP-seq tracks of PPARγ, RXR, IgG and Input, showing PPARγ-RXR occupancy ~22 kb downstream of *SOX4*. **(B)** *De novo* motif analysis of PPARγ-RXR binding sites in UC. **(C)** PPARγ-RXR genomic occupancy in UC, defined by HOMER annotate peaks. For bioinformatics analyses displayed in panels C and D, sites were defined by the following criteria: peak score ≥ 10 (≥ 1 read per million) and RXR peak called with strict overlap. **(D)** Gene ontology of PPARγ-RXR binding sites in UC, annotated to the nearest gene. **(E)** RNA-seq experimental design and Western blot for PPARγ expression following 100 nM T0070907, *PPARG* sgRNA 6 or *PPARG* sgRNA 9. **(F)** Gene ontology of significantly altered genes by both 100 nM T0070907 treatment and KO by *PPARG* sgRNA 6.

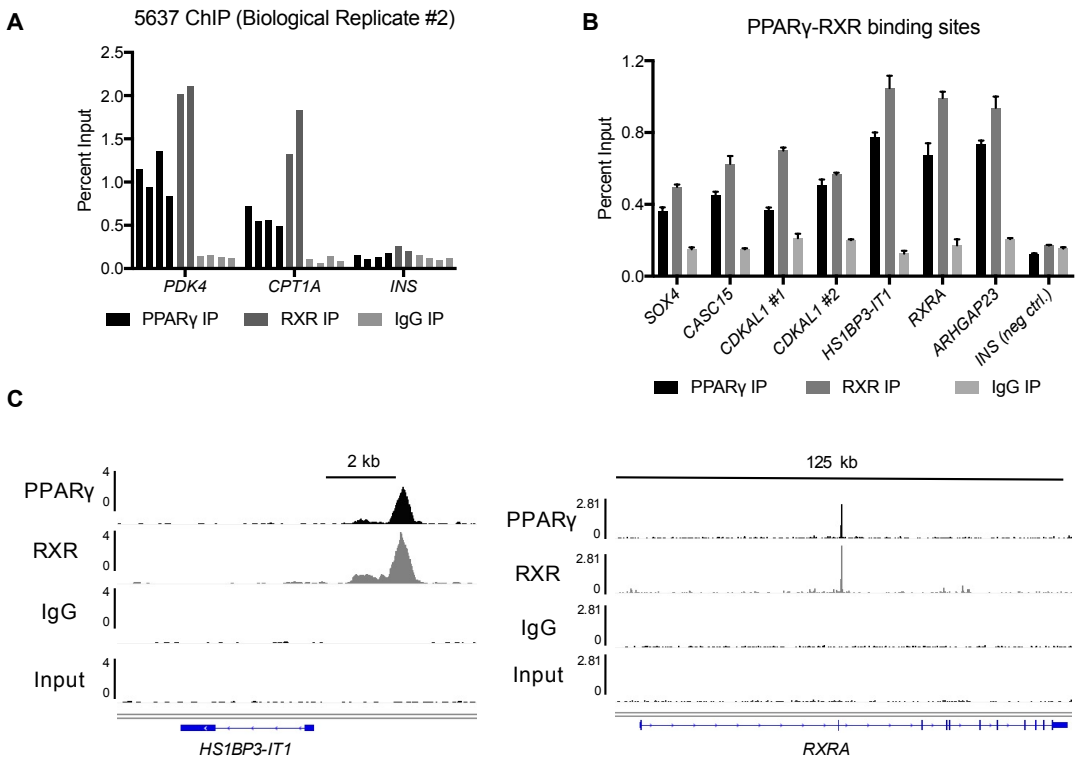

Figure 3.7 – Validation of ChIP-seq data from the 5637 cell line
(A) PPARγ, RXR, and IgG enrichment at enhancer sites near *PDK4* and *CPT1A* (*INS*, negative control) in 5637 cells, assayed by ChIP-qPCR. **(B)** ChIP-qPCR for PPARγ, RXR, and IgG enrichment at top binding sites identified by ChIP-seq. **(C)** ChIP-seq tracks of PPARγ, RXR, IgG and Input, showing PPARγ-RXR occupancy ~2 kb upstream of *HS1BP3-IT1*. ChIP-seq tracks of PPARγ, RXR, IgG and Input, showing PPARγ-RXR occupancy at *RXRA* intronic enhancer site.

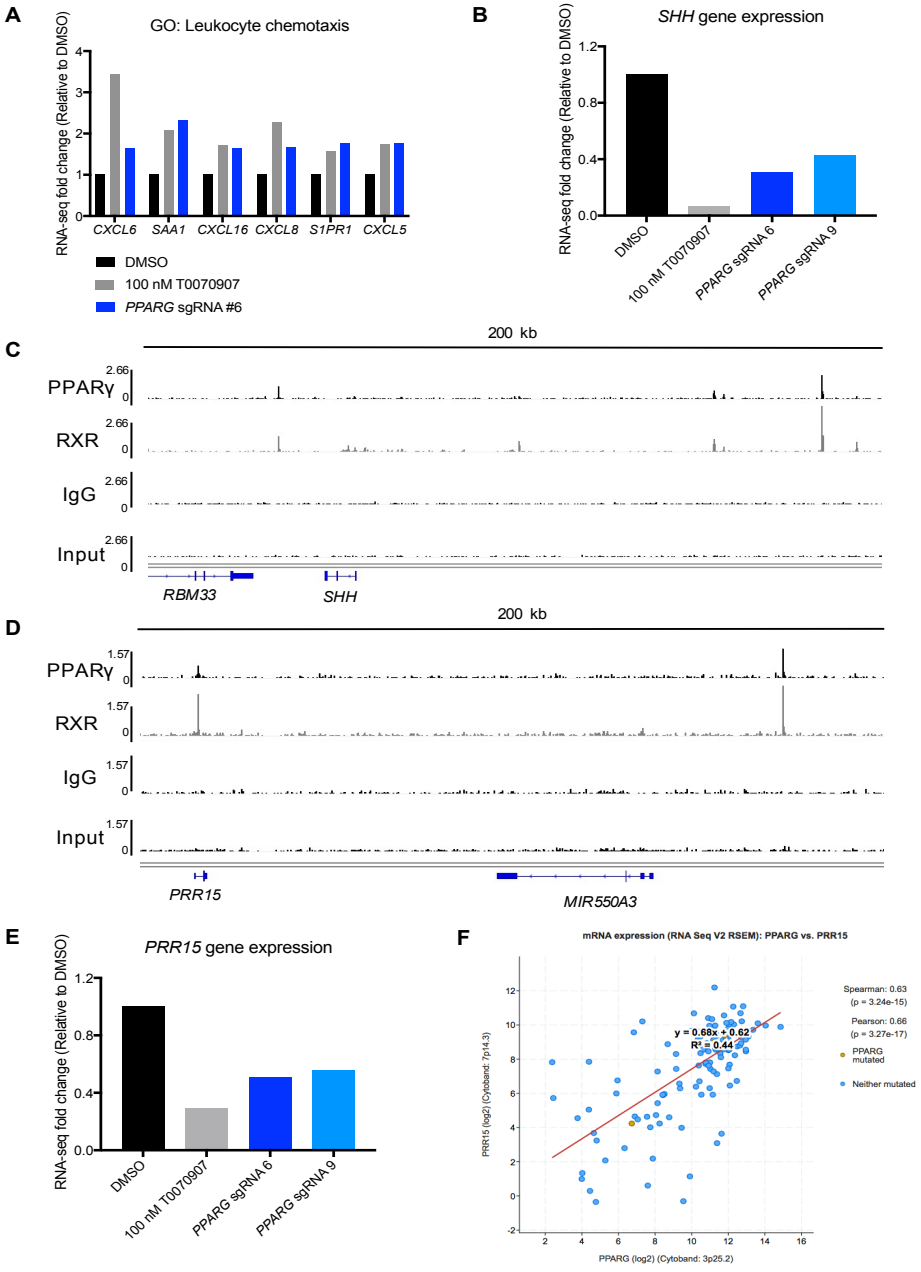

Figure 3.8 – Identification of PPARγ target genes of interest from ChIP-seq and RNA-seq data

(A) RNA-seq gene expression changes for select GO category: leukocyte chemotaxis genes following 100 nM T0070907 or *PPARG* sgRNA 6, relative to DMSO. **(B)** *SHH* gene expression data from RNA-seq in 100 nM T0070907, *PPARG* sgRNA 6, and *PPARG* sgRNA 9, relative to DMSO. **(C)** ChIP-seq tracks of PPARγ, RXR, IgG and Input, showing PPARγ-RXR occupancy within 200 kb of *SHH*. **(D)** ChIP-seq tracks of PPARγ, RXR, IgG and Input, showing PPARγ-RXR occupancy within 200 kb of *PRR15*. **(E)** *PRR15* gene expression data from RNA-seq in 100 nM T0070907, *PPARG* sgRNA 6, and *PPARG* sgRNA 9, relative to DMSO. **(F)** Co-expression data for *PPARG* and *PRR15* in UC tumors from the TCGA provisional dataset (cBioPortal).

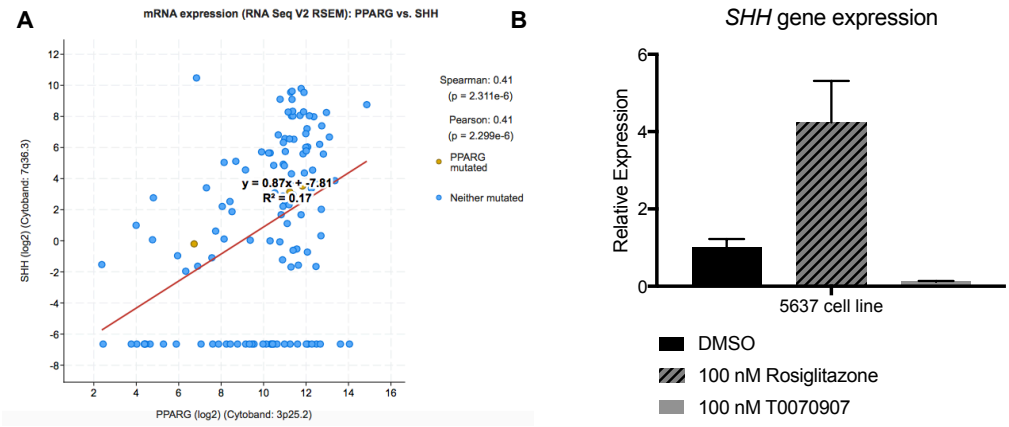

C

		CTT_v_CTD		CR6_v_CTD		CR9_v_CTD	
Ensembl Stable ID	Gene name	log2FoldChange	CTT_v_CTD padj	log2FoldChange	CR6_v_CTD padj	log2FoldChange	CR9_v_CTD padj
ENSG00000099194	SCD	-1.84836	4.75E-32	-0.967383	1.31E-08	-0.752986	3.78E-05
ENSG00000164687	FABP5	-0.99932	4.64E-22	-0.643733	6.05E-09	-0.495873	2.96E-05
ENSG00000112769	LAMA4	-1.61257	4.18E-35	-1.02366	5.47E-14	-0.627017	3.51E-05
ENSG00000152661	GJA1	-1.07888	2.00E-35	-0.964049	5.57E-28	-0.699964	1.50E-14
ENSG00000147872	PLIN2	-1.81531	1.33E-71	-0.719112	1.49E-11	-0.346714	0.008121
ENSG00000175445	LPL	-0.689581	0.000155974	-0.642038	0.00112915	-0.507711	0.0223404
ENSG00000145819	ARHGAP26	-0.974373	2.95E-06	-0.699078	0.00319829	-0.338475	0.346469
ENSG00000139668	WDFY2	-1.10349	0.000942173	-0.882333	0.0209325	-0.44463	0.450809
ENSG00000166582	CENPV	-1.09435	3.02E-13	-0.723569	9.47E-06	-0.471268	0.0148911
ENSG00000272410	AC022384.1	-0.733766	0.029615	-1.26105	5.31E-05	-0.406835	0.459134
ENSG00000164690	SHH	-3.85968	8.48E-10	-1.70939	0.0220824	-1.21403	0.199725
ENSG00000186205	MARC1	-0.872443	2.55E-05	-0.67909	0.00324381	-0.579206	0.0234548
ENSG00000270885	RASL10B	-0.980824	0.00119155	-1.01761	0.00131968	-0.406437	0.436146
ENSG00000196636	SDHAF3	-0.81483	0.00725144	-0.748726	0.0259025	-0.16698	0.825209
ENSG00000162769	FLVCR1	-0.598071	0.0041765	-0.606917	0.00618048	-0.15439	0.747874
ENSG00000088280	ASAP3	-0.752019	0.0467213	-0.905955	0.0207149	-0.362481	0.589076
ENSG00000187772	LIN28B	-1.18362	4.01E-12	-0.698968	0.000145048	-0.354951	0.155858
ENSG00000107614	TRDMT1	-0.802833	0.0411313	-0.930975	0.0236378	-0.00304135	0.997887
ENSG00000185306	C12orf56	-0.98203	0.000131536	-0.688257	0.0220165	-0.673972	0.0349877
ENSG00000056277	ZNF280C	-0.661477	0.0299821	-0.726138	0.0259025	-0.370599	0.45078
ENSG00000126562	WNK4	-1.33002	2.29E-08	-1.05148	1.72E-05	-0.563283	0.0770588
ENSG00000107295	SH3GL2	-1.52589	4.99E-06	-1.25267	0.000556914	-0.989043	0.0159139
ENSG00000176532	PRR15	-1.768	4.23E-11	-0.967951	0.000823952	-0.848442	0.00536503
ENSG00000137819	PAQR5	-0.896192	0.0303572	-0.992695	0.0215294	-0.798751	0.115044
ENSG00000007944	MYLIP	-0.669156	0.0307392	-0.925459	0.00324381	-0.374242	0.449459
ENSG00000123576	ESX1	-2.43788	7.88E-15	-0.878463	0.00763728	-0.740077	0.0428575
ENSG00000198691	ABCA4	-2.34148	0.0153891	-2.67712	0.0112151	-5.37503	1.70E-07
ENSG00000100433	KCNK10	-3.23619	0.00525737	-3.05194	0.00622587	-3.73567	0.000766383
ENSG00000257446	ZNF878	-1.10965	0.0307597	-1.31489	0.0164442	-0.776613	0.279924
ENSG00000068976	PYGM	-2.27423	0.000138108	-2.30913	0.00023289	-2.65603	3.46E-05

Denotes signficant positive association with *PPARG* mRNA expression in primary samples
CTD - Control gRNA, DMSO
CTT - Control gRNA, 100 nM T0070907
CR6 - *PPARG* sgRNA 6
CR9 - *PPARG* sgRNA 9

Figure 3.9 – Downregulated RNA-seq targets from the 5637 cell line
(A) Co-expression data for *PPARG* and *SHH* in UC tumors from the TCGA provisional dataset (cBioPortal). **(B)** *SHH* gene expression following 100 nM Rosiglitazone or T0070907 treatment, relative to DMSO. **(C)** Gene expression changes for 30 downregulated genes in both 100 nM T0070907 or *PPARG* sgRNA 6, relative to control. Red highlighting denotes significant positive association with *PPARG* mRNA expression in primary UC tumors.

Table 1 – Primers used in ChIP-qPCR experiments

Gene	Forward Primer	Reverse Primer
PDK4	GCAGAGTCAACAAGGGGAAG	ACTAGATGCCTGGGAGCTGA
FABP4	GTCCCTCTGGGGTTTTGATT	CATTTGCAGAGTTTGGCAAG
CD36	GTCATTCCATCAGCATGAGC	GGTTGGGATGAGATGAAAGC
FBXW4	TGAAATCAGAGCCACCACCT	TCCTTGCACCATTCACTTTG
PLIN1	GCAGAATGTGGGTGAGAGGT	GAACTCTATGCCCTGCAAGC
SYN2	CTGGTGAGGGGTCACACTCT	GAAGGGAGAACTTGGGGTCT
CPT1A	CACGTGACGGCTGAGAAAAG	CGGGTGGAACAGGATCCGAG
ANGPTL4	AACCTGACAGGCAATGACGC	GCCTGGCTCTATGTAAGGCAA
TRIL	GGCATTCATGGAAGCCACAC	CCAGAGTGACCAGGAAGACG
ECH1	CAAAGCGGTCAAAGAGCAGG	CAGACAGCGCCTCGGTG
SQSTM1	GCCTCCAGGTAAGAGGTCAC	CCCATGACCGCTGTCGTAAT
SLC25A42	GACCGCACAGGCAGTTTTC	CTGCTCTGAGATGTCACCTGG
DLG4	TAGGGGAAAGGTCACCGCTT	GAAGGGACTTCCGCTGTGTC
PDK2	GTGCCCTTTGCTCCACTTCA	GGCTGCTCAACAACCCTAGA
INS	GCCCACCCTCTGATGTATCT	AAAGTGACCAGCTCCCTGTG
SOX4 -22kb	TCCTGCCTGATAATGGGTGAG	CACGCTAAGCAGGAAGGAAA
CASC15 intronic	CGCACACCTGATTCACACAT	CAAAGGGCAAATGCCAGTCT
CDKAL1 intronic #1	CACAGGCTGACTAGGACCAA	TGAACTACAGCTGAGGAAGCA
CDKAL1 intronic #2	CACAAGGGCATAAAGCCAGT	GGTCATAGGATGGGCTGGAT
HS1BP3-IT1	CTTGACCCTTCCTCCCACAA	TACACAGTTCCCTGCACACA
RXRA	GGCAAGTCAGGGCAGGTG	CTGGGATCGGCGTGACTC
ARHGAP23	TTGTCAGGCGGGAGTCTCTA	CAGGCCTCTTCCACCCTTT
CDKAL1 intronic #3	TGTGAACATCCTGGCTCAGT	CACAGGTGTGGCAAAGTTGA

Chapter 4: Conclusions and Future Directions

4.1 Summary of thesis research

In my thesis research, I sought to address the following questions related to the function of the nuclear receptor PPARγ in clear cell renal cell carcinoma (ccRCC) and bladder urothelial carcinoma (UC). *1) How does PPARγ-RXR genomic occupancy differ between lineages? 2) Does PPARγ primarily regulate genes involved in lipid and glucose metabolism in these cancer subtypes, or are there unique targets that contribute to the cell-type specific functions of this nuclear receptor? 3) Does inhibiting PPARγ activity, either pharmacologically or genetically, affect tumor growth of ccRCC and UC? If so, what are the molecular mechanisms responsible for this dependency?*

Based on our ChIP-seq results in both ccRCC and UC, we determined that PPARγ binding occurs at a majority of sites in both cancers at the canonical PPAR nuclear receptor motif AGGTCA(N)AGGTCA, known as the direct repeat 1 (DR1). More than 50% of the peaks called in both our ccRCC and UC datasets contained this motif (**Figure 2.2C**, **Figure 3.6C**). In ccRCC, stratification of PPARγ-RXR peaks into "adipose-shared" and "ccRCC-specific" sites revealed ~36% similarity of binding at adipocyte locations (Soccio et al., 2011). Another striking similarity between the ccRCC and UC cistromes is the lack of the CCAAT-enhancer-binding protein (C/EBP) motif at PPARγ-RXR sites in these cancers. Even though our RNA-seq data using *PPARG* shRNA in the ccRCC model was largely unusable due to off-target effects, we did not see any evidence of downregulation of lipid or glucose metabolism-related targets in this cancer (data not shown). In UC, PPARγ inhibition largely altered the expression of genes involved in inflammatory responses, migration, and adhesion (**Figure 3.6F**). We speculate that these results are consistent with the lack of C/EBP transcription factor co-occupancy at a number of adipose-related sites and may help to explain the tissue-specific gene expression patterns observed.

Functionally, we determined that PPARγ is dispensable for ccRCC progression but required for growth in a subset of luminal MIBC tumors. Based on our *in vitro* data, we also predict that UC tumors with copy-number amplification of the *PPARG* gene, or activating point mutation in *RXRA* may be particularly dependent on this nuclear receptor for optimal growth.

Mechanistically, *PPARG* knockout by CRISPR-Cas9 or treatment with the PPARγ inverse-agonist T0070907 resulted in a block in the G_1 phase of the cell cycle, and also increased the percentage of non-cycling cells (G_0) four-fold relative to control (**Figure 3.2-3.4**). We hypothesize that PPARγ target genes such as sonic hedgehog (*SHH*) and proline-rich 15 (*PRR15*) may be important molecular mediators of this dependency (see below). These targets were chosen based on our ChIP- and RNA-seq data, as well as publicly available gene expression data from primary human UC samples. These target genes will be the subject of our future investigations.

4.2 Future directions for ccRCC project

Identification of HIF target genes involved in tumor growth and lipid metabolism

Our initial rationale and interest in exploring the role of PPARγ in ccRCC was rooted in trying to identify factors that might affect lipid uptake, storage, and/or synthesis in this disease. As described in Chapters 1 and 2, ccRCC is a cancer subtype typified by robustly lipid-laden cells. Major transcriptional regulators of this process are the hypoxia-inducible factors (HIFs), although the downstream target genes directly connected with lipid metabolism have not been entirely defined. The positive relationship between HIF activity and lipid accumulation in ccRCC was identified during von Hippel-Lindau (pVHL) reconstitution experiments, which entirely reversed the phenotype in cell culture models (Du et al., 2017). At the time of my preliminary exam, I hypothesized that PPARγ was a direct transcriptional target of HIF-1α, similarly to what had been reported in the context of cardiomyocytes following ischemic injury (Krishnan et al., 2009). However, given the results presented in Chapter 2, we determined that PPARγ was entirely dispensable for lipid storage and triglyceride synthesis in both *in vitro* and *in vivo* models of ccRCC (**Figure 2.8**). We also determined that PPARγ protein levels were not altered by shRNA knockdown of either *HIF1A* or *HIF2A* in ccRCC (data not shown).

An important future line of investigation will be identifying the direct transcriptional targets of the HIFs involved in lipid metabolism in ccRCC. Previously, our lab demonstrated that the HIF-2α target gene *PLIN2* is an important regulator of neutral lipid storage and tumor growth in this

cancer (Qiu et al., 2015). However, ectopic *PLIN2* expression in the context of HIF-2α-deficiency only rescued xenograft tumor growth by ~20%. This indicates that additional HIF-2α target genes are required for robust tumor growth. A previously published ChIP-seq dataset of both HIF-2α and HIF-1β (ARNT) in the 786-O cell line will be useful a useful tool to determine which targets explain the pVHL add-back data (Schödel et al., 2012). However, the 786-O cell culture model is still limited in that it does not express HIF-1α, which is important in early disease development even though it is commonly lost as disease progresses (Gordan et al., 2008; Kaku et al., 2004; Rankin et al., 2006). Performing ChIP-seq on primary ccRCC tumors with a combination of HIF-1α, HIF-2α, and HIF-1β will allow researchers to compare genomic occupancy of these transcription factors in cell culture models to primary tissues, which could further reveal important targets and allow us to determine the fidelity of our *in vitro* models to the human disease. These data could also be combined with RNA-seq data from 480 primary human tumors and 69 healthy kidney tissue samples available from The Cancer Genome Atlas to validate functional binding near genes of interest (Network, 2013).

As described in Chapter 2, we determined that *PPARG* knockout was dispensable for ccRCC tumor growth in several established cell culture models *in vitro* and xenograft tumor growth *in vivo*. Given these results, I do not think it is worthwhile to continue with this line of investigation in genetically-engineered mouse models of ccRCC, should they become available in the near future (**Chapter 1.2.b**).

4.3 Future directions for UC project

PPARG KO in mouse models of UC

To definitively connect PPARγ activity to UC development and progression in an *autochthonous in vivo* model, it would be useful to cross *PPARG*$^{fl/fl}$ mice with *Upk2*-Cre transgenic mice. These have the mouse uroplakin 2 (*Upk2*) gene promoter driving Cre-recombinase expression in the bladder urothelium, and are useful for studies of normal urothelial function and cancers of the bladder (de la Peña et al., 2011). *PPARG* KO experiments could be

performed using both genetic and carcinogen-induced mouse models of UC. *Upk2*-Cre inactivation of the tumor suppressors p53 and Rb by SV40 large T-antigen expression results in carcinoma *in situ* with low copy number, whereas high copy number of SV40 results in invasive and metastatic UC (Zhang et al., 1999). Given our *in vitro* results, we predict that *PPARG* KO in this model would delay tumor growth relative to control. Alternatively, the delivery of the carcinogen N-butyl-N-(4-hydroxybutyl) nitrosamine (BBN) in the drinking water of rodents has been shown to specifically induce urinary bladder tumors, 95% of which are transitional cell carcinoma with morphological characteristics similar to those seen clinically in humans (FUKUSHIMA et al., 1976). We predict that *PPARG* KO in this model would delay tumor onset and/or reduce the size of tumors in this experimental setup, inverse to the results described by dual BBN/TZD treatment (Lubet et al., 2008). One proposed explanation of the effect of PPARγ deletion on reduced tumorigenesis would be the downregulation of SHH signaling, since SHH-expressing cells have been identified as a cell-of-origin in a BBN-induced MIBC model (Shin et al., 2014a).

Mechanism of PPARγ-dependent and PPARγ-independent UC progression, and therapeutic implications

Since PPARγ is a critical factor involved in proliferation and cell cycle progression of a subset of UC cell lines, it will be important to further delineate the mechanism of action of PPARγ dependency in these tumors. We speculate that PPARγ transcriptional targets *SHH* and *PRR15* may be involved in promoting luminal UC, given the role of these targets in development and in other cancer models (**Chapter 3.4.d-3.5**), and their co-expression status with *PPARG* in primary human UC tumors. Experimentally, *SHH* or *PRR15* reconstitution in *PPARG*-deficient UC cells would allow us to determine what percentage of the growth defect is due to the loss of these genes, either alone or in combination.

Although our data suggest that PPARγ is required for growth in a subset of UC that could easily be assessed by genomic profiling, the direct use of PPARγ inhibitors would prove

challenging due to adverse effects on adipose tissue and whole-body metabolism. PPARγ is required for the development and maintenance of white and brown adipose tissue, and knockout of this factor in a fat-specific manner results in hepatosteatosis, elevated blood glucose levels, and insulin resistance (He et al., 2003; Imai et al., 2004; Wang et al., 2013). Additionally, heterozygous mutation of *PPARG* has been linked to familial partial lipodystrophy, which is associated with the loss of subcutaneous fat from the extremities and provides further evidence of the necessity of PPARγ activity in maintaining metabolic homeostasis (Agarwal and Garg, 2002). Although pharmacological inhibition of PPARγ is unlikely to produce as severe of a phenotype as genetic deletion in the entire adipose lineage, it is still reasonable to question whether the PPARγ pathway should be targeted for therapeutic benefit in cancer. I suggest the following to circumvent these challenges: 1) Use *PPARG* and/or *RXRA* amplification/mutational status as a biomarker for targeted therapy, particularly to assess likelihood of response to immunotherapy (Korpal et al., 2017) 2) Pharmacologically inhibit the downstream target genes of PPARγ-RXR rather than these nuclear receptors directly.

It is also important to note that PPARγ is absent at the protein level from 53% of all primary UC samples tested in our tissue array (**Figure 3.1B-D**). The following could explain these data and inform rational treatment strategy in the future: 1) PPARγ activity is required for disease initiation but expression is lost as the cancer progresses. 2) The PPARγ-negative samples represent a “basal” subtype of MIBC, which is characterized by expression of the biomarkers TP63 (p63), STAT3, and EGFR. This signature is distinct from the “luminal” subtype which is characterized by expression of the biomarkers ESR1, FGFR3, and the transcription factors FOXA1, GATA3, and PPARγ (Choi et al., 2014a; Warrick et al., 2016). Similarly to what we have described for PPARγ, *EGFR* amplification occurs in a subset of basal MIBCs, and cell lines with amplified *EGFR* are highly sensitive to EGFR inhibitors (Black et al., 2008; Shrader et al., 2007). Immunostaining for these various biomarkers in primary patient samples could help clinicians determine which samples are likely to respond to targeted therapy, immunotherapy, and predict prognosis given the aggressiveness of the subtype. A deeper understanding of the role of

amplified/signature proteins which characterize each subtype of MIBC will guide the development of UC-specific therapeutics that will hopefully be more precise, less toxic, and less invasive then the current standard of care.

BIBLIOGRAPHY

Aboud, O.A., Habib, S.L., Trott, J., Stewart, B., Liang, S., Chaudhari, A.J., Sutcliffe, J., and Weiss, R.H. (2017). Glutamine addiction in kidney cancer suppresses oxidative stress and can be exploited for real-time imaging. Cancer research *77*, 6746-6758.

Adams, M., Reginato, M.J., Shao, D., Lazar, M.A., and Chatterjee, V.K. (1997). Transcriptional activation by peroxisome proliferator-activated receptor γ is inhibited by phosphorylation at a consensus mitogen-activated protein kinase site. Journal of Biological Chemistry *272*, 5128-5132.

Agarwal, A.K., and Garg, A. (2002). A novel heterozygous mutation in peroxisome proliferator-activated receptor-γ gene in a patient with familial partial lipodystrophy. The Journal of Clinical Endocrinology & Metabolism *87*, 408-408.

Ahmadian, M., Suh, J.M., Hah, N., Liddle, C., Atkins, A.R., Downes, M., and Evans, R.M. (2013). PPARγ signaling and metabolism: the good, the bad and the future. Nature medicine *19*, 557.

Bailey, A.P., Koster, G., Guillermier, C., Hirst, E.M., MacRae, J.I., Lechene, C.P., Postle, A.D., and Gould, A.P. (2015). Antioxidant role for lipid droplets in a stem cell niche of Drosophila. Cell *163*, 340-353.

Bailey, S.T., Smith, A.M., Kardos, J., Wobker, S.E., Wilson, H.L., Krishnan, B., Saito, R., Lee, H.J., Zhang, J., and Eaton, S.C. (2017). MYC activation cooperates with Vhl and Ink4a/Arf loss to induce clear cell renal cell carcinoma. Nature communications *8*, 15770.

Barak, Y., Nelson, M.C., Ong, E.S., Jones, Y.Z., Ruiz-Lozano, P., Chien, K.R., Koder, A., and Evans, R.M. (1999). PPARγ is required for placental, cardiac, and adipose tissue development. Molecular cell *4*, 585-595.

Barretina, J., Caponigro, G., Stransky, N., Venkatesan, K., Margolin, A.A., Kim, S., Wilson, C.J., Lehár, J., Kryukov, G.V., and Sonkin, D. (2012). The Cancer Cell Line Encyclopedia enables predictive modelling of anticancer drug sensitivity. Nature *483*, 603.

Bensaad, K., Favaro, E., Lewis, C.A., Peck, B., Lord, S., Collins, J.M., Pinnick, K.E., Wigfield, S., Buffa, F.M., and Li, J.-L. (2014). Fatty acid uptake and lipid storage induced by HIF-1α contribute to cell growth and survival after hypoxia-reoxygenation. Cell reports *9*, 349-365.

Berdik, C. (2017). Unlocking bladder cancer. Nature *551*, S34-S34.

Beroukhim, R., Brunet, J.-P., Di Napoli, A., Mertz, K.D., Seeley, A., Pires, M.M., Linhart, D., Worrell, R.A., Moch, H., and Rubin, M.A. (2009). Patterns of gene expression and copy-number alterations in von-hippel lindau disease-associated and sporadic clear cell carcinoma of the kidney. Cancer research *69*, 4674-4681.

Bertram, J., and Craig, A. (1972). Specific induction of bladder cancer in mice by butyl-(4-hydroxybutyl)-nitrosamine and the effects of hormonal modifications on the sex difference in response. European Journal of Cancer (1965) *8*, 587-594.

Bigot, P., Colli, L.M., Machiela, M.J., Jessop, L., Myers, T.A., Carrouget, J., Wagner, S., Roberson, D., Eymerit, C., and Henrion, D. (2016). Functional characterization of the 12p12. 1 renal cancer-susceptibility locus implicates BHLHE41. Nature communications *7*, 12098.

Biton, A., Bernard-Pierrot, I., Lou, Y., Krucker, C., Chapeaublanc, E., Rubio-Pérez, C., López-Bigas, N., Kamoun, A., Neuzillet, Y., and Gestraud, P. (2014). Independent component analysis uncovers the landscape of the bladder tumor transcriptome and reveals insights into luminal and basal subtypes. Cell reports *9*, 1235-1245.

Bjornsson, J., Short, M.P., Kwiatkowski, D.J., and Henske, E. (1996). Tuberous sclerosis-associated renal cell carcinoma. Clinical, pathological, and genetic features. The American journal of pathology *149*, 1201.

Black, P.C., Brown, G.A., Inamoto, T., Shrader, M., Arora, A., Siefker-Radtke, A.O., Adam, L., Theodorescu, D., Wu, X., and Munsell, M.F. (2008). Sensitivity to epidermal growth factor receptor inhibitor requires E-cadherin expression in urothelial carcinoma cells. Clinical cancer research *14*, 1478-1486.

Böhle, A., Jocham, D., and Bock, P. (2003). Intravesical bacillus Calmette-Guerin versus mitomycin C for superficial bladder cancer: a formal meta-analysis of comparative studies on recurrence and toxicity. The Journal of urology *169*, 90-95.

Brandau, S., and Suttmann, H. (2007). Thirty years of BCG immunotherapy for non-muscle invasive bladder cancer: a success story with room for improvement. Biomedicine & Pharmacotherapy *61*, 299-305.

Cerami, E., Gao, J., Dogrusoz, U., Gross, B.E., Sumer, S.O., Aksoy, B.A., Jacobsen, A., Byrne, C.J., Heuer, M.L., and Larsson, E. (2012). The cBio cancer genomics portal: an open platform for exploring multidimensional cancer genomics data (AACR).

Chawla, A., Barak, Y., Nagy, L., Liao, D., Tontonoz, P., and Evans, R.M. (2001a). PPAR-γ dependent and independent effects on macrophage-gene expression in lipid metabolism and inflammation. Nature medicine *7*, 48.

Chawla, A., Repa, J.J., Evans, R.M., and Mangelsdorf, D.J. (2001b). Nuclear receptors and lipid physiology: opening the X-files. Science *294*, 1866-1870.

Chen, F., Zhang, Y., Şenbabaoğlu, Y., Ciriello, G., Yang, L., Reznik, E., Shuch, B., Micevic, G., De Velasco, G., and Shinbrot, E. (2016a). Multilevel genomics-based taxonomy of renal cell carcinoma. Cell reports *14*, 2476-2489.

Chen, W., Hill, H., Christie, A., Kim, M.S., Holloman, E., Pavia-Jimenez, A., Homayoun, F., Ma, Y., Patel, N., and Yell, P. (2016b). Targeting renal cell carcinoma with a HIF-2 antagonist. Nature *539*, 112.

Cho, H., Du, X., Rizzi, J.P., Liberzon, E., Chakraborty, A.A., Gao, W., Carvo, I., Signoretti, S., Bruick, R.K., and Josey, J.A. (2016). On-target efficacy of a HIF-2α antagonist in preclinical kidney cancer models. Nature *539*, 107.

Choi, W., Czerniak, B., Ochoa, A., Su, X., Siefker-Radtke, A., Dinney, C., and McConkey, D.J. (2014a). Intrinsic basal and luminal subtypes of muscle-invasive bladder cancer. Nature Reviews Urology *11*, 400.

Choi, W., Porten, S., Kim, S., Willis, D., Plimack, E.R., Hoffman-Censits, J., Roth, B., Cheng, T., Tran, M., and Lee, I.-L. (2014b). Identification of distinct basal and luminal subtypes of muscle-invasive bladder cancer with different sensitivities to frontline chemotherapy. Cancer cell *25*, 152-165.

Collet, N., Théoleyre, S., Rageul, J., Mottier, S., Jouan, F., Rioux-Leclercq, N., Fergelot, P., Patard, J.-J., Masson, D., and Denis, M.G. (2011). PPARγ is functionally expressed in clear cell renal cell carcinoma. International journal of oncology *38*, 851-857.

Dalgliesh, G.L., Furge, K., Greenman, C., Chen, L., Bignell, G., Butler, A., Davies, H., Edkins, S., Hardy, C., and Latimer, C. (2010). Systematic sequencing of renal carcinoma reveals inactivation of histone modifying genes. Nature *463*, 360.

Damrauer, J.S., Hoadley, K.A., Chism, D.D., Fan, C., Tiganelli, C.J., Wobker, S.E., Yeh, J.J., Milowsky, M.I., Iyer, G., and Parker, J.S. (2014). Intrinsic subtypes of high-grade bladder cancer reflect the hallmarks of breast cancer biology. Proceedings of the National Academy of Sciences *111*, 3110-3115.

Dasgupta, S., Lonard, D.M., and O'Malley, B.W. (2014). Nuclear receptor coactivators: master regulators of human health and disease. Annu Rev Med *65*, 279-292.

de la Peña, F.A., Kanasaki, K., Kanasaki, M., Tangirala, N., Maeda, G., and Kalluri, R. (2011). Loss of p53 and acquisition of angiogenic microRNA profile are insufficient to facilitate progression of bladder urothelial carcinoma in situ to invasive carcinoma. Journal of Biological Chemistry *286*, 20778-20787.

De Velasco, G., Miao, D., Voss, M.H., Hakimi, A.A., Hsieh, J.J., Tannir, N.M., Tamboli, P., Appleman, L.J., Rathmell, W.K., and Van Allen, E.M. (2016). Tumor mutational load and immune parameters across metastatic renal cell carcinoma risk groups. Cancer immunology research *4*, 820-822.

Demetri, G.D., Fletcher, C.D., Mueller, E., Sarraf, P., Naujoks, R., Campbell, N., Spiegelman, B.M., and Singer, S. (1999). Induction of solid tumor differentiation by the peroxisome proliferator-activated receptor-γ ligand troglitazone in patients with liposarcoma. Proceedings of the National Academy of Sciences *96*, 3951-3956.

Dibble, C.C., and Manning, B.D. (2013). Signal integration by mTORC1 coordinates nutrient input with biosynthetic output. Nature cell biology *15*, 555.

Dobin, A., Davis, C.A., Schlesinger, F., Drenkow, J., Zaleski, C., Jha, S., Batut, P., Chaisson, M., and Gingeras, T.R. (2013). STAR: ultrafast universal RNA-seq aligner. Bioinformatics *29*, 15-21.

Dondeti, V.R., Wubbenhorst, B., Lal, P., Gordan, J.D., D'Andrea, K., Attiyeh, E.F., Simon, M.C., and Nathanson, K.L. (2012). Integrative genomic analyses of sporadic clear cell renal cell carcinoma define disease subtypes and potential new therapeutic targets. Cancer research *72*, 112-121.

Drabkin, H.A., Bradley, C., Hart, I., Bleskan, J., Li, F.P., and Patterson, D. (1985). Translocation of c-myc in the hereditary renal cell carcinoma associated with at (3; 8)(p14. 2; q24. 13) chromosomal translocation. Proceedings of the National Academy of Sciences *82*, 6980-6984.

Du, W., Zhang, L., Brett-Morris, A., Aguila, B., Kerner, J., Hoppel, C.L., Puchowicz, M., Serra, D., Herrero, L., and Rini, B.I. (2017). HIF drives lipid deposition and cancer in ccRCC via repression of fatty acid metabolism. Nature communications *8*, 1769.

Duran, A., Amanchy, R., Linares, J.F., Joshi, J., Abu-Baker, S., Porollo, A., Hansen, M., Moscat, J., and Diaz-Meco, M.T. (2011). p62 is a key regulator of nutrient sensing in the mTORC1 pathway. Molecular cell *44*, 134-146.

Eckel, R.H., Grundy, S.M., and Zimmet, P.Z. (2005). The metabolic syndrome. Lancet (London, England) *365*, 1415-1428.

Fajas, L., Auboeuf, D., Raspé, E., Schoonjans, K., Lefebvre, A.-M., Saladin, R., Najib, J., Laville, M., Fruchart, J.-C., and Deeb, S. (1997). The organization, promoter analysis, and expression of the human PPARγ gene. Journal of Biological Chemistry *272*, 18779-18789.

Fu, L., Wang, G., Shevchuk, M.M., Nanus, D.M., and Gudas, L.J. (2011). Generation of a mouse model of von Hippel–Lindau kidney disease leading to renal cancers by expression of a constitutively active mutant of HIF1α. Cancer research *71*, 6848-6856.

Fujita, M., Yagami, T., Fujio, M., Tohji, C., Takase, K., Yamamoto, Y., Sawada, K., Yamamori, M., and Okamura, N. (2011). Cytotoxicity of troglitazone through PPARγ-independent pathway and p38 MAPK pathway in renal cell carcinoma. Cancer letters *312*, 219-227.

FUKUSHIMA, S., HIROSE, M., TSUDA, H., SHIRAI, T., HIRAO, K., ARAI, M., and ITO, N. (1976). Histological classification of urinary bladder cancers in rats induced by N-butyl-n-(4-hydroxybutyl) nitrosamine. GANN Japanese Journal of Cancer Research *67*, 81-90.

Gameiro, P.A., Yang, J., Metelo, A.M., Pérez-Carro, R., Baker, R., Wang, Z., Arreola, A., Rathmell, W.K., Olumi, A., and López-Larrubia, P. (2013). In vivo HIF-mediated reductive carboxylation is regulated by citrate levels and sensitizes VHL-deficient cells to glutamine deprivation. Cell metabolism *17*, 372-385.

Gao, J., Aksoy, B.A., Dogrusoz, U., Dresdner, G., Gross, B., Sumer, S.O., Sun, Y., Jacobsen, A., Sinha, R., and Larsson, E. (2013). Integrative analysis of complex cancer genomics and clinical profiles using the cBioPortal. Sci Signal *6*, pl1-pl1.

Gao, J., Huang, H.-Y., Pak, J., Cheng, J., Zhang, Z.-T., Shapiro, E., Pellicer, A., Sun, T.-T., and Wu, X.-R. (2004). p53 deficiency provokes urothelial proliferation and synergizes with activated Ha-ras in promoting urothelial tumorigenesis. Oncogene *23*, 687.

Gao, W., Li, W., Xiao, T., Liu, X.S., and Kaelin, W.G. (2017). Inactivation of the PBRM1 tumor suppressor gene amplifies the HIF-response in VHL−/− clear cell renal carcinoma. Proceedings of the National Academy of Sciences *114*, 1027-1032.

García-Closas, M., Malats, N., Silverman, D., Dosemeci, M., Kogevinas, M., Hein, D.W., Tardón, A., Serra, C., Carrato, A., and García-Closas, R. (2005). NAT2 slow acetylation, GSTM1 null genotype, and risk of bladder cancer: results from the Spanish Bladder Cancer Study and meta-analyses. The Lancet *366*, 649-659.

Gates, K.C., Goetzmann, L.N., Cantlon, J.D., Jeckel, K.M., and Anthony, R.V. (2017). Effect of proline rich 15-deficiency on trophoblast viability and survival. PloS one *12*, e0174976.

Gebhard, R., Clayman, R., Prigge, W., Figenshau, R., Staley, N., Reesey, C., and Bear, A. (1987). Abnormal cholesterol metabolism in renal clear cell carcinoma. Journal of lipid research *28*, 1177-1184.

Gerlinger, M., Horswell, S., Larkin, J., Rowan, A.J., Salm, M.P., Varela, I., Fisher, R., McGranahan, N., Matthews, N., and Santos, C.R. (2014). Genomic architecture and evolution of clear cell renal cell carcinomas defined by multiregion sequencing. Nature genetics *46*, 225.

Gerlinger, M., Rowan, A.J., Horswell, S., Larkin, J., Endesfelder, D., Gronroos, E., Martinez, P., Matthews, N., Stewart, A., and Tarpey, P. (2012). Intratumor heterogeneity and branched evolution revealed by multiregion sequencing. New England journal of medicine *366*, 883-892.

Girnun, G.D., Smith, W.M., Drori, S., Sarraf, P., Mueller, E., Eng, C., Nambiar, P., Rosenberg, D.W., Bronson, R.T., and Edelmann, W. (2002). APC-dependent suppression of colon carcinogenesis by PPARγ. Proceedings of the National Academy of Sciences *99*, 13771-13776.

Goldstein, J.T., Berger, A.C., Shih, J., Duke, F.F., Furst, L., Kwiatkowski, D.J., Cherniack, A.D., Meyerson, M., and Strathdee, C.A. (2017). Genomic activation of PPARG reveals a candidate therapeutic axis in bladder cancer. Cancer research, canres. 1701.2017.

Gordan, J.D., Bertout, J.A., Hu, C.-J., Diehl, J.A., and Simon, M.C. (2007). HIF-2α promotes hypoxic cell proliferation by enhancing c-myc transcriptional activity. Cancer cell *11*, 335-347.

Gordan, J.D., Lal, P., Dondeti, V.R., Letrero, R., Parekh, K.N., Oquendo, C.E., Greenberg, R.A., Flaherty, K.T., Rathmell, W.K., and Keith, B. (2008). HIF-α effects on c-Myc distinguish two subtypes of sporadic VHL-deficient clear cell renal carcinoma. Cancer cell *14*, 435-446.

Grubbs, C.J., Moon, R.C., Squire, R.A., Farrow, G.M., Stinson, S.F., Goodman, D.G., Brown, C.C., and Sporn, M.B. (1977). 13-cis-Retinoic acid: inhibition of bladder carcinogenesis induced in rats by N-butyl-N-(4-hydroxybutyl) nitrosamine. Science *198*, 743-744.

Gu, Y.-F., Cohn, S., Christie, A., McKenzie, T., Wolff, N., Do, Q.N., Madhuranthakam, A.J., Pedrosa, I., Wang, T., and Dey, A. (2017). Modeling renal cell carcinoma in mice: Bap1 and Pbrm1 inactivation drive tumor grade. Cancer discovery *7*, 900-917.

Guan, Y., Hao, C., Cha, D.R., Rao, R., Lu, W., Kohan, D.E., Magnuson, M.A., Redha, R., Zhang, Y., and Breyer, M.D. (2005). Thiazolidinediones expand body fluid volume through PPARγ stimulation of ENaC-mediated renal salt absorption. Nature medicine *11*, 861.

Guan, Y., Zhang, Y., Davis, L., and Breyer, M.D. (1997). Expression of peroxisome proliferator-activated receptors in urinary tract of rabbits and humans. American Journal of Physiology-Renal Physiology *273*, F1013-F1022.

Gumz, M.L., Zou, H., Kreinest, P.A., Childs, A.C., Belmonte, L.S., LeGrand, S.N., Wu, K.J., Luxon, B.A., Sinha, M., and Parker, A.S. (2007). Secreted frizzled-related protein 1 loss contributes to tumor phenotype of clear cell renal cell carcinoma. Clinical Cancer Research *13*, 4740-4749.

Guo, G., Gui, Y., Gao, S., Tang, A., Hu, X., Huang, Y., Jia, W., Li, Z., He, M., and Sun, L. (2012). Frequent mutations of genes encoding ubiquitin-mediated proteolysis pathway components in clear cell renal cell carcinoma. Nature genetics *44*, 17.

Hakimi, A.A., Ostrovnaya, I., Reva, B., Schultz, N., Chen, Y.-B., Gonen, M., Liu, H., Takeda, S., Voss, M.H., and Tickoo, S.K. (2013a). Adverse outcomes in clear cell renal cell carcinoma with mutations of 3p21 epigenetic regulators BAP1 and SETD2: a report by MSKCC and the KIRC TCGA research network. Clinical Cancer Research *19*, 3259-3267.

Hakimi, A.A., Pham, C.G., and Hsieh, J.J. (2013b). A clear picture of renal cell carcinoma. Nature genetics *45*, 849.

Hakimi, A.A., Reznik, E., Lee, C.-H., Creighton, C.J., Brannon, A.R., Luna, A., Aksoy, B.A., Liu, E.M., Shen, R., and Lee, W. (2016). An integrated metabolic atlas of clear cell renal cell carcinoma. Cancer cell *29*, 104-116.

Halstead, A.M., Kapadia, C.D., Bolzenius, J., Chu, C.E., Schriefer, A., Wartman, L.D., Bowman, G.R., and Arora, V.K. (2017). Bladder-cancer-associated mutations in RXRA activate peroxisome proliferator-activated receptors to drive urothelial proliferation. eLife *6*.

Harlander, S., Schönenberger, D., Toussaint, N.C., Prummer, M., Catalano, A., Brandt, L., Moch, H., Wild, P.J., and Frew, I.J. (2017). Combined mutation in Vhl, Trp53 and Rb1 causes clear cell renal cell carcinoma in mice. Nature medicine *23*, 869.

He, W., Barak, Y., Hevener, A., Olson, P., Liao, D., Le, J., Nelson, M., Ong, E., Olefsky, J.M., and Evans, R.M. (2003). Adipose-specific peroxisome proliferator-activated receptor γ knockout causes insulin resistance in fat and liver but not in muscle. Proceedings of the National Academy of Sciences *100*, 15712-15717.

Heinz, S., Benner, C., Spann, N., Bertolino, E., Lin, Y.C., Laslo, P., Cheng, J.X., Murre, C., Singh, H., and Glass, C.K. (2010). Simple combinations of lineage-determining transcription factors prime cis-regulatory elements required for macrophage and B cell identities. Molecular cell *38*, 576-589.

Hevener, A.L., He, W., Barak, Y., Le, J., Bandyopadhyay, G., Olson, P., Wilkes, J., Evans, R.M., and Olefsky, J. (2003). Muscle-specific Pparg deletion causes insulin resistance. Nat Med *9*, 1491-1497.

Hoffmann, K., Blaudszun, J., Brunken, C., Höpker, W.W., Tauber, R., and Steinhart, H. (2005). Lipid class distribution of fatty acids including conjugated linoleic acids in healthy and cancerous parts of human kidneys. Lipids *40*, 1057-1062.

Horiguchi, A., Asano, T., Asano, T., Ito, K., Sumitomo, M., and Hayakawa, M. (2008). Fatty acid synthase over expression is an indicator of tumor aggressiveness and poor prognosis in renal cell carcinoma. The Journal of urology *180*, 1137-1140.

Hu, E., Kim, J.B., Sarraf, P., and Spiegelman, B.M. (1996). Inhibition of adipogenesis through MAP kinase-mediated phosphorylation of PPARγ. Science *274*, 2100-2103.

Hu, X., and Lazar, M.A. (1999). The CoRNR motif controls the recruitment of corepressors by nuclear hormone receptors. Nature *402*, 93.

Hurst, C., Rosenberg, J., and Knowles, M. (2018). SnapShot: Bladder Cancer. Cancer Cell *34*, 350-350.e351.

Imai, T., Takakuwa, R., Marchand, S., Dentz, E., Bornert, J.-M., Messaddeq, N., Wendling, O., Mark, M., Desvergne, B., and Wahli, W. (2004). Peroxisome proliferator-activated receptor γ is required in mature white and brown adipocytes for their survival in the mouse. Proceedings of the National Academy of Sciences *101*, 4543-4547.

Institute, N.C. (2018). SEER Cancer Stat Facts: Kidney and Renal Pelvis Cancer.

Islam, S., Mokhtari, R., Noman, A., Uddin, M., Rahman, M., Azadi, M., Zlotta, A., van der Kwast, T., Yeger, H., and Farhat, W. (2016). Sonic hedgehog (Shh) signaling promotes tumorigenicity

and stemness via activation of epithelial-to-mesenchymal transition (EMT) in bladder cancer. Molecular carcinogenesis *55*, 537-551.

Ivanov, D.P., Parker, T.L., Walker, D.A., Alexander, C., Ashford, M.B., Gellert, P.R., and Garnett, M.C. (2014). Multiplexing spheroid volume, resazurin and acid phosphatase viability assays for high-throughput screening of tumour spheroids and stem cell neurospheres. PloS one *9*, e103817.

Jafri, M., Wake, N.C., Ascher, D.B., Pires, D.E., Gentle, D., Morris, M.R., Rattenberry, E., Simpson, M.A., Trembath, R.C., and Weber, A. (2015). Germline mutations in the CDKN2B tumor suppressor gene predispose to renal cell carcinoma. Cancer discovery *5*, 723-729.

Kaelin Jr, W.G. (2007). Von hippel-lindau disease. Annu Rev Pathol Mech Dis *2*, 145-173.

Kaku, H., Ito, S., Ebara, S., Ouchida, M., Nasu, Y., Tsushima, T., Kumon, H., and Shimizu, K. (2004). Positive correlation between allelic loss at chromosome 14q24-31 and poor prognosis of patients with renal cell carcinoma. Urology *64*, 176-181.

Kamphorst, J.J., Cross, J.R., Fan, J., de Stanchina, E., Mathew, R., White, E.P., Thompson, C.B., and Rabinowitz, J.D. (2013). Hypoxic and Ras-transformed cells support growth by scavenging unsaturated fatty acids from lysophospholipids. Proceedings of the National Academy of Sciences *110*, 8882-8887.

Kang, H.M., Ahn, S.H., Choi, P., Ko, Y.-A., Han, S.H., Chinga, F., Park, A.S.D., Tao, J., Sharma, K., and Pullman, J. (2015). Defective fatty acid oxidation in renal tubular epithelial cells has a key role in kidney fibrosis development. Nature medicine *21*, 37.

Kanu, N., Grönroos, E., Martinez, P., Burrell, R.A., Goh, X.Y., Bartkova, J., Maya-Mendoza, A., Mistrík, M., Rowan, A.J., and Patel, H. (2015). SETD2 loss-of-function promotes renal cancer branched evolution through replication stress and impaired DNA repair. Oncogene *34*, 5699.

Kapur, P., Peña-Llopis, S., Christie, A., Zhrebker, L., Pavía-Jiménez, A., Rathmell, W.K., Xie, X.-J., and Brugarolas, J. (2013). Effects on survival of BAP1 and PBRM1 mutations in sporadic clear-cell renal-cell carcinoma: a retrospective analysis with independent validation. The lancet oncology *14*, 159-167.

Keith, B., Johnson, R.S., and Simon, M.C. (2012). HIF1α and HIF2α: sibling rivalry in hypoxic tumour growth and progression. Nature Reviews Cancer *12*, 9.

Kim, K., Boo, K., Yu, Y.S., Oh, S.K., Kim, H., Jeon, Y., Bhin, J., Hwang, D., Kim, K.I., and Lee, J.-S. (2017). RORα controls hepatic lipid homeostasis via negative regulation of PPARγ transcriptional network. Nature communications *8*, 162.

Kliewer, S.A., Umesono, K., Noonan, D.J., Heyman, R.A., and Evans, R.M. (1992). Convergence of 9-cis retinoic acid and peroxisome proliferator signalling pathways through heterodimer formation of their receptors. Nature *358*, 771.

Kondo, K., Kim, W.Y., Lechpammer, M., and Kaelin Jr, W.G. (2003). Inhibition of HIF2α is sufficient to suppress pVHL-defective tumor growth. PLoS biology *1*, e83.

Kondo, K., Klco, J., Nakamura, E., Lechpammer, M., and Kaelin Jr, W.G. (2002). Inhibition of HIF is necessary for tumor suppression by the von Hippel-Lindau protein. Cancer cell *1*, 237-246.

Korpal, M., Puyang, X., Wu, Z.J., Seiler, R., Furman, C., Oo, H.Z., Seiler, M., Irwin, S., Subramanian, V., and Joshi, J.J. (2017). Evasion of immunosurveillance by genomic alterations of PPARγ/RXRα in bladder cancer. Nature communications *8*, 103.

Krishnan, J., Suter, M., Windak, R., Krebs, T., Felley, A., Montessuit, C., Tokarska-Schlattner, M., Aasum, E., Bogdanova, A., and Perriard, E. (2009). Activation of a HIF1α-PPARγ axis underlies the integration of glycolytic and lipid anabolic pathways in pathologic cardiac hypertrophy. Cell metabolism *9*, 512-524.

LaGory, E.L., Wu, C., Taniguchi, C.M., Ding, C.-K.C., Chi, J.-T., von Eyben, R., Scott, D.A., Richardson, A.D., and Giaccia, A.J. (2015). Suppression of PGC-1α is critical for reprogramming oxidative metabolism in renal cell carcinoma. Cell reports *12*, 116-127.

Lee, K., Zhang, H., Qian, D.Z., Rey, S., Liu, J.O., and Semenza, G.L. (2009). Acriflavine inhibits HIF-1 dimerization, tumor growth, and vascularization. Proceedings of the National Academy of Sciences *106*, 17910-17915.

Lefebvre, A.M., Chen, I., Desreumaux, P., Najib, J., Fruchart, J.C., Geboes, K., Briggs, M., Heyman, R., and Auwerx, J. (1998). Activation of the peroxisome proliferator-activated receptor gamma promotes the development of colon tumors in C57BL/6J-APCMin/+ mice. Nat Med *4*, 1053-1057.

Lefterova, M.I., Steger, D.J., Zhuo, D., Qatanani, M., Mullican, S.E., Tuteja, G., Manduchi, E., Grant, G.R., and Lazar, M.A. (2010). Cell-specific determinants of peroxisome proliferator-activated receptor γ function in adipocytes and macrophages. Molecular and cellular biology *30*, 2078-2089.

Lefterova, M.I., Zhang, Y., Steger, D.J., Schupp, M., Schug, J., Cristancho, A., Feng, D., Zhuo, D., Stoeckert, C.J., and Liu, X.S. (2008). PPARγ and C/EBP factors orchestrate adipocyte biology via adjacent binding on a genome-wide scale. Genes & development *22*, 2941-2952.

Lewis, J.D., Ferrara, A., Peng, T., Hedderson, M., Bilker, W.B., Quesenberry, C.P., Vaughn, D.J., Nessel, L., Selby, J., and Strom, B.L. (2011). Risk of bladder cancer among diabetic patients treated with pioglitazone: interim report of a longitudinal cohort study. Diabetes care *34*, 916-922.

Li, B., Qiu, B., Lee, D.S., Walton, Z.E., Ochocki, J.D., Mathew, L.K., Mancuso, A., Gade, T.P., Keith, B., and Nissim, I. (2014). Fructose-1, 6-bisphosphatase opposes renal carcinoma progression. Nature *513*, 251.

Li, L., Shen, C., Nakamura, E., Ando, K., Signoretti, S., Beroukhim, R., Cowley, G.S., Lizotte, P., Liberzon, E., and Bair, S. (2013). SQSTM1 is a pathogenic target of 5q copy number gains in kidney cancer. Cancer cell *24*, 738-750.

Liberti, M.V., and Locasale, J.W. (2016). The Warburg effect: how does it benefit cancer cells? Trends in biochemical sciences *41*, 211-218.

Linehan, W.M., Srinivasan, R., and Schmidt, L.S. (2010). The genetic basis of kidney cancer: a metabolic disease. Nature reviews urology *7*, 277.

Liu, L., Xu, Z., Zhong, L., Wang, H., Jiang, S., Long, Q., Xu, J., and Guo, J. (2016). Enhancer of zeste homolog 2 (EZH2) promotes tumour cell migration and invasion via epigenetic repression of E-cadherin in renal cell carcinoma. BJU international *117*, 351-362.

Love, M.I., Huber, W., and Anders, S. (2014). Moderated estimation of fold change and dispersion for RNA-seq data with DESeq2. Genome biology *15*, 550.

Lubet, R.A., Fischer, S.M., Steele, V.E., Juliana, M.M., Desmond, R., and Grubbs, C.J. (2008). Rosiglitazone, a PPAR gamma agonist: Potent promoter of hydroxybutyl (butyl) nitrosamine-induced urinary bladder cancers. International Journal of Cancer *123*, 2254-2259.

Luo, W., Hu, H., Chang, R., Zhong, J., Knabel, M., O'Meally, R., Cole, R.N., Pandey, A., and Semenza, G.L. (2011). Pyruvate kinase M2 is a PHD3-stimulated coactivator for hypoxia-inducible factor 1. Cell *145*, 732-744.

Luquet, S., Gaudel, C., Holst, D., Lopez-Soriano, J., Jehl-Pietri, C., Fredenrich, A., and Grimaldi, P.A. (2005). Roles of PPAR delta in lipid absorption and metabolism: a new target for the treatment of type 2 diabetes. Biochimica et Biophysica Acta (BBA)-Molecular Basis of Disease *1740*, 313-317.

Mandard, S., Müller, M., and Kersten, S. (2004). Peroxisome proliferator-activated receptor α target genes. Cellular and Molecular Life Sciences CMLS *61*, 393-416.

Mandriota, S.J., Turner, K.J., Davies, D.R., Murray, P.G., Morgan, N.V., Sowter, H.M., Wykoff, C.C., Maher, E.R., Harris, A.L., and Ratcliffe, P.J. (2002). HIF activation identifies early lesions in VHL kidneys: evidence for site-specific tumor suppressor function in the nephron. Cancer cell *1*, 459-468.

Martínez-Sáez, O., Borau, P.G., Alonso-Gordoa, T., Molina-Cerrillo, J., and Grande, E. (2017). Targeting HIF-2 α in clear cell renal cell carcinoma: A promising therapeutic strategy. Critical reviews in oncology/hematology *111*, 117-123.

McKenna, N.J., and O'Malley, B.W. (2002). Combinatorial control of gene expression by nuclear receptors and coregulators. Cell *108*, 465-474.

Medicine, U.S.N.L.o. (2018). Renal Carcinoma Clinical Trials.

Meierhofer, D., Mayr, J.A., Foetschl, U., Berger, A., Fink, K., Schmeller, N., Hacker, G.W., Hauser-Kronberger, C., Kofler, B., and Sperl, W. (2004). Decrease of mitochondrial DNA content and energy metabolism in renal cell carcinoma. Carcinogenesis *25*, 1005-1010.

Metallo, C.M., Gameiro, P.A., Bell, E.L., Mattaini, K.R., Yang, J., Hiller, K., Jewell, C.M., Johnson, Z.R., Irvine, D.J., and Guarente, L. (2012). Reductive glutamine metabolism by IDH1 mediates lipogenesis under hypoxia. Nature *481*, 380.

Meunier, D., Patra, K., Smits, R., Hägebarth, A., Lüttges, A., Jaussi, R., Wieduwilt, M.J., Quintanilla-Fend, L., Himmelbauer, H., and Fodde, R. (2011). Expression analysis of proline rich 15 (Prr15) in mouse and human gastrointestinal tumors. Molecular carcinogenesis *50*, 8-15.

Meyers, R.M., Bryan, J.G., McFarland, J.M., Weir, B.A., Sizemore, A.E., Xu, H., Dharia, N.V., Montgomery, P.G., Cowley, G.S., and Pantel, S. (2017). Computational correction of copy number effect improves specificity of CRISPR–Cas9 essentiality screens in cancer cells. Nature genetics *49*, 1779.

Miao, D., Margolis, C.A., Gao, W., Voss, M.H., Li, W., Martini, D.J., Norton, C., Bossé, D., Wankowicz, S.M., and Cullen, D. (2018). Genomic correlates of response to immune checkpoint therapies in clear cell renal cell carcinoma. Science, eaan5951.

Morán-Salvador, E., López-Parra, M., García-Alonso, V., Titos, E., Martínez-Clemente, M., González-Périz, A., López-Vicario, C., Barak, Y., Arroyo, V., and Clària, J. (2011). Role for PPARγ in obesity-induced hepatic steatosis as determined by hepatocyte-and macrophage-specific conditional knockouts. The FASEB Journal *25*, 2538-2550.

Motzer, R.J., Escudier, B., McDermott, D.F., George, S., Hammers, H.J., Srinivas, S., Tykodi, S.S., Sosman, J.A., Procopio, G., and Plimack, E.R. (2015). Nivolumab versus everolimus in advanced renal-cell carcinoma. New England Journal of Medicine *373*, 1803-1813.

Motzer, R.J., Escudier, B., Oudard, S., Hutson, T.E., Porta, C., Bracarda, S., Grünwald, V., Thompson, J.A., Figlin, R.A., and Hollaender, N. (2008). Efficacy of everolimus in advanced renal cell carcinoma: a double-blind, randomised, placebo-controlled phase III trial. The Lancet *372*, 449-456.

Mucaj, V., Shay, J.E., and Simon, M.C. (2012). Effects of hypoxia and HIFs on cancer metabolism. International journal of hematology *95*, 464-470.

Nakamura, Y., Suzuki, T., Sugawara, A., Arai, Y., and Sasano, H. (2009). Peroxisome proliferator-activated receptor gamma in human prostate carcinoma. Pathology international *59*, 288-293.

Nargund, A.M., Pham, C.G., Dong, Y., Wang, P.I., Osmangeyoglu, H.U., Xie, Y., Aras, O., Han, S., Oyama, T., and Takeda, S. (2017). The SWI/SNF protein PBRM1 restrains VHL-loss-driven clear cell renal cell carcinoma. Cell reports *18*, 2893-2906.

Nedjadi, T., Salem, N., Khayyat, D., Al-Sayyad, A., Al-Ammari, A., and Al-Maghrabi, J. (2018). Sonic Hedgehog Expression is Associated with Lymph Node Invasion in Urothelial Bladder Cancer. Pathology & Oncology Research, 1-7.

Nelson, V.L., Nguyen, H.C.B., Garcia-Canaveras, J.C., Briggs, E.R., Ho, W.Y., DiSpirito, J.R., Marinis, J.M., Hill, D.A., and Lazar, M.A. (2018). PPARgamma is a nexus controlling alternative activation of macrophages via glutamine metabolism. Genes Dev *32*, 1035-1044.

Network, C.G.A.R. (2013). Comprehensive molecular characterization of clear cell renal cell carcinoma. Nature *499*, 43.

Network, C.G.A.R. (2014). Comprehensive molecular characterization of urothelial bladder carcinoma. Nature *507*, 315.

Neumann, A., Weill, A., Ricordeau, P., Fagot, J., Alla, F., and Allemand, H. (2012). Pioglitazone and risk of bladder cancer among diabetic patients in France: a population-based cohort study. Diabetologia *55*, 1953-1962.

Nickerson, M.L., Jaeger, E., Shi, Y., Durocher, J.A., Mahurkar, S., Zaridze, D., Matveev, V., Janout, V., Kollarova, H., and Bencko, V. (2008). Improved identification of von Hippel-Lindau gene alterations in clear cell renal tumors. Clinical cancer research *14*, 4726-4734.

Nicol, C.J., Yoon, M., Ward, J.M., Yamashita, M., Fukamachi, K., Peters, J.M., and Gonzalez, F.J. (2004). PPARγ influences susceptibility to DMBA-induced mammary, ovarian and skin carcinogenesis. Carcinogenesis *25*, 1747-1755.

Nilsson, H., Lindgren, D., Forsberg, A.M., Mulder, H., Axelson, H., and Johansson, M. (2015). Primary clear cell renal carcinoma cells display minimal mitochondrial respiratory capacity

resulting in pronounced sensitivity to glycolytic inhibition by 3-Bromopyruvate. Cell death & disease *6*, e1585.

Okuno, A., Tamemoto, H., Tobe, K., Ueki, K., Mori, Y., Iwamoto, K., Umesono, K., Akanuma, Y., Fujiwara, T., Horikoshi, H.*, et al.* (1998). Troglitazone increases the number of small adipocytes without the change of white adipose tissue mass in obese Zucker rats. J Clin Invest *101*, 1354-1361.

Parikh, M., and Lara, J., Primo N (2017). Modern Systemic Therapy for Metastatic Renal Cell Carcinoma of the Clear Cell Type. Annual review of medicine.

Patro, R., Duggal, G., Love, M.I., Irizarry, R.A., and Kingsford, C. (2017). Salmon provides fast and bias-aware quantification of transcript expression. Nature methods *14*, 417.

Pavlova, N.N., and Thompson, C.B. (2016). The emerging hallmarks of cancer metabolism. Cell metabolism *23*, 27-47.

Peña-Llopis, S., Christie, A., Xie, X.-J., and Brugarolas, J. (2013). Cooperation and antagonism among cancer genes: the renal cancer paradigm. Cancer research *73*, 4173-4179.

Peña-Llopis, S., Vega-Rubín-de-Celis, S., Liao, A., Leng, N., Pavía-Jiménez, A., Wang, S., Yamasaki, T., Zhrebker, L., Sivanand, S., and Spence, P. (2012). BAP1 loss defines a new class of renal cell carcinoma. Nature genetics *44*, 751.

Puigserver, P., Wu, Z., Park, C.W., Graves, R., Wright, M., and Spiegelman, B.M. (1998). A cold-inducible coactivator of nuclear receptors linked to adaptive thermogenesis. Cell *92*, 829-839.

Purdue, M.P., Hutchings, S.J., Rushton, L., and Silverman, D.T. (2015). The proportion of cancer attributable to occupational exposures. Annals of epidemiology *25*, 188-192.

Purdue, M.P., Johansson, M., Zelenika, D., Toro, J.R., Scelo, G., Moore, L.E., Prokhortchouk, E., Wu, X., Kiemeney, L.A., and Gaborieau, V. (2011). Genome-wide association study of renal cell carcinoma identifies two susceptibility loci on 2p21 and 11q13. 3. Nature genetics *43*, 60.

Puzio-Kuter, A.M., Castillo-Martin, M., Kinkade, C.W., Wang, X., Shen, T.H., Matos, T., Shen, M.M., Cordon-Cardo, C., and Abate-Shen, C. (2009). Inactivation of p53 and Pten promotes invasive bladder cancer. Genes & development *23*, 675-680.

Qiu, B., Ackerman, D., Sanchez, D.J., Li, B., Ochocki, J.D., Grazioli, A., Bobrovnikova-Marjon, E., Diehl, J.A., Keith, B., and Simon, M.C. (2015). HIF2α-dependent lipid storage promotes endoplasmic reticulum homeostasis in clear-cell renal cell carcinoma. Cancer discovery *5*, 652-667.

Rafnar, T., Vermeulen, S.H., Sulem, P., Thorleifsson, G., Aben, K.K., Witjes, J.A., Grotenhuis, A.J., Verhaegh, G.W., Hulsbergen-van de Kaa, C.A., and Besenbacher, S. (2011). European genome-wide association study identifies SLC14A1 as a new urinary bladder cancer susceptibility gene. Human molecular genetics *20*, 4268-4281.

Rankin, E.B., Tomaszewski, J.E., and Haase, V.H. (2006). Renal cyst development in mice with conditional inactivation of the von Hippel-Lindau tumor suppressor. Cancer research *66*, 2576-2583.

Raval, R.R., Lau, K.W., Tran, M.G., Sowter, H.M., Mandriota, S.J., Li, J.-L., Pugh, C.W., Maxwell, P.H., Harris, A.L., and Ratcliffe, P.J. (2005). Contrasting properties of hypoxia-inducible factor 1 (HIF-1) and HIF-2 in von Hippel-Lindau-associated renal cell carcinoma. Molecular and cellular biology *25*, 5675-5686.

Ravaud, A., Motzer, R.J., Pandha, H.S., George, D.J., Pantuck, A.J., Patel, A., Chang, Y.-H., Escudier, B., Donskov, F., and Magheli, A. (2016). Adjuvant sunitinib in high-risk renal-cell carcinoma after nephrectomy. New England Journal of Medicine *375*, 2246-2254.

Ricketts, C.J., Crooks, D.R., and Linehan, W.M. (2016). Targeting HIF2α in Clear-Cell Renal Cell Carcinoma. Cancer cell *30*, 515-517.

Rimkus, T., Carpenter, R., Qasem, S., Chan, M., and Lo, H.-W. (2016). Targeting the sonic hedgehog signaling pathway: review of smoothened and GLI inhibitors. Cancers *8*, 22.

Rini, B.I., Campbell, S.C., and Escudier, B. (2009). Renal cell carcinoma. The Lancet *373*, 1119-1132.

Robertson, A.G., Kim, J., Al-Ahmadie, H., Bellmunt, J., Guo, G., Cherniack, A.D., Hinoue, T., Laird, P.W., Hoadley, K.A., and Akbani, R. (2017). Comprehensive molecular characterization of muscle-invasive bladder cancer. Cell *171*, 540-556. e525.

Rochel, N., Krucker, C., Coutos-Thévenot, L., Osz, J., Zhang, R., Guyon, E., Zita, W., Vanthong, S., Hernandez, O.A., and Bourguet, M. (2019). Recurrent activating mutations of PPARγ associated with luminal bladder tumors. Nature communications *10*, 253.

Rosen, E.D., Hsu, C.-H., Wang, X., Sakai, S., Freeman, M.W., Gonzalez, F.J., and Spiegelman, B.M. (2002). C/EBPα induces adipogenesis through PPARγ: a unified pathway. Genes & development *16*, 22-26.

Rothman, N., Garcia-Closas, M., Chatterjee, N., Malats, N., Wu, X., Figueroa, J.D., Real, F.X., Van Den Berg, D., Matullo, G., and Baris, D. (2010). A multi-stage genome-wide association study of bladder cancer identifies multiple susceptibility loci. Nature genetics *42*, 978.

Roussel, M.F. (1999). The INK4 family of cell cycle inhibitors in cancer. Oncogene *18*, 5311.

Rydzanicz, M., Wrzesiński, T., Bluyssen, H.A., and Wesoły, J. (2013). Genomics and epigenomics of clear cell renal cell carcinoma: recent developments and potential applications. Cancer letters *341*, 111-126.

Rysman, E., Brusselmans, K., Scheys, K., Timmermans, L., Derua, R., Munck, S., Van Veldhoven, P.P., Waltregny, D., Daniëls, V.W., and Machiels, J. (2010). De novo lipogenesis protects cancer cells from free radicals and chemotherapeutics by promoting membrane lipid saturation. Cancer research *70*, 8117-8126.

Saez, E., Tontonoz, P., Nelson, M.C., Alvarez, J.G., Ming, U.T., Baird, S.M., Thomazy, V.A., and Evans, R.M. (1998). Activators of the nuclear receptor PPARgamma enhance colon polyp formation. Nat Med *4*, 1058-1061.

Saito, K., Arai, E., Maekawa, K., Ishikawa, M., Fujimoto, H., Taguchi, R., Matsumoto, K., Kanai, Y., and Saito, Y. (2016). Lipidomic signatures and associated transcriptomic profiles of clear cell renal cell carcinoma. Scientific reports *6*, 28932.

Sanchez, D.J., Steger, D.J., Skuli, N., Bansal, A., and Simon, M.C. (2018). PPARγ is dispensable for clear cell renal cell carcinoma progression. Molecular metabolism.

Sanjana, N.E., Shalem, O., and Zhang, F. (2014). Improved vectors and genome-wide libraries for CRISPR screening. Nature methods *11*, 783.

Sanli, O., Dobruch, J., Knowles, M.A., Burger, M., Alemozaffar, M., Nielsen, M.E., and Lotan, Y. (2017). Bladder cancer. Nature reviews Disease primers *3*, 17022.

Sato, Y., Yoshizato, T., Shiraishi, Y., Maekawa, S., Okuno, Y., Kamura, T., Shimamura, T., Sato-Otsubo, A., Nagae, G., and Suzuki, H. (2013). Integrated molecular analysis of clear-cell renal cell carcinoma. Nature genetics *45*, 860.

Sauer, S. (2015). Ligands for the nuclear peroxisome proliferator-activated receptor gamma. Trends in pharmacological sciences *36*, 688-704.

Scelo, G., Purdue, M.P., Brown, K.M., Johansson, M., Wang, Z., Eckel-Passow, J.E., Ye, Y., Hofmann, J.N., Choi, J., and Foll, M. (2017). Genome-wide association study identifies multiple risk loci for renal cell carcinoma. Nature communications *8*, 15724.

Scelo, G., Riazalhosseini, Y., Greger, L., Letourneau, L., Gonzàlez-Porta, M., Wozniak, M.B., Bourgey, M., Harnden, P., Egevad, L., and Jackson, S.M. (2014). Variation in genomic landscape of clear cell renal cell carcinoma across Europe. Nature communications *5*, 5135.

Schmidt, S.F., Jørgensen, M., Chen, Y., Nielsen, R., Sandelin, A., and Mandrup, S. (2011). Cross species comparison of C/EBPα and PPARγ profiles in mouse and human adipocytes reveals interdependent retention of binding sites. BMC genomics *12*, 152.

Schödel, J., Bardella, C., Sciesielski, L.K., Brown, J.M., Pugh, C.W., Buckle, V., Tomlinson, I.P., Ratcliffe, P.J., and Mole, D.R. (2012). Common genetic variants at the 11q13. 3 renal cancer susceptibility locus influence binding of HIF to an enhancer of cyclin D1 expression. Nature genetics *44*, 420.

Schumacher, T.N., and Schreiber, R.D. (2015). Neoantigens in cancer immunotherapy. Science *348*, 69-74.

Sever, R., and Glass, C.K. (2013). Signaling by nuclear receptors. Cold Spring Harbor perspectives in biology *5*, a016709.

Shao, D., Rangwala, S.M., Bailey, S.T., Krakow, S.L., Reginato, M.J., and Lazar, M.A. (1998). Interdomain communication regulating ligand binding by PPAR-γ. Nature *396*, 377.

Shao, X., Somlo, S., and Igarashi, P. (2002). Epithelial-specific Cre/lox recombination in the developing kidney and genitourinary tract. Journal of the American Society of Nephrology *13*, 1837-1846.

Shapira, S.N., and Seale, P. (2019). Transcriptional Control of Brown and Beige Fat Development and Function. Obesity *27*, 13-21.

Shen, C., Beroukhim, R., Schumacher, S., Zhou, J., Chang, M., Signoretti, S., and Kaelin, W. (2011). Genetic and functional studies implicate HIF1α as a 14q kidney cancer suppressor gene. Cancer discovery, CD-11-0098.

Shenoy, N., Vallumsetla, N., Zou, Y., Galeas, J.N., Shrivastava, M., Hu, C., Susztak, K., and Verma, A. (2015). Role of DNA methylation in renal cell carcinoma. Journal of hematology & oncology *8*, 88.

Shiau, C.-W., Yang, C.-C., Kulp, S.K., Chen, K.-F., Chen, C.-S., Huang, J.-W., and Chen, C.-S. (2005). Thiazolidenediones mediate apoptosis in prostate cancer cells in part through inhibition of Bcl-xL/Bcl-2 functions independently of PPARγ. Cancer research *65*, 1561-1569.

Shin, K., Lim, A., Odegaard, J.I., Honeycutt, J.D., Kawano, S., Hsieh, M.H., and Beachy, P.A. (2014a). Cellular origin of bladder neoplasia and tissue dynamics of its progression to invasive carcinoma. Nature cell biology *16*, 469.

Shin, K., Lim, A., Zhao, C., Sahoo, D., Pan, Y., Spiekerkoetter, E., Liao, J.C., and Beachy, P.A. (2014b). Hedgehog signaling restrains bladder cancer progression by eliciting stromal production of urothelial differentiation factors. Cancer cell *26*, 521-533.

Shinagare, A.B., Ramaiya, N.H., Jagannathan, J.P., Fennessy, F.M., Taplin, M.-E., and Van den Abbeele, A.D. (2011). Metastatic pattern of bladder cancer: correlation with the characteristics of the primary tumor. American Journal of Roentgenology *196*, 117-122.

Shrader, M., Pino, M.S., Brown, G., Black, P., Adam, L., Bar-Eli, M., Dinney, C.P., and McConkey, D.J. (2007). Molecular correlates of gefitinib responsiveness in human bladder cancer cells. Molecular cancer therapeutics *6*, 277-285.

Shroff, E.H., Eberlin, L.S., Dang, V.M., Gouw, A.M., Gabay, M., Adam, S.J., Bellovin, D.I., Tran, P.T., Philbrick, W.M., and Garcia-Ocana, A. (2015). MYC oncogene overexpression drives renal cell carcinoma in a mouse model through glutamine metabolism. Proceedings of the National Academy of Sciences *112*, 6539-6544.

Siegel Rebecca, L., Miller Kimberly, D., and Jemal, A. (2018). Cancer statistics, 2018. CA: a cancer journal for clinicians *68*, 7-30.

Simonnet, H., Alazard, N., Pfeiffer, K., Gallou, C., Béroud, C., Demont, J., Bouvier, R., Schägger, H., and Godinot, C. (2002). Low mitochondrial respiratory chain content correlates with tumor aggressiveness in renal cell carcinoma. Carcinogenesis *23*, 759-768.

Sjödahl, G., Lauss, M., Lövgren, K., Chebil, G., Gudjonsson, S., Veerla, S., Patschan, O., Aine, M., Fernö, M., and Ringnér, M. (2012). A molecular taxonomy for urothelial carcinoma. Clinical cancer research *18*, 3377-3386.

Soccio, R.E., Tuteja, G., Everett, L.J., Li, Z., Lazar, M.A., and Kaestner, K.H. (2011). Species-specific strategies underlying conserved functions of metabolic transcription factors. Molecular endocrinology *25*, 694-706.

Soneson, C., Love, M.I., and Robinson, M.D. (2015). Differential analyses for RNA-seq: transcript-level estimates improve gene-level inferences. F1000Research *4*.

Srivastava, N., Kollipara, R.K., Singh, D.K., Sudderth, J., Hu, Z., Nguyen, H., Wang, S., Humphries, C.G., Carstens, R., and Huffman, K.E. (2014). Inhibition of cancer cell proliferation by PPARγ is mediated by a metabolic switch that increases reactive oxygen species levels. Cell metabolism *20*, 650-661.

Stein, J.P., Lieskovsky, G., Cote, R., Groshen, S., Feng, A.-C., Boyd, S., Skinner, E., Bochner, B., Thangathurai, D., and Mikhail, M. (2001). Radical cystectomy in the treatment of invasive bladder cancer: long-term results in 1,054 patients. Journal of clinical oncology *19*, 666-675.

Sternberg, C.N., Bellmunt, J., Sonpavde, G., Siefker-Radtke, A.O., Stadler, W.M., Bajorin, D.F., Dreicer, R., George, D.J., Milowsky, M.I., and Theodorescu, D. (2013). ICUD-EAU International Consultation on Bladder Cancer 2012: chemotherapy for urothelial carcinoma—neoadjuvant and adjuvant settings. European urology *63*, 58-66.

Sundelin, J.P., Ståhlman, M., Lundqvist, A., Levin, M., Parini, P., Johansson, M.E., and Borén, J. (2012). Increased expression of the very low-density lipoprotein receptor mediates lipid accumulation in clear-cell renal cell carcinoma. PloS one *7*, e48694.

Syed, I.S., Pedram, A., and Farhat, W.A. (2016). Role of Sonic Hedgehog (Shh) signaling in bladder cancer stemness and tumorigenesis. Current urology reports *17*, 11.

Tang, S.-W., Chang, W.-H., Su, Y.-C., Chen, Y.-C., Lai, Y.-H., Wu, P.-T., Hsu, C.-I., Lin, W.-C., Lai, M.-K., and Lin, J.-Y. (2009). MYC pathway is activated in clear cell renal cell carcinoma and essential for proliferation of clear cell renal cell carcinoma cells. Cancer letters *273*, 35-43.

Tannir, N.M., Fan, A.C., Lee, R.J., Carthon, B.C., Iliopoulos, O., Mier, J.W., Patel, M.R., Meric-Bernstam, F., DeMichele, A., and Voss, M.H. (2018). Phase 1 study of glutaminase (GLS) inhibitor CB-839 combined with either everolimus (E) or cabozantinib (Cabo) in patients (pts) with clear cell (cc) and papillary (pap) metastatic renal cell cancer (mRCC) (American Society of Clinical Oncology).

Tontonoz, P., Hu, E., and Spiegelman, B.M. (1994). Stimulation of adipogenesis in fibroblasts by PPARγ2, a lipid-activated transcription factor. Cell *79*, 1147-1156.

Tontonoz, P., Singer, S., Forman, B.M., Sarraf, P., Fletcher, J.A., Fletcher, C.D., Brun, R.P., Mueller, E., Altiok, S., and Oppenheim, H. (1997). Terminal differentiation of human liposarcoma cells induced by ligands for peroxisome proliferator-activated receptor γ and the retinoid X receptor. Proceedings of the National Academy of Sciences *94*, 237-241.

Tontonoz, P., and Spiegelman, B.M. (2008). Fat and beyond: the diverse biology of PPARγ. Annu Rev Biochem *77*, 289-312.

Tsai, M.-J., and O'Malley, B.W. (1994). Molecular mechanisms of action of steroid/thyroid receptor superfamily members. Annual review of biochemistry *63*, 451-486.

Tuccori, M., Filion, K.B., Yin, H., Oriana, H.Y., Platt, R.W., and Azoulay, L. (2016). Pioglitazone use and risk of bladder cancer: population based cohort study. Bmj *352*, i1541.

Tun, H.W., Marlow, L.A., Von Roemeling, C.A., Cooper, S.J., Kreinest, P., Wu, K., Luxon, B.A., Sinha, M., Anastasiadis, P.Z., and Copland, J.A. (2010). Pathway signature and cellular differentiation in clear cell renal cell carcinoma. PloS one *5*, e10696.

Turajlic, S., Larkin, J., and Swanton, C. (2015). SnapShot: renal cell carcinoma. Cell *163*, 1556-1556. e1551.

Van Haaften, G., Dalgliesh, G.L., Davies, H., Chen, L., Bignell, G., Greenman, C., Edkins, S., Hardy, C., O'meara, S., and Teague, J. (2009). Somatic mutations of the histone H3K27 demethylase gene UTX in human cancer. Nature genetics *41*, 521.

Vanharanta, S., Shu, W., Brenet, F., Hakimi, A.A., Heguy, A., Viale, A., Reuter, V.E., Hsieh, J.J., Scandura, J.M., and Massagué, J. (2013). Epigenetic expansion of VHL-HIF signal output drives multiorgan metastasis in renal cancer. Nature medicine *19*, 50.

Varela, I., Tarpey, P., Raine, K., Huang, D., Ong, C.K., Stephens, P., Davies, H., Jones, D., Lin, M.-L., and Teague, J. (2011). Exome sequencing identifies frequent mutation of the SWI/SNF complex gene PBRM1 in renal carcinoma. Nature *469*, 539.

Villavicencio, E.H., Walterhouse, D.O., and Iannaccone, P.M. (2000). The sonic hedgehog–patched–gli pathway in human development and disease. The American Journal of Human Genetics *67*, 1047-1054.

Vinci, M., Gowan, S., Boxall, F., Patterson, L., Zimmermann, M., Lomas, C., Mendiola, M., Hardisson, D., and Eccles, S.A. (2012). Advances in establishment and analysis of three-dimensional tumor spheroid-based functional assays for target validation and drug evaluation. BMC biology *10*, 29.

Von Roemeling, C.A., Marlow, L.A., Wei, J.J., Cooper, S.J., Caulfield, T.R., Wu, K., Tan, W.W., Tun, H.W., and Copland, J.A. (2013). Stearoyl-CoA desaturase 1 is a novel molecular therapeutic target for clear cell renal cell carcinoma. Clinical Cancer Research *19*, 2368-2380.

Wallace, E.M., Rizzi, J.P., Han, G., Wehn, P.M., Cao, Z., Du, X., Cheng, T., Czerwinski, R.M., Dixon, D.D., and Goggin, B.S. (2016). A small-molecule antagonist of HIF2α is efficacious in preclinical models of renal cell carcinoma. Cancer research *76*, 5491-5500.

Walther, T.C., and Farese Jr, R.V. (2012). Lipid droplets and cellular lipid metabolism. Annual review of biochemistry *81*, 687-714.

Wang, F., Mullican, S.E., DiSpirito, J.R., Peed, L.C., and Lazar, M.A. (2013). Lipoatrophy and severe metabolic disturbance in mice with fat-specific deletion of PPARγ. Proceedings of the National Academy of Sciences *110*, 18656-18661.

Wang, S.-S., Gu, Y.-F., Wolff, N., Stefanius, K., Christie, A., Dey, A., Hammer, R.E., Xie, X.-J., Rakheja, D., and Pedrosa, I. (2014). Bap1 is essential for kidney function and cooperates with Vhl in renal tumorigenesis. Proceedings of the National Academy of Sciences *111*, 16538-16543.

Ward, P.S., and Thompson, C.B. (2012). Metabolic reprogramming: a cancer hallmark even warburg did not anticipate. Cancer cell *21*, 297-308.

Warrick, J.I., Walter, V., Yamashita, H., Chung, E., Shuman, L., Amponsa, V.O., Zheng, Z., Chan, W., Whitcomb, T.L., and Yue, F. (2016). FOXA1, GATA3 and PPARɣ Cooperate to Drive Luminal Subtype in Bladder Cancer: A Molecular Analysis of Established Human Cell Lines. Scientific reports *6*, 38531.

Wellen, K.E., and Thompson, C.B. (2012). A two-way street: reciprocal regulation of metabolism and signalling. Nature reviews Molecular cell biology *13*, 270.

Wettersten, H.I., Aboud, O.A., Lara Jr, P.N., and Weiss, R.H. (2017). Metabolic reprogramming in clear cell renal cell carcinoma. Nature Reviews Nephrology *13*, 410.

Wiederschain, D., Susan, W., Chen, L., Loo, A., Yang, G., Huang, A., Chen, Y., Caponigro, G., Yao, Y.-m., and Lengauer, C. (2009). Single-vector inducible lentiviral RNAi system for oncology target validation. Cell cycle *8*, 498-504.

Wu, X.-R., Kong, X.-P., Pellicer, A., Kreibich, G., and Sun, T.-T. (2009). Uroplakins in urothelial biology, function, and disease. Kidney international *75*, 1153-1165.

Wu, Z., Bucher, N., and Farmer, S.R. (1996). Induction of peroxisome proliferator-activated receptor gamma during the conversion of 3T3 fibroblasts into adipocytes is mediated by C/EBPbeta, C/EBPdelta, and glucocorticoids. Molecular and cellular biology *16*, 4128-4136.

Wu, Z., Xie, Y., Bucher, N., and Farmer, S.R. (1995). Conditional ectopic expression of C/EBP beta in NIH-3T3 cells induces PPAR gamma and stimulates adipogenesis. Genes & development *9*, 2350-2363.

Xie, H., and Simon, M.C. (2017). Oxygen availability and metabolic reprogramming in cancer. Journal of Biological Chemistry *292*, 16825-16832.

Yang, J.C., Haworth, L., Sherry, R.M., Hwu, P., Schwartzentruber, D.J., Topalian, S.L., Steinberg, S.M., Chen, H.X., and Rosenberg, S.A. (2003). A randomized trial of bevacizumab, an anti–vascular endothelial growth factor antibody, for metastatic renal cancer. New England Journal of Medicine *349*, 427-434.

Yki-Jarvinen, H. (2004). Thiazolidinediones. The New England journal of medicine *351*, 1106-1118.

Yoshida, S., Imam, A., Olson, C., and Taylor, C. (1986). Proximal renal tubular surface membrane antigens identified in primary and metastatic renal cell carcinomas. Archives of pathology & laboratory medicine *110*, 825-832.

Yoshimura, K., Chen, L.C., Mandal, M.K., Nakazawa, T., Yu, Z., Uchiyama, T., Hori, H., Tanabe, K., Kubota, T., and Fujii, H. (2012). Analysis of renal cell carcinoma as a first step for developing mass spectrometry-based diagnostics. Journal of The American Society for Mass Spectrometry *23*, 1741-1749.

Young, R.M., Ackerman, D., Quinn, Z.L., Mancuso, A., Gruber, M., Liu, L., Giannoukos, D.N., Bobrovnikova-Marjon, E., Diehl, J.A., and Keith, B. (2013). Dysregulated mTORC1 renders cells critically dependent on desaturated lipids for survival under tumor-like stress. Genes & development *27*, 1115-1131.

Zhang, H., Gao, P., Fukuda, R., Kumar, G., Krishnamachary, B., Zeller, K.I., Dang, C.V., and Semenza, G.L. (2007). HIF-1 inhibits mitochondrial biogenesis and cellular respiration in VHL-deficient renal cell carcinoma by repression of C-MYC activity. Cancer cell *11*, 407-420.

Zhang, Z.-T., Pak, J., Shapiro, E., Sun, T.-T., and Wu, X.-R. (1999). Urothelium-specific expression of an oncogene in transgenic mice induced the formation of carcinoma in situ and invasive transitional cell carcinoma. Cancer research *59*, 3512-3517.

Zhu, C., Wei, J., Tian, X., Li, Y., and Li, X. (2015). Prognostic role of PPAR-γ and PTEN in the renal cell carcinoma. International journal of clinical and experimental pathology *8*, 12668.

Zhu, Y., Qi, C., Korenberg, J.R., Chen, X.-N., Noya, D., Rao, M.S., and Reddy, J.K. (1995). Structural organization of mouse peroxisome proliferator-activated receptor gamma (mPPAR gamma) gene: alternative promoter use and different splicing yield two mPPAR gamma isoforms. Proceedings of the National Academy of Sciences *92*, 7921-7925.